MMNSA

Mathematical Modelling and Numerical Simulation with Applications

ISSN Online : 2791-8564

Year : 2021

Volume : 1

Issue : 2

www.mmnsa.org

EDITOR-IN-CHIEF
Mehmet Yavuz, PhD,
Necmettin Erbakan University, Turkey

VOLUME: 1 ISSUE: 2
ISSN ONLINE: 2791-8564

December 2021
http://mmnsa.org

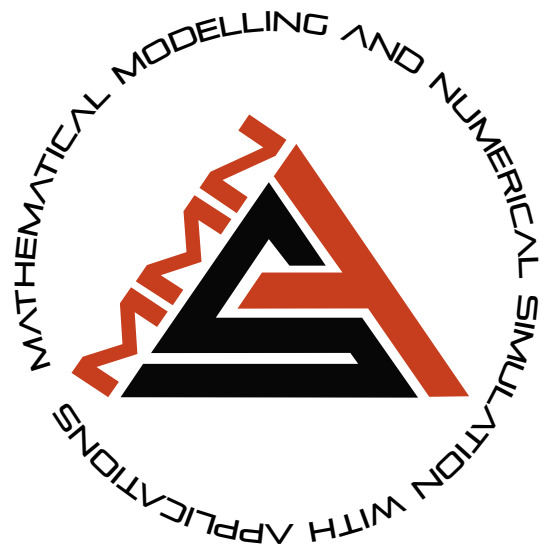

MATHEMATICAL MODELLING AND NUMERICAL SIMULATION WITH APPLICATIONS

Technical Editor

Halil İbrahim Özer
Department of Computer and Instructional Technologies
Education, Ahmet Keleşoğlu Faculty of Education,
Necmettin Erbakan University, Meram Yeniyol, 42090
Meram, Konya/TURKEY
hiozer@gmail.com

English Editor

Abdulkadir Ünal
School of Foreign Languages, Foreign Languages, Alanya
Alaaddin Keykubat University, Alanya,
Antalya/TURKEY
abdulkadir.unal@alanya.edu.tr

Editorial Secretariat

Fatma Özlem Coşar
Department of Mathematics and Computer Sciences,
Faculty of Science, Necmettin Erbakan University,
Meram Yeniyol, 42090 Meram, Konya/TURKEY

Müzeyyen Akman
Department of Mathematics and Computer Sciences,
Faculty of Science, Necmettin Erbakan University,
Meram Yeniyol, 42090 Meram, Konya/TURKEY

Contents

Research Articles

Mathematical Modelling and Numerical Simulation with Applications, 2021, 1(2), 56–66

https://www.mmnsa.org
ISSN Online: 2791-8564 / Open Access
https://doi.org/10.53391/mmnsa.2021.01.006

RESEARCH PAPER

Vaccination effect conjoint to fraction of avoided contacts for a Sars-Cov-2 mathematical model

Stefania Allegretti[1,†], Iulia Martina Bulai[1,2,*,†], Roberto Marino[1,†], Margherita Anna Menandro[1,†] and Katia Parisi[1,†]

[1]Department of Mathematics, Informatics and Economics, University of Basilicata, Viale dell'Ateneo Lucano, 10, 85100 Potenza, Italy, [2]Member of the research group GNCS of INdAM.

*Corresponding Author
†stefania.allegretti@studenti.unibas.it (Stefania Allegretti); iulia.bulai@unibas.it (Iulia Martina Bulai); roberto.marino@studenti.unibas.it (Roberto Marino); margheritaanna.menandro@studenti.unibas.it (Margherita Anna Menandro); katia.parisi@studenti.unibas.it (Katia Parisi)

Abstract

In this paper, we consider a modified SIR (susceptible-infected-recovered/removed) model that describes the evolution in time of the infectious disease caused by Sars-Cov-2 (Severe Acute Respiratory Syndrome-Coronavirus-2). We take into consideration that this disease can be both symptomatic and asymptomatic. By formulating a suitable mathematical model via a system of ordinary differential equations (ODEs), we investigate how the vaccination rate and the fraction of avoided contacts affect the population dynamics.

Key words: COVID-19; SIR model; asymptomatic cases; avoided contacts; vaccination effect
AMS 2020 Classification: 34A34; 92D30; 92D25

1 Introduction

The mathematical epidemiology research area, related to modeling infectious diseases, began to develop in 1771 having Daniel Bernoulli as one of the pioneers, [2]. The SIR models and their modified versions are simple tools that can be used to better understand the dynamics of an epidemic, and they gave a significant contribute also for Covid-19 (coronavirus-19 disease) pandemic. The global pandemic status, due to Sars-Cov-2, has been declared, by World Health Organization, at the beginning of 2020, while the virus started to spread around the globe already at the end of 2019 and beginning of 2020 [1].

In the last year an increasing amount of papers for modeling Covid-19 pandemic was published, only to cite few of them see [3]-[31]. The modeling approach helped in a better understanding of the epidemic evolution, such as transmission dynamics of Covid-19 [17]-[19], Covid-19 forecasting, [3], the importance of implementing population-wide interventions, [24]-[25], the role of asymptomatic individuals in the disease transmission, [30]-[31], the vaccination effect on the pandemic outcome, [32]-[34], etc.

Motivated by the importance of a better understanding of the vaccination effect and of the non-pharmaceutical interventions (NPIs) on the disease spreading, here, we consider an extended version of the already studied modified SIR model, [35], considering susceptible individuals, infected individuals that can show symptoms (symptomatic) or not (asymptomatic), and recovered/removed individuals, respectively. The model is characterized by assuming that the infection rate can change depending on NPIs. The novelty here is to consider also the vaccination rate for the susceptible individuals. For a qualitative analysis of the model we compute the equilibrium points and we study their stability by analyzing the Jacobian matrix eigenvalues. We also compute the basic reproduction number. Moreover, for a

➤ **Received:** 13.10.2021 ➤ **Revised:** 18.11.2021 ➤ **Accepted:** 22.11.2021 ➤ **Published:** 26.11.2021

quantitative analysis, via numerical simulation, we investigate how the fraction of avoided contacts and the vaccination rate affects the model outcome, separately using one parameter bifurcation diagrams and jointly by approximating the two strain parameter surface.

The paper outline is as follows. In the first Section, we introduce the model describing all the hypothesis used to build it. In the second Section, we compute a qualitative analysis of the model. In the third Section, via numerical simulations we investigate the importance of both vaccination rate and the fraction of avoided contacts, respectively. Last we present the conclusions of the paper.

2 Mathematical model formulation

In this study we introduce a new mathematical model, generalizing the classical SIR model used to describe the transmission and evolution in time of infectious diseases that leads to the immunization of the diseased individual, for the specific case of Sars-Cov-2. In the SIR model we can distinguish three classes of individuals:

Susceptible $H(t)$: healthy individuals that can get the disease.
Infected $I(t)$: individuals that are infected and can transmit the disease.
Removed $R(t)$: individuals that, after being infected, once they recover become immune to the disease, are isolated or died.

For Sars-Cov-2 transmission we consider two different subgroups of the infective classes:

Asymptomatic $A(t)$: infected individuals that does not present symptoms. We denote with ϕ the probability that the disease presents itself in this form.
Symptomatic $S(t)$: infected individuals that present symptoms. The probability that the disease manifests itself in this form is $1-\phi$.

From now on for simplicity we will abbreviate the new model with SASR (Susceptible-Asymptomatic-Symptomatic-Removed). We assume to have a constant total population in time, N, this is reasonable for two reasons: (i) if we consider the beginning of the epidemic it means that only a short interval of time will be considered; (ii) while if we consider a long time after the onset of the epidemic we can assume that the mortality rate due to the disease is lower and lower due to a better understanding of the virus and improvement of the effects of the cure. We also consider the demographic parameters such as constant birth/immigration term, Ω, in the susceptible class and a mortality rate, μ_N, due to other causes besides the disease, present in all the considered classes.
The infection rate take into consideration also the effect of non-pharmaceutical interventions (NPIs) by means of a parameter ψ, the fraction of avoided contacts, the infection rate reads $\beta = \lambda(1-\psi)$. Here we assume that the contact rate between susceptible and infected is reduced thanks to NPIs adopted by individuals or by institutions, in order to avoid the contagion.
Once infected, a fraction $1-\phi$ of individuals can develop symptoms and the remaining ones ϕ stay asymptomatic. We also assume that the asymptomatic individuals can develop symptoms at rate δ. Last, we assume that both asymptomatic and symptomatic individuals can move in the removed class at rate γ_A and γ_S, respectively, and that exist a vaccine and the susceptible individuals can be vaccinated and get a permanent immunity at rate μ.
Given the assumptions introduced above the model reads:

$$\begin{aligned}
\frac{dH}{dt} &= \Omega - \beta\frac{H(A+S)}{N} - \mu_N H - \mu H,\\
\frac{dA}{dt} &= \phi\beta\frac{H(A+S)}{N} - \gamma_A A - \mu_N A - \delta A,\\
\frac{dS}{dt} &= (1-\phi)\beta\frac{H(A+S)}{N} - \gamma_S S - \mu_N S + \delta A - \mu_S S,\\
\frac{dR}{dt} &= \gamma_A A + \gamma_S S - \mu_N R + \mu H,
\end{aligned} \tag{1}$$

with $\phi, \psi \in [0,1]$. In Figure 1, we have represented a sketch of the main interactions between the four classes of the SASR model.

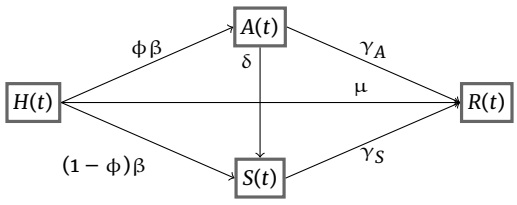

Figure 1. The diagram for the main interaction between the four classes of the SASR model, without considering the mortality rates and birth/immigration term.

3 Qualitative analysis of the model

Boundedness

It is important to establish that the variables cannot grow unbounded. We show now that the system's trajectories remain within a compact set. We consider the function

$$\varphi(t) = H(t) + A(t) + S(t) + R(t).$$

Summing up the equations in (1), we then have

$$\frac{d\varphi(t)}{dt} + \mu_N \varphi(t) = \Omega - \mu_S S \quad \Leftrightarrow \quad \frac{d\varphi(t)}{dt} + \mu_N \varphi(t) \leq \Omega.$$

Since $\varphi(0) = N$, we can solve the corresponding differential equation, and find that:

$$\varphi(t) \leq max\left\{\frac{\Omega}{\mu_N}, N\right\},$$

which guarantees that every single variable must have the same upper bound as well.

Equilibrium points

In order to find the equilibrium points we assume $a = \gamma_A + \mu_N + \delta$, $b = \gamma_S + \mu_S + \mu_N$ and $W = \frac{H(A+S)}{N}$ in (1), and get the new simplified version of the model by equating to zero the right hand side of the obtained model:

$$\begin{cases} \Omega - \beta W - \mu_N H - \mu H = 0, \\ \phi\beta W - aA = 0, \\ (1-\phi)\beta W - bS + \delta A = 0, \\ \gamma_A A + \gamma_S S - \mu_N R + \mu H = 0, \\ W = \frac{H(A+S)}{N}, \end{cases} \tag{2}$$

which is equivalent to

$$\begin{cases} H = \frac{\Omega - \beta W}{\mu_N + \mu}, \\ A = \frac{\phi\beta W}{a}, \\ S = \frac{\beta W(a(1-\phi) + \delta\phi)}{ab}, \\ \gamma_A\left(\frac{\phi\beta W}{a}\right) + \gamma_S\left(\frac{\beta W(a(1-\phi)+\delta\phi)}{ab}\right) - \mu_N R + \mu\left(\frac{\Omega - \beta W}{\mu_N + \mu}\right) = 0, \\ W = \frac{\left(\frac{\Omega - \beta W}{\mu_N + \mu}\right)\left(\frac{\phi\beta W}{a} + \frac{\beta W(a(1-\phi)+\delta\phi)}{ab}\right)}{N}. \end{cases} \tag{3}$$

Solving the last equation of (3) we get

$$W_1 = 0$$
$$or$$
$$W_2 = \frac{-\phi\beta b\Omega - a\beta\Omega + a\beta\phi\Omega - \delta\phi\beta\Omega + Nab(\mu_N + \mu)}{\beta^2(-\phi b - a + a\phi - \delta\phi)}.$$

- For W_1 we get the disease free equilibrium (DFE)

$$E_0 = (H_0, A_0, S_0, R_0) = \left(\frac{\Omega}{\mu_N + \mu}, 0, 0, \frac{\mu\Omega}{\mu_N(\mu_N + \mu)}\right),$$

  that is always feasible.
- For W_2 we get the coexistence equilibrium

$$E_* = (H_*, A_*, S_*, R_*)$$

  with

$$H_* = \frac{Nab}{\beta(a(1-\phi) + \phi(b+\delta))},$$
$$A_* = \frac{\phi[\beta\Omega(a(1-\phi) + \phi(b+\delta)) - Nab(\mu_N + \mu)]}{a\beta(a(1-\phi) + \phi(b+\delta))},$$
$$S_* = \frac{(a(1-\phi) + \delta\phi)[\beta\Omega(a(1-\phi) + \phi(b+\delta)) - Nab(\mu_N + \mu)]}{ab\beta(a(1-\phi) + \phi(b+\delta))},$$
$$R_* = \frac{(b\gamma_A\phi + \gamma_S(a(1-\phi) + \delta\phi)[\Omega\beta(a(1-\phi) + \phi(b+\delta)) - Nab(\mu_N + \mu)] - \mu Na^2b^2}{\mu_N ab\beta(a(1-\phi) + \phi(b+\delta))}.$$

Notice that $H_* > 0$, while

$$A_* > 0 \quad \Leftrightarrow \quad \frac{\phi[\beta\Omega(a(1-\phi)+\phi(b+\delta)) - Nab(\mu_N+\mu)]}{a\beta(a(1-\phi)+\phi(b+\delta))} > 0,$$

solving the inequality for μ we get that

$$\mu < \frac{\beta\Omega(a(1-\phi)+\phi(b+\delta))}{Nab} - \mu_N$$

must hold. Assuming $A_* > 0$ also $S_* > 0$ and $R_* > 0$ hold and the coexistence equilibrium E_* is feasible.

Jacobian matrix and characteristic polynomial

In order to study the stability of the equilibrium points we need to compute the eigenvalues of the Jacobian matrix associated to system (1), evaluated at the equilibrium points. The Jacobian matrix is

$$J = \begin{pmatrix} -\beta\frac{(A+S)}{N} - \mu_N - \mu & -\beta\frac{H}{N} & -\beta\frac{H}{N} & 0 \\ \phi\beta\frac{(A+S)}{N} & \phi\beta\frac{H}{N} - a & \phi\beta\frac{H}{N} & 0 \\ (1-\phi)\beta\frac{(A+S)}{N} & (1-\phi)\beta\frac{H}{N} + \delta & (1-\phi)\beta\frac{H}{N} - b & 0 \\ \mu & \gamma_A & \gamma_S & -\mu_N \end{pmatrix}. \tag{4}$$

We compute the characteristic polynomial associated to J by computing $det(J - xI)$, and we get

$$\begin{aligned} p(x) = \frac{(-\mu_N - x)}{N} \cdot \Big[& Nx^3 + x^2(\beta(A+S-H) + N(a+b+\mu_N+\mu)) + \\ & + x(-\beta H(\mu_N+\mu+a(1-\phi)+\phi(b+\delta)) + \beta(A+S)(a+b) + N(ab+(\mu_N+\mu)(a+b))) + \\ & - \beta H((\mu_N+\mu)(a(1-\phi)+\phi(b+\delta))) + ab\beta(A+S) + Nab(\mu_N+\mu)\Big]. \end{aligned} \tag{5}$$

Substituting in (5) the values of E_0 we get

$$p_0(x) = (\mu_N + x)(\mu_N + \mu + x)\left[x^2 + \left(a + b - \frac{\beta\Omega}{N(\mu_N+\mu)}\right)x + ab - \frac{\beta\Omega[a(1-\phi)+\phi(b+\delta)]}{N(\mu_N+\mu)}\right],$$

that has two negative eigenvalues $x_1 = -\mu_N$ e $x_2 = -(\mu_N + \mu)$. In order to have a stable DFE we should analyze the sign of the real parts of the roots of the second degree polynomial

$$x^2 + \left(a + b - \frac{\beta\Omega}{N(\mu_N+\mu)}\right)x + ab - \frac{\beta\Omega[a(1-\phi)+\phi(b+\delta)]}{N(\mu_N+\mu)}. \tag{6}$$

Notice that, $\forall\phi, \psi \in [0,1]$, the two roots of (6) are real. Imposing the second and the third coefficients of (6) to be positive and solving with respect to the vaccination rate, μ, we get the condition

$$\mu > \max\left\{\frac{\beta\Omega}{N(a+b)} - \mu_N, \quad \frac{\beta\Omega[a(1-\phi)+\phi(b+\delta)]}{Nab} - \mu_N\right\},$$

that guaranties that the second degree equation, (6), has two negative real roots and thus the stability of E_0.
In analogues way we study the stability of the coexistence equilibrium. We evaluate the Jacobian matrix (4) at E_* and we compute the associated characteristic polynomial

$$p_{*\mu}(x) = (\mu_N + x)\left(x^3 + a_2x^2 + a_1x + a_0\right) \tag{7}$$

with

$$\begin{aligned} a_2 &= \frac{1}{N}\left[\frac{Nab}{(a(1-\phi)+\phi(b+\delta))} + \frac{\beta\Omega(a(1-\phi)+\phi(b+\delta))}{ab} + N(a+b)\right], \\ a_1 &= \frac{1}{N}\left[\frac{-Nab(\mu_N+\mu)}{(a(1-\phi)+\phi(b+\delta))} + \frac{[\beta\Omega(a(1-\phi)+\phi(b+\delta))](a+b)}{ab}\right], \\ a_0 &= \frac{1}{N}\left[\beta\Omega(a(1-\phi)+\phi(b+\delta)) - Nab(\mu_N+\mu)\right]. \end{aligned}$$

The root $x_1 = -\mu_N$ is always negative while for the coexistence equilibrium to be stable the Routh–Hurwitz criterion must hold $a_0 > 0$ (true if the equilibrium is feasible), $a_2 > 0$ (true) and $a_1a_2 > a_0$.

Table 1. Parameters of the model for data considering Italy. [a] [36](ISTAT 2018), [b] Ω was chosen such that $H(0) \simeq \Omega/\mu_N$, [c] [38], [d] [39], [e] Fitted using data from [37].

Parameters	Name	Value	Unit
N	total population	60.36×10^6 [a]	human
Ω	birth and immigration	633780 [b]	human/day
λ	infection rate	0.292 [c]	day^{-1}
ψ	fraction of avoided contacts	test	pure number
ϕ	prob. of undergoing asympt. infection	0.5 [d]	pure number
γ_A	per capita recovery rate A	0.028	day^{-1}
γ_S	per capita recovery rate S	0.028 [e]	day^{-1}
μ_N	mortality rate due to other causes	0.0105 [a]	day^{-1}
μ	vaccination rate	test	day^{-1}
δ	transition from $A \to S$	0.067 [d]	day^{-1}
μ_S	mortality rate due Covid-19	0.0069 [e]	day^{-1}
a	$\gamma_A + \mu_N + \delta$	0.1055	day^{-1}
b	$\gamma_S + \mu_S + \mu_N$	0.0454	day^{-1}

Basic reproduction number R_0

The basic reproduction number, R_0, is "the expected number of secondary cases produced, in a completely susceptible population, by a typical infective individual", (e.g. [40]). The importance of R_0 in the spreading of a disease is related to its value. The ideal scenario is $R_0 < 1$, in this case the infection cannot grow. This means that on average an infected individual produces less than one new infected individual over the course of its infectious period. Conversely if $R_0 > 1$, the disease spread over the population, in fact each infected individual produces, on average, more than one new infection. We compute the basic reproduction number using the next generation matrix technique, (for a detailed description of the method see [40], [41]), and we get

$$R_0 = \frac{\lambda(1-\psi)\Omega}{(\mu_N+\mu)Nab}\left[(1-\phi)a + \phi(b+\delta)\right], \tag{8}$$

where we used that $\beta = \lambda(1-\psi)$. From (8) one can see that also in presence of the vaccine the epidemic can evolve and the stability of the coexistence equilibrium is reached. In order to have the stability of the DFE the vaccination efficiency must be greater than a certain threshold

$$\mu > (R_0 - 1)\mu_N = \frac{\lambda(1-\psi)\Omega(a(1-\phi) + \phi(b+\delta))}{Nab} - \mu_N. \tag{9}$$

For values of μ for which (9) does not hold the disease spread and the coexistence equilibrium stability is reached.

4 Numerical analysis of the model

In this section we will analyze, from a numerical perspective, how the vaccination rate and the fraction of avoided contacts affects the solutions of the system of ordinary differential equations, defined in (1). We also find the transcritical bifurcation value for μ fixing all the other parameter values as in Table 1 and $\psi = 0$. Assuming that $\mu = 0$, no vaccination is available, we investigate the importance of the fraction of avoided contact parameter, ψ. In Figure 2 are reported the solutions of system (1) for 5 different values of ψ in $[0, 1]$ with step 0.2. Notice that if $\psi = 1$, meaning that the virus does not circulate and the infection rate is zero, the DFE become stable, on the other side for $\psi = 0$ no measures to avoid contact are taken and the coexistence equilibrium reach its stability. It is worth noting that increasing the NPIs the maximum value of the peak in the asymptomatic and symptomatic populations not only decrease but is also shifted to the right, so there is a delay which can give an advantage in those situations where the ICU (Intensive Care Units) are overloads. In Figure 3 we have plotted the six numerical solutions of the ODE system (1), fixing all the parameter values as in Table 1, $\psi = 0$ and μ assuming 6 different values in the interval $[0, 0.5]$ with step 0.1. Notice that without a vaccine ($\mu = 0$) both asymptomatic and symptomatic individuals reaches their highest peak, with all the other solution pressed against the abscissa axis, though they are not zero. In fact in Figure 4 we have reported a zoomed version of this two populations for values of μ much closer to 0, that confirm the stability of the coexistence equilibrium (for the first three lowest values) where the disease it is not yet eradicated and for $\mu = 0.06$ the stability of the DFE. In Figure 5 we have plotted one parameter bifurcation diagram with respect to μ (left panel) and ψ (right panel), respectively. For $\mu \simeq 0.059$ (or for $\psi \simeq 0.81$) a transcritical bifurcation arises and for system (1) the coexistence equilibrium interchanges its stability with the disease free equilibrium. In Figure 6 we have represented a two strain parameter plot with respect to both μ and ψ. We can see that without vaccination the system reach the DFE stability only for values of the fraction of avoided contact close to 1, that means strict measures are needed in order to have an infection rate close to 0. Moreover if we assume that the fraction of avoided contacts is 0, which means no measures are taken, the DFE it is stable for a vaccination rate higher than 0.06 ($\leqslant$ 17 days). In Figure 7 we represented the contour plots of the surfaces introduced in Figure 6.

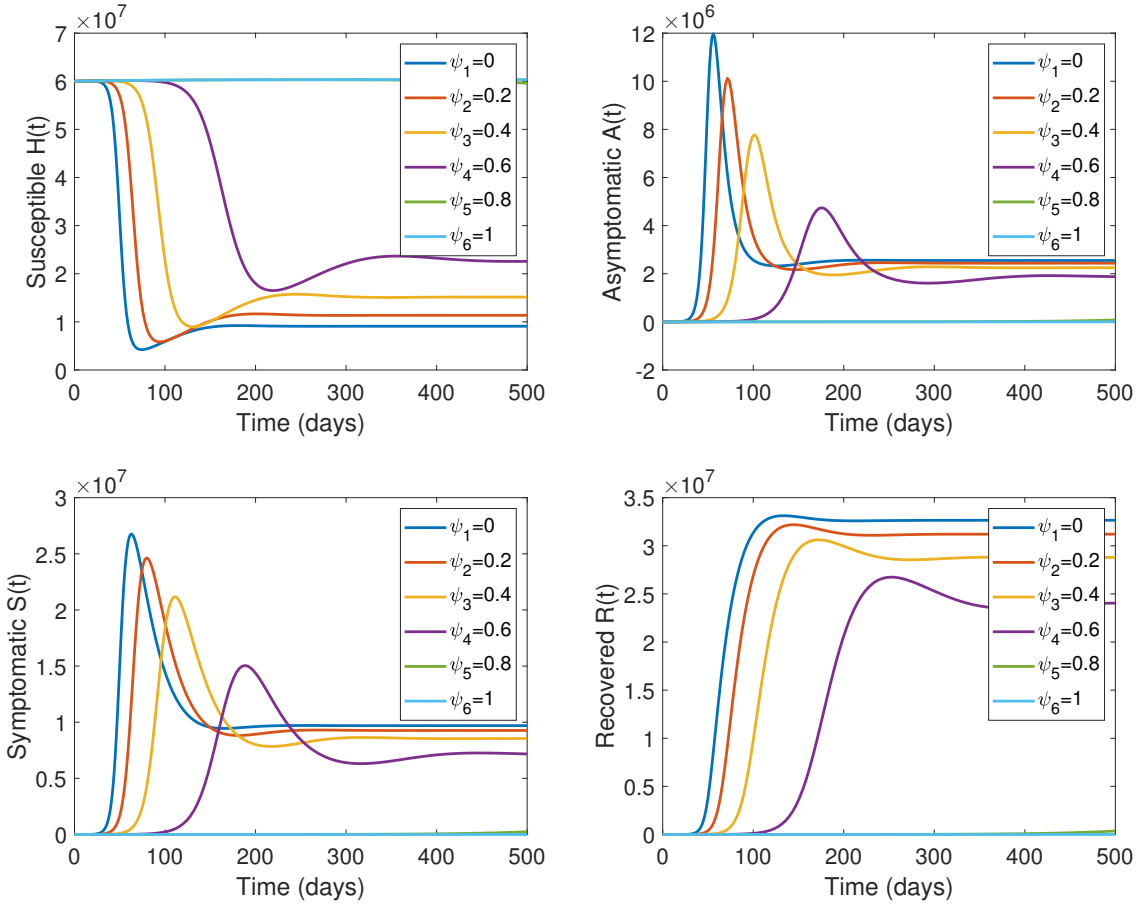

Figure 2. The numerical solutions of system (1) fixing all the parameter values as in Table 1, $\mu = 0$ (no vaccination) and ψ assuming 6 different values in the interval $[0, 1]$ with step 0.2. Top row: Susceptible individuals in time (left panel) and asymptomatic individuals in time (right panel). Bottom row: symptomatic individuals in time (left panel) and recovered/removed individuals in time (right panel).

5 Conclusions

In this paper we have introduced a SASR (Susceptible-Asymptomatic-Symptomatic-Recovered/Removed) model to describe the dynamics of four different classes of individuals where Sars-Cov-2 virus infection is considered. In this model we have also considered the vaccination rate and a parameter in the infection rate that represent the avoided contacts between individuals due to NPIs. We computed the disease free equilibrium and the coexistence equilibrium and analyzed their local stability. Moreover we have computed the basic reproduction number.

From the numerical investigation we can conclude that: (i) increasing the fraction of avoided contacts ψ leads to, not only to delay the peak, but also to lower the maximum value, with a direct consequence on decreasing the pressure on the ICU; (ii) assuming to have an efficient vaccine with a permanent immunity, we found a critical value for the vaccination rate, bellow which the disease free equilibrium is locally asymptotically stable, while if above this threshold we have the confirmation that higher the efficiency of vaccine lower the peak of infected individuals at the coexistence equilibrium. From the two strain parameter analysis we can conclude that both an efficient vaccine and a high fraction of avoided contacts lead to the stability of the disease free equilibrium, but also that higher the efficiency of the vaccine smaller the fraction of avoided contact must be.

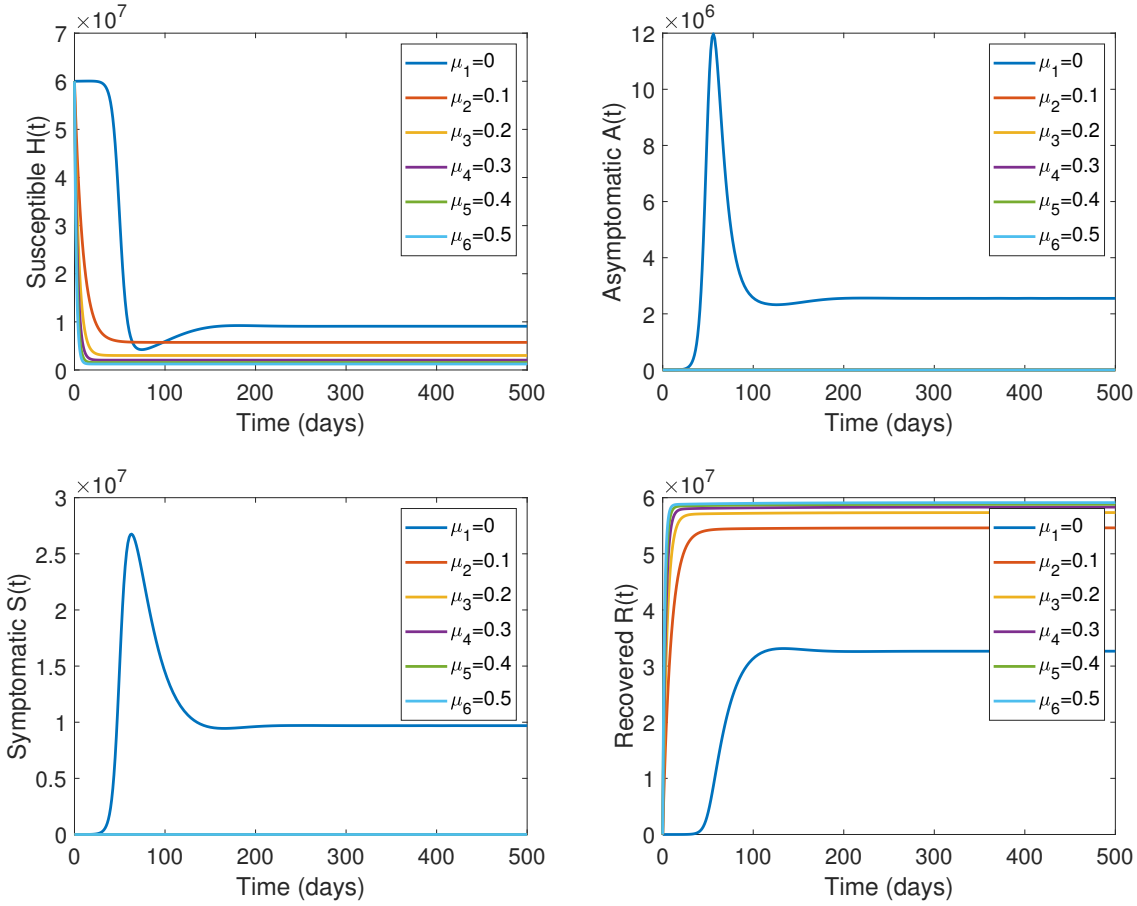

Figure 3. The numerical solutions of system (1) fixing all the parameter values as in Table 1, $\psi = 0$ and μ assuming 6 different values in the interval $[0, 0.5]$ with step 0.1. Top row: Susceptible individuals in time (left panel) and asymptomatic individuals in time (right panel). Bottom row: symptomatic individuals in time (left panel) and recovered/removed individuals in time (right panel).

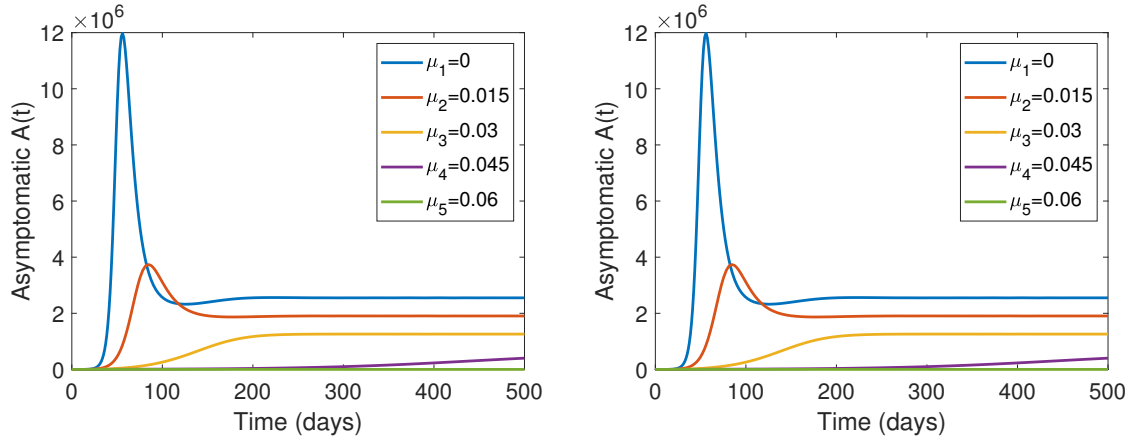

Figure 4. Zoomed version of Figure 3 for asymptomatic (left) and symptomatic (right) populations, respectively, assuming μ varying in $[0, 0.06]$ with step 0.015.

Declarations

Availability of data and material

Not applicable.

Consent for publication

Not applicable.

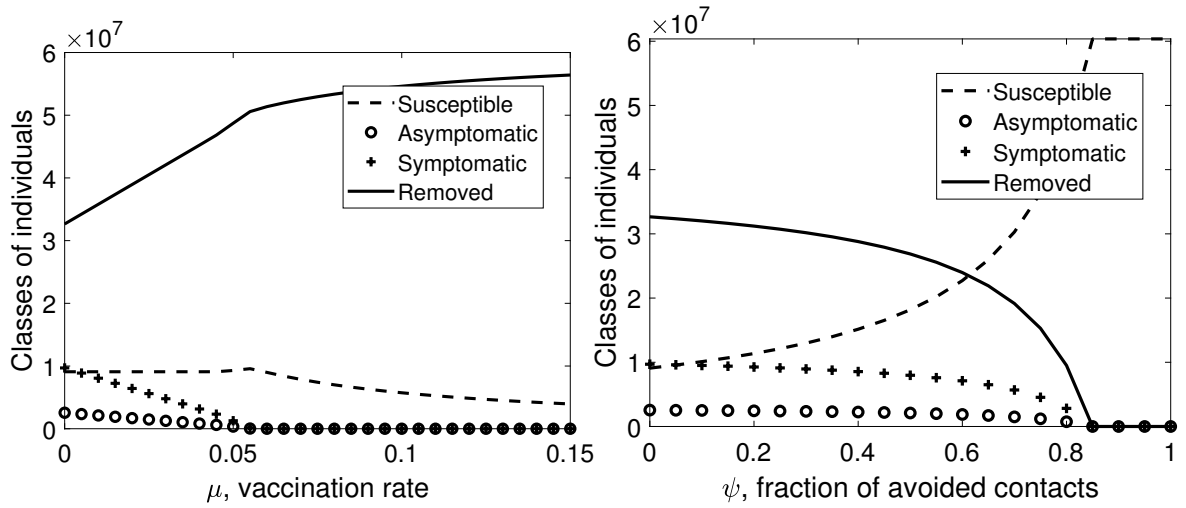

Figure 5. One parameter bifurcation diagram with respect to the vaccination rate μ (left panel) and to fraction of avoided contacts ψ (right panel). All the other parameter values fixed as in Table 1, $\psi = 0$ (left panel) and $\mu = 0$ (right panel). For $\mu \simeq 0.059$ (and $\psi \simeq 0.81$) a transcritical bifurcation arises, (the coexistence equilibrium interchanges its stability with the disease free equilibrium).

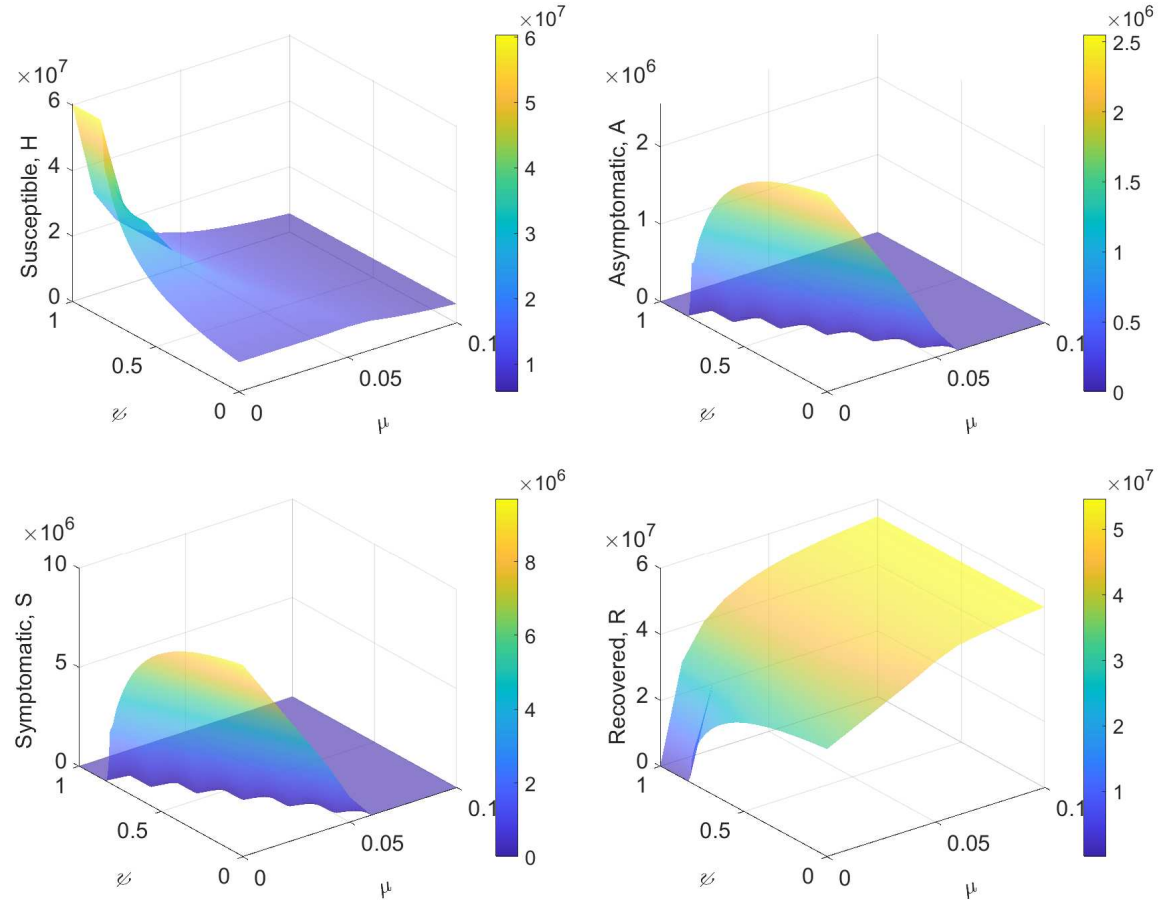

Figure 6. The numerical solutions of system (1) fixing all the parameter values as in Table 1, and varying $\psi \in [0, 1]$ and $\mu \in [0, 0.1]$. Top row: Susceptible individuals (left panel) and Asymptomatic individuals (right panel). Bottom row: Symptomatic individuals (left panel) and Recovered individuals (right panel).

Conflicts of interest

The authors declare that they have no conflict of interests.

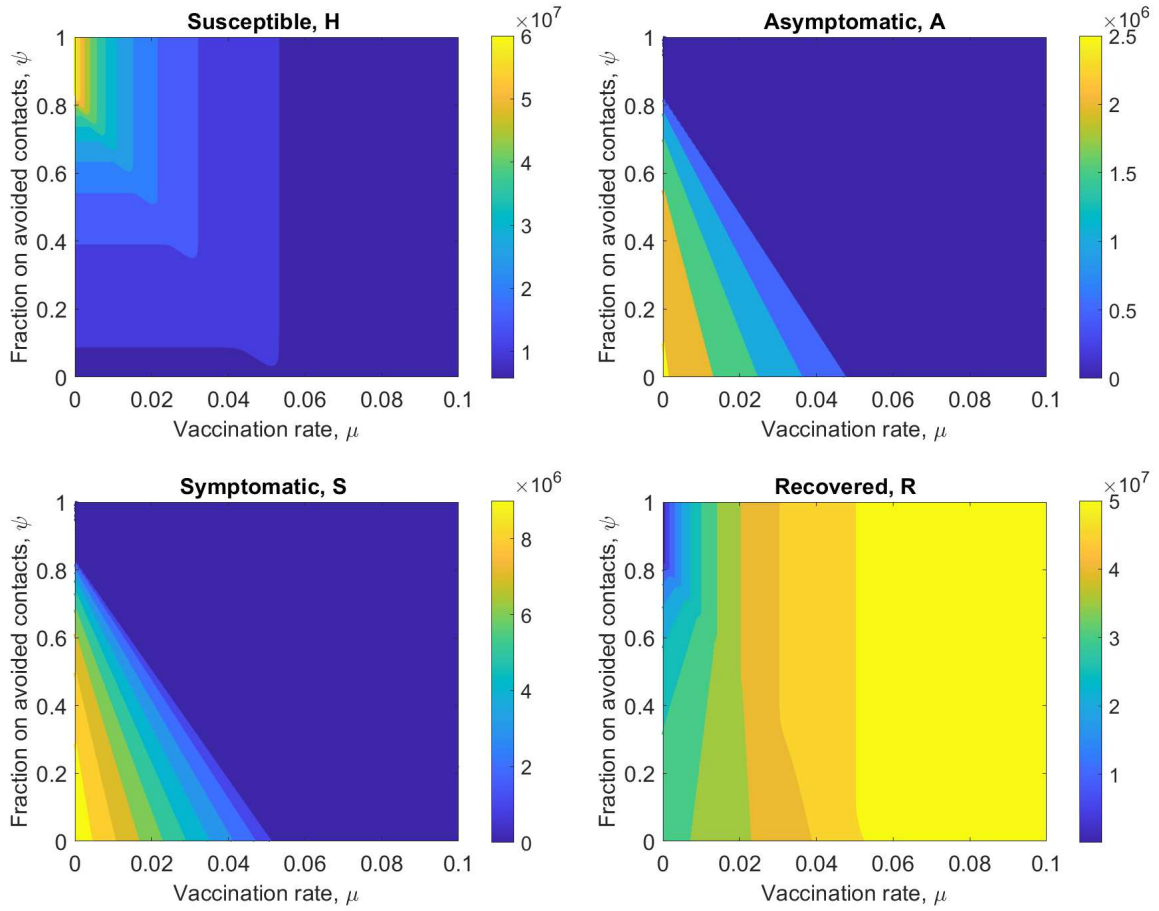

Figure 7. Contour plot of the surfaces represented in Figure 6.

Funding

This work was supported by MIUR through PON-AIM Linea 1 (AIM1852570-1) and by Research Grant "Finanziamento giovanni ricercatori" 2020/2021 GNCS to I.M.B.

Author's contributions

IMB: Conceptualization, Methodology, Investigation, Writing-Original draft preparation. SA, IMB, RM, MAM and KP: Data Curation, Software, Validation, Writing-Reviewing and Editing. All authors discussed the results and contributed to the final manuscript.

Acknowledgements

This research has been accomplished within the UMI Group TAA "Approximation Theory and Application".

References

[1] https://www.who.int/health-topics/coronavirus.
[2] Bernoulli, D., Blower, S. An attempt at a new analysis of the mortality caused by smallpox and of the advantages of inoculation to prevent it. *Reviews in medical virology,* 14(5), 275-288, (2004). [CrossRef]
[3] Rahimi, I., Chen, F. and Gandomi, A.H. A review on COVID-19 forecasting models. *Neural Computing and Applications*, 1-11, (2021). [CrossRef]
[4] Akgül, A., Ahmed, N., Raza, A., et al. New applications related to Covid-19. *Results in Physics,* 20, 103663, (2021). [CrossRef]
[5] Farman, M., Akgül, A., Ahmad, A., Baleanu, D., Saleem, M.U. Dynamical Transmission of Coronavirus Model with Analysis and Simulation. *CMES-Computer Modeling in Engineering and Sciences*, 127(2), 753–769, (2021). [CrossRef]
[6] Amico, E., Bulai, I.M. How political choices shaped Covid connectivity: the Italian case study, Plos One, (2021). [CrossRef].
[7] Zeb, A., Alzahrani, E., Erturk, V.S., Zaman, G. Mathematical model for Coronavirus Disease 2019 (COVID-19) Containing Isolation Class. *BioMed Research International*, (2020). [CrossRef]
[8] Zhang, Z., Zeb, A., Hussain, S., Alzahrani, E. Dynamics of COVID-19 mathematical model with stochastic perturbation. *Advances in Difference Equations*, 2020(1), 1-12, (2020). [CrossRef]

[9] Naik, P.A., Yavuz, M., Qureshi, S., Zu, J. & Townley, S. Modeling and analysis of COVID-19 epidemics with treatment in fractional derivatives using real data from Pakistan. *The European Physical Journal Plus*, 135(10), 1-42, (2020). [CrossRef]

[10] Zhang, Z., Zeb, A., Egbelowo, O.F., Erturk, V.S. Dynamics of a fractional order mathematical model for COVID-19 epidemic. *Advances in Difference Equations*, 2020(1), 1-16, (2020). [CrossRef]

[11] Özköse, F., Yavuz, M. Investigation of interactions between COVID-19 and diabetes with hereditary traits using real data: A case study in Turkey. *Computers in Biology and Medicine*, 105044, (2021). [CrossRef]

[12] Nazir, G., Zeb, A., Shah, K., Saeed, T., Khan, R.A. & Khan, S.I.U. Study of COVID-19 mathematical model of fractional order via modified Euler method. *Alexandria Engineering Journal*, 60(6), 5287-5296, (2021). [CrossRef]

[13] Bushnaq, S., Saeed, T., Torres, D.F.M., Zeb, A. Control of COVID-19 dynamics through a fractional-order model. *Alexandria Engineering Journal*, 60(4), 3587-3592, (2021). [CrossRef]

[14] Yavuz, M., Coşar, F.Ö, Günay, F., Özdemir, F.N. A new mathematical modeling of the COVID-19 pandemic including the vaccination campaign. *Open Journal of Modelling and Simulation*, 9(3), 299-321, (2021). [CrossRef]

[15] Zhang, Z., Zeb, A., Alzahrani, E. & Iqbal, S. Crowding effects on the dynamics of COVID-19 mathematical model. *Advances in Difference Equations*, 2020(1), 1-13, (2020). [CrossRef]

[16] Li, X.P., Al Bayatti, H., Din, A. & Zeb, A. A vigorous study of fractional order COVID-19 model via ABC derivatives. *Results in Physics*, 29, 104737, (2021). [CrossRef]

[17] Guan, J., Wei, Y., Zhao, Y., Chen, F. Modeling the transmission dynamics of COVID-19 epidemic: a systematic review. *Journal of Biomedical Research*, 34(6), 422-430, (2020). [CrossRef]

[18] Atangana, A., Araz, S.İ. Mathematical model of COVID-19 spread in Turkey and South Africa: theory, methods, and applications. *Advances in Difference Equations*, 2020(1), 1-89, (2020). [CrossRef]

[19] Amaro, J.E., Dudouet, J., Orce, J.N. Global analysis of the COVID-19 pandemic using simple epidemiological models. *Applied Mathematical Modelling*, 90, 995-1008, (2021). [CrossRef]

[20] Buonomo, B., Della Marca, R. Effects of information-induced behavioural changes during the COVID-19 lockdowns: the case of Italy. *Royal Society Open Science*, 7(10), 201635, (2020). [CrossRef]

[21] Zhu, H., Li, Y., Jin, X., Huang, J., Liu, X., Qian, Y., Tan, J. Transmission dynamics and control methodology of COVID-19: A modeling study. *Applied Mathematical Modelling*, 89(2), 1983-1998, (2021). [CrossRef]

[22] Pellis, L. et al. & University of Manchester COVID-19 Modelling Group. Challenges in control of Covid-19: short doubling time and long delay to effect of interventions. *Philosophical Transactions of the Royal Society B*, 376(1829), 20200264, (2021). [CrossRef]

[23] Sun, D., Duan, L., Xiong, J. & Wang, D. Modeling and forecasting the spread tendency of the COVID-19 in China. *Advances in Difference Equations*, 2020(1), 1-16, (2020). [CrossRef]

[24] Giordano, G., Blanchini, F., Bruno, R., Colaneri, P., Di Filippo, A., Di Matteo, A. & Colaneri, M. Modelling the COVID-19 epidemic and implementation of population-wide interventions in Italy. *Nature medicine*, 26(6), 855–860, (2020). [CrossRef]

[25] Pedersen, M.G., Meneghini, M. Data-driven estimation of change points reveals correlation between face mask use and accelerated curtailing of the first wave of the COVID-19 epidemic in Italy. *Infectious Diseases*, 53(4), 243-251, (2021). [CrossRef]

[26] Viguerie, A., et al. Simulating the spread of COVID-19 via a spatially-resolved susceptible–exposed–infected–recovered–deceased (SEIRD) model with heterogeneous diffusion. *Applied Mathematics Letters*, 111, 106617, (2021). [CrossRef]

[27] Ferguson, N., et al. Report 9: Impact of non-pharmaceutical interventions (NPIs) to reduce COVID19 mortality and healthcare demand.*Imperial College London*, (2020). [CrossRef]

[28] Chowdhury, R., Heng, K., Shawon, M.S.R., Goh, G., Okonofua, D., Ochoa-Rosales, C., ... & Franco, O.H. Dynamic interventions to control COVID-19 pandemic: a multivariate prediction modelling study comparing 16 worldwide countries. *European journal of epidemiology*, 35(5), 389-399, (2020). [CrossRef]

[29] Jiao, J., Liu, Z., Cai, S. Dynamics of an SEIR model with infectivity in incubation period and homestead-isolation on the susceptible. *Applied Mathematics Letters*, 107, 106442, (2020). [CrossRef]

[30] Bai, Y., Yao, L., Wei, T., Tian, F., Jin, D.Y., Chen, L. & Wang, M. Presumed Asymptomatic Carrier Transmission of COVID-19. *JAMA*, 323(14), 1406-1407, (2020). [CrossRef]

[31] Sakurai, A., Sasaki, T., Kato, S., Hayashi, M., Tsuzuki, S.I., Ishihara, T., et al. Natural History of Asymptomatic SARS-CoV-2 Infection. *N Engl J Med*, 383(9), 885-886, (2020). [CrossRef]

[32] Moore, S., Hill, E.M., Tildesley, M.J., Dyson, L., Keeling, M.J. Vaccination and non-pharmaceutical interventions for COVID-19: a mathematical modelling study. *The Lancet Infectious Diseases*, 21(6), 793-802, (2021). [CrossRef]

[33] Aniţa, S., Banerjee, M., Ghosh, S., Volpert, V. Vaccination in a two-group epidemic model. *Applied Mathematics Letters*, 119, 107197, (2021). [CrossRef]

[34] Estrada, E. COVID-19 and SARS-CoV-2: Modeling the present, looking at the future. *Physics Reports*, 869, 1-51, (2020). [CrossRef]

[35] Bulai, I.M. Modeling Covid-19 Considering Asymptomatic Cases and Avoided Contacts. Chapter in Trends in Biomathematics: Chaos and Control in Epidemics, Ecosystems, and Cells, Springer, (2021). [CrossRef]

[36] https://www.istat.it/storage/rapporto-annuale/2018/Rapportoannuale2018.pdf.

[37] https://raw.githubusercontent.com/pcm-dpc/COVID-19/master/dati-json/dpc-covid19-ita-andamento-nazionale.json

[38] Pedersen, M.G., Meneghini, M. Quantifying undetected COVID-19 cases and effects of containment measures in Italy, (2020).[Preprint].

[39] National Institute of Infectious Diseases Japan. Field Briefing: Diamond Princess COVID-19 Cases, 20 Feb Update. Last accessed March 12, 2020. Available from: https://www. niid.go.jp/niid/en/2019-ncov-e/9417-covid-dp-fe-02.html.

[40] O. Diekmann, J.A.P. Heesterbeek, J.A.J. Metz. On the definition and the computation of the basic reproduction ratio R 0 in models for infectious diseases in heterogeneous populations. *Journal of mathematical biology*, 28, 365-382, (1990). [CrossRef]

[41] P. Van den Driessche, J. Watmough. Reproduction numbers and sub-threshold endemic equilibria for compartmental models of disease transmission. *Math Biosci*, 180(1), 29–48, (2002). [CrossRef]

Mathematical Modelling and Numerical Simulation with Applications (MMNSA) (http://www.mmnsa.org)

Mathematical Modelling and Numerical Simulation with Applications, 2021, 1(2), 67–83

https://www.mmnsa.org
ISSN Online: 2791-8564 / Open Access
https://doi.org/10.53391/mmnsa.2021.01.007

RESEARCH PAPER

Fractional-order mathematical modelling of cancer cells-cancer stem cells-immune system interaction with chemotherapy

Fatma Özköse[1,*,‡], Mehmet Tamer Şenel[1,‡] and Rafla Habbireeh[2,3,‡]

[1]Department of Mathematics, Faculty of Science, Erciyes University, Kayseri 38039, Turkey, [2]Institute of Science, Erciyes University, Kayseri 38039, Turkey, [3]Department of Mathematics, Faculty of Science, Misurata University, Misurata, Libya

*Corresponding Author
‡fpeker@erciyes.edu.tr (Fatma Özköse); senel@erciyes.edu.tr (Mehmet Tamer Şenel); r.habbireeh@sci.misuratau.edu.ly (Rafla Habbireeh)

Abstract

In this paper, we present a mathematical model of stem cells and chemotherapy for cancer treatment, in which the model is represented by fractional order differential equations. Local stability of equilibrium points is discussed. Then, the existence and uniqueness of the solution are studied. In addition, in order to point out the advantages of the fractional order modeling, the memory trace and hereditary traits are taken into consideration. Numerical simulations have been used to investigate how the fractional order derivative and different parameters affect the population dynamics, the graphs have been illustrated according to different values of fractional order α and different parameter values. Moreover, we have examined the effect of chemotherapy on tumor cells and stem cells over time. Furthermore, we concluded that the memory effect occurs as the α decreases from 1 and the chemotherapy drug is quite effective on the populations. We hope that this work will contribute to helping medical scientists take the necessary measures during the screening process and treatment.

Key words: Fractional-order differential equations; cancer stem cells; immune system; numerical solutions; memory effect; existence and uniqueness
AMS 2020 Classification: 92D25; 26A33; 34A08

1 Introduction

Cancer is a general term that includes a wide range of diseases that can affect any part of the body. One of the distinguishing features of cancer is the rapid generation of abnormal cells that grow outside their normal limits and can then invade neighboring parts of the body and spread to other parts of it. Despite the scientific and technological development, cancer is a major cause of death worldwide, and it claimed the lives of 10 million people in 2020. According to the World Health Organization (WHO), between 30% and 50% of cancer cases can be prevented by avoiding risk factors for the disease to prevent it. The burden of cancer can also be reduced by detecting the disease early and providing patients with adequate treatment and care, given that the chances of recovery from many types of cancer increase if they are diagnosed early and treated appropriately. Many researchers have described the interactions between the immune system especially effector cells and tumor cells, where a mathematical modeling was used to clarify the relationship between them as in [1, 2, 3, 30, 31]. Recently, researches were directed to study the effect of stem cell therapy to reduce the growth of tumor cells due to the importance of stem cells in blood formation, as they grow into different types of blood cells such as red and white blood cells and platelets that contribute to stimulating

➤ **Received:** 13.11.2021 ➤ **Revised:** 11.12.2021 ➤ **Accepted:** 13.12.2021 ➤ **Published:** 13.12.2021

the patient's immune system and that were destroyed by Chemotherapy, radiotherapy, or both. A fractional-order model of tumor-immune system interaction has been proposed in [4], and a Chaotic dynamics of a fractional order HIV-1 model involving AIDS-related cancer cells has been given to understand the mechanism that underlies AIDS-related cancers in [8]. As in [13, 14, 15, 16] the effectiveness of using stem cells to boost the patient's immune system has been shown, which may in the future be a treatment for most types of cancer. In this work, we extend the study [17]. Taking into account the interaction of stem cells, tumor cells and chemotherapy for the treatment of cancer, we propose a fractional-order instead of integer-order model to show how effective stem cells are in improving the immune system, which in turn better fights tumor cells [10, 11, 12, 18]. Many real life systems are described better by fractional differential equations, e.g. heat equation, telegraph equation, social systems, medical imaging, pollution control, cancer dynamics, infectious diseases, and a lossy electric transmission line are all involved with fractional order operators [8, 9, 18, 19]. We propose a model motivated by Manar A. Alqudah's work [17], Manar presented a study of ordinary differential equations model that describes the stem cells and chemotherapy for treatment of cancer to show how the stem cells support the effector cells which fighting the tumor cells to improve the immune system of the cancer patient while the chemotherapy kills the infected cells. The mathematical model of treatment of cancer studied in [17] is presented by:

$$\begin{cases} \frac{dS}{dt} = \gamma_1 S - k_s MS, \\ \frac{dT}{dt} = r(1 - bT)T - (p_3 E + k_T M)T, \\ \frac{dE}{dt} = \sigma - \mu E + \frac{p_1 ES}{S+1} - p_2(T + M)E, \\ \frac{dM}{dt} = -\gamma_2 M + V(t). \end{cases} \tag{1}$$

In the previous model $S(t)$ stem cells, $T(t)$ tumor cells, $E(t)$ effector cells, $M(t)$ chemotherapy concentration drug, and the initial conditions are: $S(0) = S_0$, $E(0) = E_0$, $T(0) = T_0$, $0 \leq t \leq \infty$ and $M(0) = 0$ if $V_0 = 0$.

In our paper, the fractional order form of the model (1) is considered with the Caputo sense [20]. In addition, so that the system (1) is dimensionally consistent: the units of measurement from the left- and right-hand sides of the equations agree. It has been achieved by modifying the parameters involved in the right-hand side of the equations, e.g. raising them to power α. The new system as follows:

$$\begin{cases} {}_C D^\alpha S(t) = \gamma_1^\alpha S - k_s^\alpha MS, \\ {}_C D^\alpha T(t) = r^\alpha (1 - b^\alpha T)T - (p_3^\alpha E + k_T^\alpha M)T, \\ {}_C D^\alpha E(t) = \sigma^\alpha - \mu^\alpha E + \frac{p_1^\alpha ES}{S+1} - p_2^\alpha (T + M)E, \\ {}_C D^\alpha M(t) = -\gamma_2^\alpha M + V(t), \end{cases} \tag{2}$$

with the same initial conditions in (1) and α is the order of the model $0 < \alpha \leq 1$.

The parameters description are summarized in Table 1. Some values are taken arbitrarily to easy solving the model numerically and the others are taken from [17] to be compatible with the description of model (2). We assumed that all of the parameters to be non-negative was γ_1 non-positive as stated in [17].

Table 1. Parameter values used for numerical analysis

Parameters	Description	Values	Reference
S_0	Stem cells initial concentration	1	[17]
T_0	Density of free tumors	1	[17]
E_0	Effector cells initial concentration	1	[17]
M_0	Chemotherapy concentration drug	1	[17]
V_0	The time dependent external influx of chemotherapy drug	0.18	[17]
r	Tumor growth rate	0	[17]
γ_1	Decay rate of concentration of stem cells	-0.02825	[17]
γ_2	Decay rate of chemotherapy drug	6.4	[17]
σ	The rate of produced effector cells	0.17	[17]
μ	The natural death rate of the effector cell	0.03	[17]
p_1	Maximum rate of effector cells	0.1245	[17]
p_2	Decay rate of effector cells killed by tumor cells and chemotherapy	1	[17]
p_3	Decay rate of tumor cells killed by effector cells	0.9	[17]
b	Carrying capacity of tumor cells	10^{-9}	[17]
k_s	Fractional stem cells killed by chemotherapy	1	[17]
k_T	Fractional tumor cells killed by chemotherapy	0.9	[17]
$V(t)$	The time dependent external influx of chemotherapy drug	1	[17]

Motivated by the above discussion, the aim of this study is to investigate a fractional-order mathematical model of stem cell- cancer cell- immune system interaction. The reason of using fractional order differential equations is that they are naturally related to systems with memory which exists in cancer cells-immune system interactions. The most essential property of these models is their nonlocal property which does not exist in the integer order differential operators. Mathematical models, using ordinary differential equations with integer order have been proved valuable in understanding the dynamics of diseases. But, they have some limitations when compared with the fractional order derivatives. Integer order derivatives only describe the instantaneous biological events. Fractional order's nonlocal

property says that the next stage of a model depends not only upon its current state but also upon all of its historical states. Therefore, models with fractional order differential equations provide more advantages than integer order mathematical models. In this study, both fractional modeling has been taken into account and estimated data have been used. Meanwhile, dimensional compatibility has been considered in order to better reveal the effect of fractional-order in the proposed fractional-order stem cell-cancer cell-immune system interaction. Additionally, we have aimed to point out the advantages of the fractional order modeling, taking into consideration the memory trace and hereditary traits which are capable of integrating all past activities and taking into account the long-term history of the system. In this context, it can be seen that the memory trace dynamics are highly dependent on time. When the fractional-order α is decreased from the unit, the memory trace nonlinearly increases from 0. Hence, the fractional-order system dynamics are quite different from the integer-order dynamics. It is thought that there is no such study in the literature that deals with the stem cell-cancer relationship, and making the fractional order model dimensionally consistent, and taking into account the memory effect/hereditary characteristics.

The remaining part of this paper is prepared as follows. In Sec. (2), some definitions of a fractional order derivative (FOD) and some important theorems for FODs are given. In Sec. (3), the existence and uniqueness conditions of the solutions are given. In Sec. (4), stability theorems for the equilibrium points are examined. In Sec. (5), the numerical simulation and data analysis have been given. In Sec. (6), the effects of the memory trace on the behaviour of the system (2) are examined. In Sec. (7), to investigate the effects of different parameter values and different values of α on the dynamic behavior of the proposed model, the numerical solutions have been carried out. Finally, the Results and Discussion are given in Sec. (8).

2 Preliminaries

The fractional-order derivation and the fractional-order integration have many definitions such that the Riemann-Liouville definition, Caputo definition, Hadamard fractional integral, Atangana-Baleanu fractional integral, Riesz derivative, and Generalized Functions approaches [5, 7, 20, 26]. The most commonly used of these are Riemann-Liouville and Caputo definitions. Caputo reformulated the definition of the Riemann–Liouville fractional derivative by switching the order of the ordinary derivative with the fractional integral operator. By doing so, the Laplace transform of this new derivative depends on integer order initial conditions, differently from the initial conditions when we use the Riemann–Liouville fractional derivative, which involves fractional order conditions, give a well understanding of the properties of many physical phenomena which makes it applicable to the problems of our real world.

Definition 1 *[20, 26] The fractional integral of order $\alpha > 0$, of the function $f(t)$, $t > 0$ is given by*

$$I^{\alpha} f(t) = \int_0^t \frac{(t-s)^{\alpha-1}}{\Gamma(\alpha)} f(s) ds.$$

and the fractional derivative of order $\alpha \in (n-1, n)$ of $f(t)$, $t > 0$ is given by

$$D^{\alpha} f(t) = I^{n-\alpha} D^n f(t) \quad (D = \frac{d}{dt}).$$

Definition 2 *[20] Let $f : R_+ \to R$ continuous function. The Caputo fractional-order derivative is given by*

$${}_C D^{\alpha}_{t_0,t} f(t) = \frac{1}{\Gamma(m-\alpha)} \int_0^t (t-\tau)^{m-\alpha-1} f^{(m)}(\tau) d\tau.$$

where $m-1 < \alpha < m \in Z^+$. For the special case of $0 < \alpha < 1$, we have

$${}_C D^{\alpha}_{0,t} f(t) = \frac{1}{\Gamma(1-\alpha)} \int_0^t (t-\tau)^{-\alpha} f'(\tau) d\tau.$$

For convenience, we use the notation ${}_C D^{\alpha} f(t)$ instead of ${}_C D^{\alpha}_{0,t} f(t)$ to denote the Caputo fractional-order derivative operator.

Theorem 1 *[27, 28] If X^* is the equilibrium point of system (2), then system (2) is*

(1) Asymptotically stable $\iff$ all the eigenvalues $\lambda_i, i = 1, 2, \ldots, n$ of the Jacobian matrix $J(X^*)$ satisfy that $|arg(\lambda_i)| > \frac{\alpha\pi}{2}$.
(2) Stable $\iff$ it is asymptotically stable or the eigenvalues $\lambda_i, i = 1, 2, \ldots, n$ of $J(X^*)$ that satisfy $|arg(\lambda_i)| = \frac{\alpha\pi}{2}$ have the same geometric and geometric multiplicity for λ_i is 1.
(3) Unstable $\iff$ eigenvalues λ_i for some $i = 1, 2, \ldots, n$ of $J(X^*)$ satisfy $|arg(\lambda_i)| < \frac{\alpha\pi}{2}$.

3 Existence and uniqueness

Consider system (2) with the initial conditions $S(0) = S_0$, $E(0) = E_0$, $T(0) = T_0$, $M(0) = 0$ if $V_0 = 0$. System (2) can be written in the following form:

$$\begin{cases} {}_C D^{\alpha} X(t) = B_1 X(t) + S(t) B_2 X(t) + T(t) B_3 X(t) + E(t) B_4 X(t) + M(t) B_5 X(t) + \vartheta, \\ X(t_0) = X_0, \end{cases} \tag{3}$$

where

$$X(t) = \begin{pmatrix} S(t) \\ T(t) \\ E(t) \\ M(t) \end{pmatrix}, \quad X(0) = \begin{pmatrix} S(0) \\ T(0) \\ E(0) \\ M(0) \end{pmatrix}, \quad B_1 = \begin{pmatrix} \gamma_1^{\alpha} & 0 & 0 & 0 \\ 0 & r^{\alpha} & 0 & 0 \\ 0 & 0 & -\mu^{\alpha} & 0 \\ 0 & 0 & 0 & -\gamma_2^{\alpha} \end{pmatrix},$$

$$B_2 = \begin{pmatrix} 0 & 0 & 0 & -k_S^{\alpha} \\ 0 & 0 & 0 & 0 \\ 0 & 0 & 0 & 0 \\ 0 & 0 & 0 & 0 \end{pmatrix}, \quad B_3 = \begin{pmatrix} 0 & 0 & 0 & 0 \\ 0 & -b^{\alpha} & 0 & 0 \\ 0 & 0 & -p_2^{\alpha} & 0 \\ 0 & 0 & 0 & 0 \end{pmatrix}, \quad B_4 = \begin{pmatrix} 0 & 0 & 0 & 0 \\ 0 & -p_3^{\alpha} & 0 & 0 \\ \frac{p_1^{\alpha}}{S+1} & 0 & 0 & 0 \\ 0 & 0 & 0 & 0 \end{pmatrix},$$

$$B_5 = \begin{pmatrix} 0 & 0 & 0 & 0 \\ 0 & -k_T^{\alpha} & 0 & 0 \\ 0 & 0 & -p_2^{\alpha} & 0 \\ 0 & 0 & 0 & 0 \end{pmatrix}, \quad \vartheta = \begin{pmatrix} 0 \\ 0 \\ \sigma^{\alpha} \\ V(t) \end{pmatrix}.$$

In view of [4, 25, 26] desired definitions for the existence and uniqueness are defined as follows:

Definition 3 *Let $C^*[0,\tau]$ be the class of continuous column vector $X(t)$ whose components $S, T, E, M \in C^*[0,\tau]$ are the class of continuous functions on the interval $[0,\tau]$. The norm of $X \in C^*[0,\tau]$ is given by*

$$\|X\| = \sup_t \mid e^{-Nt}S(t) \mid + \sup_t \mid e^{-Nt}T(t) \mid + \sup_t \mid e^{-Nt}E(t) \mid + \sup_t \mid e^{-Nt}M(t) \mid,$$

where N is a natural number and when $t > \delta \geq m$, we write $C_{\delta}^*[0,\tau]$ and $C_{\delta}[0,\tau]$.

Definition 4 *$X \in C^*[0,\tau]$ is a solution of IVP (3) if*

(1) $(t, X(t)) \in \mathcal{D}, t \in [0,\tau]$ where $\mathcal{D} = [0,\tau] \times \mathcal{K}$, $\mathcal{K} = \{(S,T,E,M) \in \mathcal{R}_+^4 : |S| \leq p, \ |T| \leq r, \ |E| \leq w, \ |M| \leq q\}$; $p, r, w, q \in R_+$ are constants.
(2) $X(t)$ satisfies (3).

Theorem 2 *The solution X of IVP (3) is unique and $X \in C^*[0,\tau]$.*

Proof From the properties of fractional calculus, Eq. (3) can be written as

$$I^{1-\alpha}\frac{d}{dt}X(t) = B_1X(t) + S(t)B_2X(t) + T(t)B_3X(t) + E(t)B_4X(t) + M(t)B_5X(t) + \vartheta.$$

Operating by I^{α}, we obtain

$$X(t) = X(0) + I^{\alpha}(B_1X(t) + S(t)B_2X(t) + T(t)B_3X(t) + E(t)B_4X(t) + M(t)B_5X(t) + \vartheta). \tag{4}$$

Now let $F : C^*[0,\tau] \to C^*[0,\tau]$ defined by

$$FX(t) = X(0) + I^{\alpha}(B_1X(t) + S(t)B_2X(t) + T(t)B_3X(t) + E(t)B_4X(t) + M(t)B_5X(t) + \vartheta). \tag{5}$$

Then

$$\begin{aligned} e^{-Nt}(FX - FY) &= e^{-Nt}I^{\alpha}(B_1(X(t) - Y(t)) + S(t)B_2(X(t) - Y(t)) + T(t)B_3(X(t) - Y(t)) + E(t)B_4(X(t) - Y(t)) + M(t)B_5(X(t) - Y(t))) \\ &\leq \mid \frac{1}{\Gamma(\alpha)}\int_0^t (t-s)^{\alpha-1}e^{-N(t-s)}(X(s) - Y(s))\, e^{-Ns}ds \mid (B_1 + pB_2 + rB_3 + wB_4 + qB_5) \\ &\leq \frac{(B_1 + pB_2 + rB_3 + wB_4 + qB_5)\mid\gamma(\alpha,u)\mid}{N^{\alpha}}\|X - Y\|, \end{aligned}$$

where $\gamma(\alpha,u)$ is the lower incomplete gamma function and $u = t - s$. If we choose N such that $N^{\alpha} \geq |\gamma(\alpha,u)|\, B_1 + pB_2 + rB_3 + wB_4 + qB_5$, then we obtain $\|FX - FY\| \leq \|X - Y\|$. Operator F in (5) has a fixed point. Thus, (4) has a unique solution $X \in C^*[0,\tau]$. From (4) we have

$$\begin{aligned} X(t) &= X(0) + \frac{t^{\alpha}}{\Gamma(\alpha+1)}\left(B_1X(0) + S(0)B_2X(0) + T(0)B_3X(0) + E(0)B_4X(0) + M(0)B_5X(0) + \vartheta\right) + I^{\alpha+1}(B_1X'(t) + S'(t)B_2X(t) \\ &\quad + S(t)B_2X'(t) + T'(t)B_3X(t) + T(t)B_3X'(t) + E'(t)B_4X(t) + E(t)B_4X'(t) + M'(t)B_5X(t) + M(t)B_5X'(t). \\ e^{-Nt}X' &= e^{-Nt}\Big[\frac{t^{\alpha-1}}{\Gamma(\alpha)}(B_1X(0) + S(0)B_2X(0) + T(0)B_3X(0) + E(0)B_4X(0) + M(0)B_5X(0) + \vartheta) + I^{\alpha}(B_1X'(t) + S'(t)B_2X(t) \\ &\quad + S(t)B_2X'(t) + T'(t)B_3X(t) + T(t)B_3X'(t) + E'(t)B_4X(t) + E(t)B_4X'(t) + M'(t)B_5X(t) + M(t)B_5X'(t)\Big]. \end{aligned}$$

from which we can deduce that $X' \in C^*_\sigma[0,\tau]$. From (4) we get

$$\frac{dX}{dt} = \frac{d}{dt}I^\alpha(B_1X(t) + S(t)B_2X(t) + T(t)B_3X(t) + E(t)B_4X(t) + M(t)B_5X(t) + \vartheta).$$

Operating by $I^{1-\alpha}$ we get

$$I^{1-\alpha}\frac{dX}{dt} = I^{1-\alpha}\frac{d}{dt}I^\alpha(B_1X(t) + S(t)B_2X(t) + T(t)B_3X(t) + E(t)B_4X(t) + M(t)B_5X(t) + V(t)C + \vartheta).$$
$${}_CD^\alpha X(t) = B_1X(t) + S(t)B_2X(t) + T(t)B_3X(t) + E(t)B_4X(t) + M(t)B_5X(t) + \vartheta),$$

and

$$X(0) = X_0 + I^\alpha(B_1X(t) + S(t)B_2X(t) + T(t)B_3X(t) + E(t)B_4X(t) + M(t)B_5X(t) + \vartheta).$$

Therefore, Eq. (4) is equivalent to IVP (3). ■

4 Equilibrium points and stability analysis

To calculate the equilibrium points of system (2) let [29]

$$\begin{cases} {}_CD^\alpha S(t) = 0, \\ {}_CD^\alpha T(t) = 0, \\ {}_CD^\alpha E(t) = 0, \\ {}_CD^\alpha M(t) = 0. \end{cases}$$

Thus,

$$\begin{cases} \gamma_1^\alpha S - k_S^\alpha MS = 0, \\ r^\alpha(1 - b^\alpha T)T - (p_3^\alpha E + k_T^\alpha M)T = 0, \\ \sigma^\alpha - \mu^\alpha E + \dfrac{p_1^\alpha ES}{S+1} - p_2^\alpha(T+M)E = 0, \\ -\gamma_2^\alpha M + V(t) = 0. \end{cases}$$

Then the equilibrium points are:

$$Eq_1 = (S_1, T_1, E_1, M_1) = (0, 0, \frac{\sigma^\alpha\gamma_2^\alpha}{p_2^\alpha V + \gamma_2^\alpha\mu^\alpha}, \frac{V}{\gamma_2^\alpha}),$$

$$Eq_2 = (S_2, T_2, E_2, M_2) = (0, \frac{p_2^\alpha V(r^\alpha b^\alpha - k_T^\alpha) + r^\alpha\gamma_2^\alpha(p_2^\alpha - b^\alpha\mu^\alpha) - \sqrt{-4\sigma^\alpha b^\alpha p_2^\alpha p_3^\alpha r^\alpha\gamma_2^{2\alpha} + a^2}}{2p_2^\alpha\gamma_2^\alpha r^\alpha b^\alpha},$$
$$\frac{p_2^\alpha V(r^\alpha b^\alpha - k_T^\alpha) + r^\alpha\gamma_2^\alpha(p_2^\alpha + b^\alpha\mu^\alpha) + \sqrt{-4\sigma^\alpha b^\alpha p_2^\alpha p_3^\alpha r^\alpha\gamma_2^{2\alpha} + a^2}}{2p_2^\alpha p_3^\alpha\gamma_2^\alpha}, \frac{V}{\gamma_2^\alpha}),$$

$$Eq_3 = (S_3, T_3, E_3, M_3) = (0, \frac{p_2^\alpha V(r^\alpha b^\alpha - k_T^\alpha) + r^\alpha\gamma_2^\alpha(p_2^\alpha - b^\alpha\mu^\alpha) + \sqrt{-4\sigma^\alpha b^\alpha p_2^\alpha p_3^\alpha r^\alpha\gamma_2^{2\alpha} + a^2}}{2p_2^\alpha\gamma_2^\alpha r^\alpha b^\alpha},$$
$$\frac{p_2^\alpha V(r^\alpha b^\alpha - k_T^\alpha) + r^\alpha\gamma_2^\alpha(p_2^\alpha + b^\alpha\mu^\alpha) - \sqrt{-4\sigma^\alpha b^\alpha p_2^\alpha p_3^\alpha r^\alpha\gamma_2^{2\alpha} + a^2}}{2p_2^\alpha p_3^\alpha\gamma_2^\alpha}, \frac{V}{\gamma_2^\alpha}),$$

where $a = ((k_T^\alpha - r^\alpha b^\alpha)p_2^\alpha V - \gamma_2^\alpha r^\alpha(p_2^\alpha + b^\alpha\mu^\alpha)$, and equilibrium points must verify $Eq_1, Eq_2, Eq_3 > 0$. Hence, $p_2^\alpha, p_3^\alpha, \mu^\alpha, \gamma_2^\alpha, \sigma^\alpha, r^\alpha, b^\alpha, V, k_T^\alpha \in D_1$, where $\mathcal{D}_1 = \{(p_2^\alpha, p_3^\alpha, \mu^\alpha, \gamma_2^\alpha, \sigma^\alpha, r^\alpha, b^\alpha, V, k_T^\alpha) \in \mathcal{R}_+^9 : Vk_T^\alpha - r^\alpha(b^\alpha + \gamma_2^\alpha) + \sigma^\alpha\gamma_2^\alpha > 0\} \cap \{(p_2^\alpha, p_3^\alpha, \mu^\alpha, \gamma_2^\alpha, \sigma^\alpha, r^\alpha, b^\alpha, V, k_T^\alpha) \in \mathcal{R}_+^9 : (Vp_2^\alpha(k_T^\alpha - r^\alpha b^\alpha) - r^\alpha\gamma_2^\alpha(p_2^\alpha + b^\alpha\mu^\alpha))^2 \geq 4\sigma^\alpha b^\alpha p_2^\alpha p_3^\alpha\gamma_2^{2\alpha}\}$.

Theorem 3 *Let $Eq_1 \in D_1$ be the equilibrium point of system (2) and the following conditions are valid:*
$\gamma_1^\alpha\gamma_2^\alpha < k_S^\alpha V$, $(p_2^\alpha V + \gamma_2^\alpha\mu^\alpha)(\gamma_2^\alpha r^\alpha + k_T^\alpha V) < p_3^\alpha\sigma^\alpha\gamma_2^{2\alpha}$ *and* $p_2^\alpha V + \gamma_2^\alpha\mu^\alpha > 0$.
Then Eq_1 is locally asymptotically stable.

Proof The Jacobian matrix of the model (2) at Eq_1 is

$$J(Eq_1) = \begin{pmatrix} \gamma_1^\alpha - k_S^\alpha\frac{V}{\gamma_2^\alpha} & 0 & 0 & 0 \\ 0 & r^\alpha - p_3^\alpha\frac{\sigma^\alpha\gamma_2^\alpha}{p_2^\alpha V + \gamma_2^\alpha\mu^\alpha} + k_T^\alpha\frac{V}{\gamma_2^\alpha} & 0 & 0 \\ p_1^\alpha\frac{\sigma^\alpha\gamma_2^\alpha}{p_2^\alpha V + \gamma_2^\alpha\mu^\alpha} & -p_2^\alpha\frac{\sigma^\alpha\gamma_2^\alpha}{p_2^\alpha V + \gamma_2^\alpha\mu^\alpha} & -\mu^\alpha - p_2^\alpha\frac{V}{\gamma_2^\alpha} & -p_2^\alpha\frac{\sigma^\alpha\gamma_2^\alpha}{p_2^\alpha V + \gamma_2^\alpha\mu^\alpha} \\ 0 & 0 & 0 & -\gamma_2^\alpha \end{pmatrix}.$$

The characteristic equation is $|J(Eq_1) - \lambda I| = 0$. Hence, $(\gamma_1^\alpha - k_S^\alpha\frac{V}{\gamma_2^\alpha} - \lambda)(r^\alpha - p_3^\alpha\frac{\sigma^\alpha\gamma_2^\alpha}{p_2^\alpha V + \gamma_2^\alpha\mu^\alpha} + k_T^\alpha\frac{V}{\gamma_2^\alpha} - \lambda)(-\gamma_2^\alpha - \lambda)(-\mu^\alpha - p_2^\alpha\frac{V}{\gamma_2^\alpha} - \lambda) = 0$.

Eigenvalues of $J(Eq_1)$ are $\lambda_1 = \gamma_1^\alpha - k_s^\alpha \frac{V}{\gamma_2^\alpha}$, $\lambda_2 = r^\alpha - p_3^\alpha \frac{\sigma^\alpha \gamma_2^\alpha}{p_2^\alpha V + \gamma_2^\alpha \mu^\alpha} - k_T^\alpha \frac{V}{\gamma_2^\alpha}$, $\lambda_3 = -\mu^\alpha - p_2^\alpha \frac{V}{\gamma_2^\alpha}$, $\lambda_4 = -\gamma_2^\alpha$. From the conditions we have $\lambda_i < 0$ *for* $i = 1, 2, 3, 4$. Therefore, $|arg(\lambda_i)| > \frac{\alpha\pi}{2}$. By Theorem (1), Eq_1 is locally asymptotically stable. ■

Theorem 4 *Let* $Eq_2 \in D_1$ *be the equilibrium point of system (2) and* $(p_2^\alpha, p_3^\alpha, \mu^\alpha, \gamma_2^\alpha, \sigma^\alpha, r^\alpha, b^\alpha, V, k_T^\alpha) \in D_1 \cap (Q^* \cup P^*)$, *where*
$Q^* = \{(p_2^\alpha, p_3^\alpha, \mu^\alpha, \gamma_2^\alpha, \sigma^\alpha, r^\alpha, b^\alpha, V, k_T^\alpha) \in R_+^9 : d^2, d_1 \geq 0, \gamma_1^\alpha \gamma_2^\alpha < k_s^\alpha V$ *and* $((2b^\alpha + p_2^\alpha)(d + k_T^\alpha p_2^\alpha V) r^\alpha \gamma_2^\alpha - b^\alpha r^{3\alpha} \gamma_2^\alpha (b^\alpha p_2^\alpha V - p_2^\alpha \gamma_2^\alpha + b^\alpha \gamma_2^\alpha \mu^\alpha) + r^{2\alpha} \gamma_2 (-p_2^{2\alpha} \gamma_2^\alpha + 2b^{2\alpha}(p_2^\alpha V + \gamma_2^\alpha \mu^\alpha) - b^\alpha (d + p_2^\alpha ((k_T^\alpha + p_2^\alpha)V + \gamma_2^\alpha (2 + \mu^\alpha)))) - d_1) < 0\}$. $P^* = \{(p_2^\alpha, p_3^\alpha, \mu^\alpha, \gamma_2^\alpha, \sigma^\alpha, r^\alpha, b^\alpha, V, k_T^\alpha) \in R_+^9 : d^2$ *or* $d_1 < 0, \gamma_1^\alpha \gamma_2^\alpha < k_s^\alpha V$ *and*
$Re(((2b^\alpha + p_2^\alpha)(d + k_T^\alpha p_2^\alpha V) r^\alpha \gamma_2^\alpha - b^\alpha r^{3\alpha} \gamma_2^\alpha (b^\alpha p_2^\alpha V - p_2^\alpha \gamma_2^\alpha + b^\alpha \gamma_2^\alpha \mu^\alpha) + r^{2\alpha} \gamma_2 (-p_2^{2\alpha} \gamma_2^\alpha + 2b^{2\alpha}(p_2^\alpha V + \gamma_2^\alpha \mu^\alpha) - b^\alpha (d + p_2^\alpha ((k_T^\alpha + p_2^\alpha)V + \gamma_2^\alpha (2 + \mu^\alpha)))) - d_1)) < 0\}$,
where $d = \sqrt{-4\sigma^\alpha b^\alpha p_2^\alpha p_3^\alpha r^\alpha \gamma_2^{2\alpha} + (k_T^\alpha p_2^\alpha V - b^\alpha p_2^\alpha r^\alpha V - p_2^\alpha r^\alpha \gamma_2^\alpha - b^\alpha r^\alpha \gamma_2^\alpha \mu^\alpha)^2}$ *and* $d_1 = (r^{2\alpha} \gamma_2^{2\alpha}((-p_2^\alpha (d + k_T^\alpha p_2^\alpha V - p_2^\alpha r^\alpha \gamma_2^\alpha) + b^{2\alpha}(-2 + r^\alpha) r^\alpha (p_2^\alpha V + \gamma_2^\alpha \mu^\alpha) + b^\alpha (d(-2 + r^\alpha) - 2k_T^\alpha p_2^\alpha V + p_2^\alpha r^\alpha ((k_T^\alpha + p_2^\alpha)V + \gamma_2^\alpha (2 - r^\alpha + \mu^\alpha))))^2 - 8b^\alpha p_2^\alpha (-k_T^{2\alpha} p_2^{2\alpha}(-2 + r^\alpha) V^2 - 2k_T^\alpha p_2^\alpha r^\alpha V(-p_2^\alpha (-2 + r^\alpha)\gamma_2^\alpha + b^\alpha (p_2^\alpha V + \gamma_2^\alpha \mu^\alpha)) + r^\alpha (-p_2^{2\alpha}(-2 + r^\alpha) r^\alpha \gamma_2^{2\alpha} + b^{2\alpha} r^{2\alpha}(p_2^\alpha V + \gamma_2^\alpha \mu^\alpha)^2 + 2b^\alpha p_2^\alpha \gamma_2^\alpha (p_2^\alpha r^\alpha V - 2\sigma^\alpha p_3^\alpha \gamma_2^\alpha + r^\alpha \gamma_2^\alpha \mu^\alpha)) + d(-k_T^\alpha p_2^\alpha (-2 + r^\alpha) V + r^\alpha (p_2^\alpha (-2 + r^\alpha)\gamma_2^\alpha + b^\alpha r^\alpha (p_2^\alpha V + \gamma_2^\alpha \mu^\alpha))))))$.
Then Eq_2 *is locally asymptotically stable.*

Proof The Jacobian matrix of the model (2) at Eq_2 is

$$J(Eq_2) = \begin{pmatrix} \gamma_1^\alpha - k_s^\alpha \frac{V}{\gamma_2^\alpha} & 0 & 0 & 0 \\ 0 & j_{22} & j_{23} & j_{24} \\ j_{31} & j_{32} & j_{33} & j_{34} \\ 0 & 0 & 0 & -\gamma_2^\alpha \end{pmatrix},$$

where

$$j_{22} = r^\alpha - \left(\frac{p_2^\alpha V(r^\alpha b^\alpha - k_T^\alpha) + r^\alpha \gamma_2^\alpha (p_2^\alpha - b^\alpha \mu^\alpha) - \sqrt{-4\sigma^\alpha b^\alpha p_2^\alpha p_3^\alpha r^\alpha \gamma_2^{2\alpha} + a^2}}{p_2^\alpha \gamma_2^\alpha r^\alpha} \right)$$
$$- \left(\frac{p_2^\alpha V(r^\alpha b^\alpha - k_T^\alpha) + r^\alpha \gamma_2^\alpha (p_2^\alpha + b^\alpha \mu^\alpha) + \sqrt{-4\sigma^\alpha b^\alpha p_2^\alpha p_3^\alpha r^\alpha \gamma_2^{2\alpha} + a^2}}{2p_2^\alpha \gamma_2^\alpha} - k_T^\alpha \frac{V}{\gamma_2^\alpha} \right).$$

$$j_{23} = -p_3^\alpha \frac{p_2^\alpha V(r^\alpha b^\alpha - k_T^\alpha) + r^\alpha \gamma_2^\alpha (p_2^\alpha - b^\alpha \mu^\alpha) - \sqrt{-4\sigma^\alpha b^\alpha p_2^\alpha p_3^\alpha r^\alpha \gamma_2^{2\alpha} + a^2}}{2p_2^\alpha \gamma_2^\alpha r^\alpha b^\alpha}$$
$$j_{24} = -k_T^\alpha \frac{p_2^\alpha V^\alpha (r^\alpha b^\alpha - k_T^\alpha) + r^\alpha \gamma_2^\alpha (p_2^\alpha - b^\alpha \mu^\alpha) - \sqrt{-4\sigma^\alpha b^\alpha p_2^\alpha p_3^\alpha r^\alpha \gamma_2^{2\alpha} + a^2}}{2p_2^\alpha \gamma_2^\alpha r^\alpha b^\alpha}.$$

$$j_{31} = p_1^\alpha \frac{p_2^\alpha V(r^\alpha b^\alpha - k_T^\alpha) + r^\alpha \gamma_2^\alpha (p_2^\alpha + b^\alpha \mu^\alpha) + \sqrt{-4\sigma^\alpha b^\alpha p_2^\alpha p_3^\alpha r^\alpha \gamma_2^{2\alpha} + a^2}}{2p_2^\alpha p_3^\alpha \gamma_2^\alpha}.$$

$$j_{32} = j_{34} = -\frac{p_2^\alpha V(r^\alpha b^\alpha - k_T^\alpha) + r^\alpha \gamma_2^\alpha (p_2^\alpha + b^\alpha \mu^\alpha) + \sqrt{-4\sigma^\alpha b^\alpha p_2^\alpha p_3^\alpha r^\alpha \gamma_2^{2\alpha} + a^2}}{2p_3^\alpha \gamma_2^\alpha}.$$

$$j_{33} = -\mu^\alpha - p_2 \left(\frac{p_2^\alpha V(r^\alpha b^\alpha - k_T^\alpha) + r^\alpha \gamma_2^\alpha (p_2^\alpha - b^\alpha \mu^\alpha) - \sqrt{-4\sigma^\alpha b^\alpha p_2^\alpha p_3^\alpha r^\alpha \gamma_2^{2\alpha} + a^2}}{2p_2^\alpha \gamma_2^\alpha r^\alpha b^\alpha} + \frac{V}{\gamma_2^\alpha} \right). \quad (6)$$

The characteristic equation is $|J(Eq_2) - \lambda I| = 0$. Hence,

$$(\gamma_1^\alpha - k_s^\alpha \frac{V}{\gamma_2^\alpha} - \lambda)(-\gamma_2^\alpha - \lambda) \left(\left(r^\alpha - \frac{p_2^\alpha V(r^\alpha b^\alpha - k_T^\alpha) + r^\alpha \gamma_2^\alpha (p_2^\alpha - b^\alpha \mu^\alpha) - \sqrt{-4\sigma^\alpha b^\alpha p_2^\alpha p_3^\alpha r^\alpha \gamma_2^{2\alpha} + a^2}}{p_2^\alpha \gamma_2^\alpha r^\alpha} \right.\right.$$
$$\left. - \left(\frac{p_2^\alpha V(r^\alpha b^\alpha - k_T^\alpha) + r^\alpha \gamma_2^\alpha (p_2^\alpha + b^\alpha \mu^\alpha) + \sqrt{-4\sigma^\alpha b^\alpha p_2^\alpha p_3^\alpha r^\alpha \gamma_2^{2\alpha} + a^2}}{2p_2^\alpha \gamma_2^\alpha} \right) - k_T^\alpha \frac{V}{\gamma_2^\alpha} - \lambda \right)$$
$$\left(\left(-\mu^\alpha - p_2^\alpha \left(\frac{p_2^\alpha V(r^\alpha b^\alpha - k_T^\alpha) + r^\alpha \gamma_2^\alpha (p_2^\alpha - b^\alpha \mu^\alpha) - \sqrt{-4\sigma^\alpha b^\alpha p_2^\alpha p_3^\alpha r^\alpha \gamma_2^{2\alpha} + a^2}}{2p_2^\alpha \gamma_2^\alpha r^\alpha b^\alpha} + \frac{V}{\gamma_2^\alpha} - \lambda \right) \right) \right.$$
$$\left. - \frac{p_2^\alpha V(r^\alpha b^\alpha - k_T^\alpha) + r^\alpha \gamma_2^\alpha (p_2^\alpha - b^\alpha \mu^\alpha) - \sqrt{-4\sigma^\alpha b^\alpha p_2^\alpha p_3^\alpha r^\alpha \gamma_2^{2\alpha} + a^2}}{2\gamma_2^\alpha r^\alpha b^\alpha} \right.$$
$$\left. \left(\frac{p_2^\alpha V(r^\alpha b^\alpha - k_T^\alpha) + r^\alpha \gamma_2^\alpha (p_2^\alpha + b^\alpha \mu^\alpha) + \sqrt{-4\sigma^\alpha b^\alpha p_2^\alpha p_3^\alpha r^\alpha \gamma_2^{2\alpha} + a^2}}{2p_2^\alpha \gamma_2^\alpha} \right) \right) = 0.$$

Eigenvalues of $J(Eq_2)$ are $\lambda_1 = \gamma_1^\alpha - k_s^\alpha \frac{V}{\gamma_2^\alpha}$, $\lambda_2 = -\gamma_2^\alpha$,

$$\begin{aligned}
\lambda_3 =& \frac{1}{(4b^\alpha p_2^\alpha r^{2\alpha}\gamma_2^{2\alpha})}((2b^\alpha + p_2^\alpha)r^\alpha(d + k_T^\alpha p_2^\alpha V)\gamma_2^\alpha - b^\alpha r^{3\alpha}\gamma_2^\alpha(b^\alpha p_2^\alpha V - p_2^\alpha\gamma_2^\alpha + b^\alpha\gamma_2^\alpha\mu^\alpha)+\\
& r^{2\alpha}\gamma_2^\alpha(-p_2^{2\alpha}\gamma_2^\alpha + 2b^{2\alpha}(p_2^\alpha V + \gamma_2^\alpha\mu^\alpha) - b^\alpha(d + p_2^\alpha((k_T^\alpha + p_2^\alpha)V + \gamma_2^\alpha(2 + \mu^\alpha))))\\
& - \sqrt{(r^{2\alpha}\gamma_2^{2\alpha}((-p_2^\alpha(d + k_T^\alpha p_2^\alpha V - p_2^\alpha r^\alpha\gamma_2^\alpha) + b^{2\alpha}(-2 + r^\alpha)r^\alpha(p_2^\alpha V + \gamma_2^\alpha\mu^\alpha) + b^\alpha(d(-2 + r^\alpha)}\\
& - 2k_T^\alpha p_2^\alpha V + p_2^\alpha r^\alpha((k_T^\alpha + p_2^\alpha)V + \gamma_2^\alpha(2 - r^\alpha + \mu^\alpha))))^2 - 8b^\alpha p_2^\alpha(-k_T^{2\alpha}p_2^{2\alpha}(-2 + r^\alpha)V^2\\
& - 2k_T^\alpha p_2^\alpha r^\alpha V(-p_2^\alpha(-2 + r^\alpha)\gamma_2^\alpha + b^\alpha(p_2^\alpha V + \gamma_2^\alpha\mu^\alpha))\\
& + r^\alpha(-p_2^{2\alpha}(-2 + r^\alpha)r^\alpha\gamma_2^{2\alpha} + b^{2\alpha}r^{2\alpha}(p_2^\alpha V + \gamma_2^\alpha\mu^\alpha)^2 + 2b^\alpha p_2^\alpha\gamma_2^\alpha(p_2^\alpha r^\alpha V - 2\sigma^\alpha p_3^\alpha\gamma_2^\alpha + r^\alpha\gamma_2^\alpha\mu^\alpha))\\
& + d(-k_T^\alpha p_2^\alpha(-2 + r^\alpha)V + r^\alpha(p_2^\alpha(-2 + r^\alpha)\gamma_2^\alpha + b^\alpha r^\alpha(p_2^\alpha V + \gamma_2^\alpha\mu^\alpha))))))).\\
\lambda_4 =& \frac{1}{(4b^\alpha p_2^\alpha r^{2\alpha}\gamma_2^{2\alpha})}((2b^\alpha + p_2^\alpha)r^\alpha(d + k_T^\alpha p_2^\alpha V)\gamma_2^\alpha - b^\alpha r^{3\alpha}\gamma_2^\alpha(b^\alpha p_2^\alpha V - p_2^\alpha\gamma_2^\alpha + b^\alpha\gamma_2^\alpha\mu^\alpha)\\
& + r^{2\alpha}\gamma_2^\alpha(-p_2^{2\alpha}\gamma_2^\alpha + 2b^{2\alpha}(p_2^\alpha V + \gamma_2^\alpha\mu^\alpha) - b^\alpha(d + p_2^\alpha((k_T^\alpha + p_2^\alpha)V + \gamma_2^\alpha(2 + \mu^\alpha))))\\
& + \sqrt{(r^{2\alpha}\gamma_2^{2\alpha}((-p_2^\alpha(d + k_T^\alpha p_2^\alpha V - p_2^\alpha r^\alpha\gamma_2^\alpha) + b^{2\alpha}(-2 + r^\alpha)r^\alpha(p_2^\alpha V + \gamma_2^\alpha\mu^\alpha)}\\
& + b^\alpha(d(-2 + r^\alpha) - 2k_T^\alpha p_2^\alpha V + p_2^\alpha r^\alpha((k_T^\alpha + p_2^\alpha)V + \gamma_2^\alpha(2 - r^\alpha + \mu^\alpha))))^2\\
& - 8b^\alpha p_2^\alpha(-k_T^{2\alpha}p_2^{2\alpha}(-2 + r^\alpha)V^2 - 2k_T^\alpha p_2^\alpha r^\alpha V^\alpha(-p_2^\alpha(-2 + r^\alpha)\gamma_2^\alpha + b^\alpha(p_2^\alpha V + \gamma_2^\alpha\mu^\alpha)) + r^\alpha\\
& (-p_2^{2\alpha}(-2 + r^\alpha)r^\alpha\gamma_2^{2\alpha} + b^{2\alpha}r^{2\alpha}(p_2^\alpha V + \gamma_2^\alpha\mu^\alpha)^2 + 2b^\alpha p_2^\alpha\gamma_2^\alpha(p_2^\alpha r^\alpha V - 2\sigma^\alpha p_3^\alpha\gamma_2^\alpha + r^\alpha\gamma_2^\alpha\mu^\alpha))\\
& + d(-k_T^\alpha p_2^\alpha(-2 + r^\alpha)V + r^\alpha(p_2^\alpha(-2 + r^\alpha)\gamma_2^\alpha + b^\alpha r^\alpha(p_2^\alpha V + \gamma_2^\alpha\mu^\alpha))))))).
\end{aligned}$$

From the conditions we have $\lambda_i < 0$ *for* $i = 1, 2, 3, 4$. Therefore, $|arg(\lambda_i)| > \frac{\alpha\pi}{2}$ by Theorem (1) and Eq_2 is locally asymptotically stable. ■

Theorem 5 *Let* $Eq_3 \in D_1$ *be the equilibrium point of system (2) and* $(p_2^\alpha, p_3^\alpha, \mu^\alpha, \gamma_2^\alpha, \sigma^\alpha, r^\alpha, b^\alpha, V, k_T^\alpha) \in D_1 \cap (Q^* \cup P^*)$, *where* $Q^* = \{(p_2^\alpha, p_3^\alpha, \mu^\alpha, \gamma_2^\alpha, \sigma^\alpha, r^\alpha, b^\alpha, V, k_T^\alpha) \in R_+^9 : d^2, d1 \geq 0, \gamma_1^\alpha\gamma_2^\alpha < k_s^\alpha V$ *and* $((2b^\alpha + p_2^\alpha)(-d + k_T^\alpha p_2^\alpha V)r^\alpha\gamma_2^\alpha - b^\alpha r^{3\alpha}\gamma_2^\alpha(b^\alpha p_2^\alpha V - p_2^\alpha\gamma_2^\alpha + b^\alpha\gamma_2^\alpha\mu^\alpha) + r^{2\alpha}\gamma_2^\alpha(-p_2^{2\alpha}\gamma_2^\alpha + 2b^{2\alpha}(p_2^\alpha V + \gamma_2^\alpha\mu^\alpha) - b^\alpha(-d + p_2^\alpha((k_T^\alpha + p_2^\alpha)V + \gamma_2^\alpha(2 + \mu^\alpha)))) - \sqrt{d_1}) < 0\}$.
$P^* = \{(p_2^\alpha, p_3^\alpha, \mu^\alpha, \gamma_2^\alpha, \sigma^\alpha, r^\alpha, b^\alpha, V, k_T^\alpha) \in R_+^9 : d^2$ *or* $d1 < 0, \gamma_1^\alpha\gamma_2^\alpha < k_s^\alpha V$ *and* $Re(((2b^\alpha + p_2^\alpha)(-d + k_T^\alpha p_2^\alpha V)r^\alpha\gamma_2^\alpha - b^\alpha r^{3\alpha}\gamma_2^\alpha(b^\alpha p_2^\alpha V - p_2^\alpha\gamma_2^\alpha + b^\alpha\gamma_2^\alpha\mu^\alpha) + r^{2\alpha}\gamma_2^\alpha(-p_2^{2\alpha}\gamma_2^\alpha + 2b^{2\alpha}(p_2^\alpha V + \gamma_2^\alpha\mu^\alpha) - b^\alpha(-d + p_2^\alpha((k_T^\alpha + p_2^\alpha)V + \gamma_2^\alpha(2 + \mu^\alpha)))) + \sqrt{d_1})) < 0\}$,
where $d = \sqrt{-4\sigma^\alpha b^\alpha p_2^\alpha p_3^\alpha r^\alpha\gamma_2^{2\alpha} + (k_T^\alpha p_2^\alpha V - b^\alpha p_2^\alpha r^\alpha V - p_2^\alpha r^\alpha\gamma_2^\alpha - b^\alpha r^\alpha\gamma_2^\alpha\mu^\alpha)^2}$ *and* $d_1 = (r^{2\alpha}\gamma_2^{2\alpha}((-p_2^\alpha(d + k_T^\alpha p_2^\alpha V - p_2^\alpha r^\alpha\gamma_2^\alpha) + b^{2\alpha}(-2 + r^\alpha)r^\alpha(p_2^\alpha V + \gamma_2^\alpha\mu^\alpha) + b^\alpha(d(-2 + r^\alpha) - 2k_T^\alpha p_2^\alpha V + p_2^\alpha r^\alpha((k_T^\alpha + p_2^\alpha)V + \gamma_2^\alpha(2 - r^\alpha + \mu^\alpha))))^2 - 8b^\alpha p_2^\alpha(-k_T^{2\alpha}p_2^{2\alpha}(-2 + r^\alpha)V^2 - 2k_T^\alpha p_2^\alpha r^\alpha V(-p_2^\alpha(-2 + r^\alpha)\gamma_2^\alpha + b^\alpha(p_2^\alpha V + \gamma_2^\alpha\mu^\alpha)) + r^\alpha(-p_2^{2\alpha}(-2 + r^\alpha)r^\alpha\gamma_2^{2\alpha} + b^{2\alpha}r^{2\alpha}(p_2^\alpha V + \gamma_2^\alpha\mu^\alpha)^2 + 2b^\alpha p_2^\alpha\gamma_2^\alpha(p_2^\alpha rV - 2\sigma^\alpha p_3^\alpha\gamma_2^\alpha + r^\alpha\gamma_2^\alpha\mu^\alpha)) + d(-k_T^\alpha p_2^\alpha(-2 + r^\alpha)V + r^\alpha(p_2^\alpha(-2 + r^\alpha)\gamma_2^\alpha + b^\alpha r^\alpha(p_2^\alpha V + \gamma_2^\alpha\mu^\alpha))))))$.
Then Eq_3 *is locally asymptotically stable*.

Proof The Jacobian matrix of the model (2) at Eq_3 is

$$J(Eq_3) = \begin{pmatrix} \gamma_1^\alpha - k_s^\alpha\frac{V}{\gamma_2^\alpha} & 0 & 0 & 0 \\ 0 & j_{22}^* & j_{23}^* & j_{24} \\ j_{31}^* & j_{32}^* & j_{33}^* & j_{34}^* \\ 0 & 0 & 0 & -\gamma_2^\alpha \end{pmatrix},$$

where

$$\begin{aligned}
j_{22}^* =& r^\alpha - \left(\frac{p_2^\alpha V(r^\alpha b^\alpha - k_T^\alpha) + r^\alpha\gamma_2^\alpha(p_2^\alpha - b^\alpha\mu^\alpha) + \sqrt{-4\sigma^\alpha b^\alpha p_2^\alpha p_3^\alpha r^\alpha\gamma_2^{2\alpha} + a^2}}{p_2^\alpha\gamma_2^\alpha r^\alpha}\right)\\
& - \left(\frac{p_2^\alpha V(r^\alpha b^\alpha - k_T^\alpha) + r^\alpha\gamma_2^\alpha(p_2^\alpha + b^\alpha\mu^\alpha) - \sqrt{-4\sigma^\alpha b^\alpha p_2^\alpha p_3^\alpha r^\alpha\gamma_2^{2\alpha} + a^2}}{2p_2^\alpha\gamma_2^\alpha} - k_T^\alpha\frac{V}{\gamma_2^\alpha}\right).\\
j_{23}^* =& -p_3^\alpha\frac{p_2^\alpha V(rb^\alpha - k_T^\alpha) + r^\alpha\gamma_2^\alpha(p_2^\alpha - b^\alpha\mu^\alpha) + \sqrt{-4\sigma^\alpha b^\alpha p_2^\alpha p_3^\alpha r^\alpha\gamma_2^{2\alpha} + a^2}}{2p_2^\alpha\gamma_2^\alpha r^\alpha b^\alpha}.\\
j_{24}^* =& -k_T^\alpha\frac{p_2^\alpha V(r^\alpha b^\alpha - k_T^\alpha) + r^\alpha\gamma_2^\alpha(p_2^\alpha - b^\alpha\mu^\alpha) + \sqrt{-4\sigma^\alpha b^\alpha p_2^\alpha p_3^\alpha r^\alpha\gamma_2^{2\alpha} + a^2}}{2p_2^\alpha\gamma_2^\alpha r^\alpha b^\alpha}.\\
j_{31}^* =& p_1^\alpha\frac{p_2^\alpha V(r^\alpha b^\alpha - k_T^\alpha) + r^\alpha\gamma_2^\alpha(p_2^\alpha + b^\alpha\mu^\alpha) - \sqrt{-4\sigma^\alpha b^\alpha p_2^\alpha p_3^\alpha r^\alpha\gamma_2^2 + a^2}}{2p_2^\alpha p_3^\alpha\gamma_2^\alpha}.\\
j_{32}^* =& j_{34}^* = -\frac{p_2^\alpha V(r^\alpha b^\alpha - k_T^\alpha) + r^\alpha\gamma_2^\alpha(p_2^\alpha + b^\alpha\mu^\alpha) - \sqrt{-4\sigma^\alpha b^\alpha p_2^\alpha p_3^\alpha r^\alpha\gamma_2^{2\alpha} + a^2}}{2p_3^\alpha\gamma_2^\alpha}.\\
j_{33}^* =& -\mu^\alpha - p_2^\alpha\left(\frac{p_2^\alpha V(r^\alpha b^\alpha - k_T^\alpha) + r^\alpha\gamma_2^\alpha(p_2^\alpha - b^\alpha\mu^\alpha) + \sqrt{-4\sigma^\alpha b^\alpha p_2^\alpha p_3^\alpha r^\alpha\gamma_2^{2\alpha} + a^2}}{2p_2^\alpha\gamma_2^\alpha r^\alpha b^\alpha} + \frac{V}{\gamma_2^\alpha}\right).
\end{aligned}$$

The characteristic equation is $|J(Eq_3) - \lambda I| = 0$. Hence,

$$(\gamma_1^\alpha - k_s^\alpha \frac{V}{\gamma_2^\alpha} - \lambda)(-\gamma_2^\alpha - \lambda)((r^\alpha - \frac{p_2^\alpha V(r^\alpha b^\alpha - k_T^\alpha) + r^\alpha \gamma_2^\alpha (p_2^\alpha - b^\alpha \mu^\alpha) + \sqrt{-4\sigma^\alpha b^\alpha p_2^\alpha p_3^\alpha r^\alpha \gamma_2^{2\alpha} + a^2}}{p_2^\alpha \gamma_2^\alpha r^\alpha}$$
$$- (\frac{p_2^\alpha V(r^\alpha b^\alpha - k_T^\alpha) + r^\alpha \gamma_2^\alpha (p_2^\alpha + b^\alpha \mu^\alpha) - \sqrt{-4\sigma^\alpha b^\alpha p_2^\alpha p_3^\alpha r^\alpha \gamma_2^{2\alpha} + a^2}}{2p_2^\alpha \gamma_2^\alpha}) - k_T^\alpha \frac{V}{\gamma_2^\alpha} - \lambda)$$
$$((-\mu^\alpha - (\frac{p_2^\alpha V(r^\alpha b^\alpha - k_T^\alpha) + r^\alpha \gamma_2^\alpha (p_2^\alpha - b^\alpha \mu^\alpha) + \sqrt{-4\sigma^\alpha b^\alpha p_2^\alpha p_3^\alpha r^\alpha \gamma_2^{2\alpha} + a^2}}{2\gamma_2^\alpha r^\alpha b^\alpha} + \frac{V}{\gamma_2^\alpha} - \lambda))$$
$$- \frac{p_2^\alpha V(r^\alpha b^\alpha - k_T^\alpha) + r^\alpha \gamma_2^\alpha (p_2^\alpha - b^\alpha \mu^\alpha) + \sqrt{-4\sigma^\alpha b^\alpha p_2^\alpha p_3^\alpha r^\alpha \gamma_2^{2\alpha} + a^2}}{2\gamma_2^\alpha r^\alpha b^\alpha}$$
$$(\frac{p_2^\alpha V(r^\alpha b^\alpha - k_T^\alpha) + r^\alpha \gamma_2^\alpha (p_2^\alpha + b^\alpha \mu^\alpha) - \sqrt{-4\sigma^\alpha b^\alpha p_2^\alpha p_3^\alpha r^\alpha \gamma_2^{2\alpha} + a^2}}{2p_2^\alpha \gamma_2^\alpha})) = 0.$$

Eigenvalues of $J(Eq_3)$ are $\lambda_1 = \gamma_1^\alpha - k_s^\alpha \frac{V}{\gamma_2^\alpha}$, $\lambda_2 = -\gamma_2^\alpha$,

$$\lambda_3 = \frac{1}{(4b^\alpha p_2^\alpha r^{2\alpha} \gamma_2^{2\alpha})}((2b^\alpha + p_2^\alpha) r^\alpha (-d + k_T^\alpha p_2^\alpha V)\gamma_2^\alpha - b^\alpha r^{3\alpha} \gamma_2^\alpha (b^\alpha p_2^\alpha V - p_2^\alpha \gamma_2^\alpha + b^\alpha \gamma_2^\alpha \mu^\alpha)$$
$$+ r^{2\alpha} \gamma_2^\alpha (-p_2^{2\alpha} \gamma_2^\alpha + 2b^{2\alpha}(p_2^\alpha V + \gamma_2^\alpha \mu^\alpha) - b^\alpha (d + p_2^\alpha ((k_T^\alpha + p_2^\alpha)V + \gamma_2^\alpha (2 + \mu^\alpha))))$$
$$- (r^{2\alpha} \gamma_2^{2\alpha}((-p_2^\alpha (-d + k_T^\alpha p_2^\alpha V - p_2^\alpha r^\alpha \gamma_2^\alpha) + b^{2\alpha}(-2 + r^\alpha) r^\alpha (p_2^\alpha V + \gamma_2^\alpha \mu^\alpha)$$
$$+ b^\alpha (-d(-2 + r^\alpha) - 2k_T^\alpha p_2^\alpha V + p_2^\alpha r^\alpha ((k_T^\alpha + p_2^\alpha)V + \gamma_2^\alpha (2 - r^\alpha + \mu^\alpha))))^2$$
$$- 8b^\alpha p_2^\alpha (-k_T^{2\alpha} p_2^{2\alpha}(-2 + r^\alpha)V^2 - 2k_T^\alpha p_2^\alpha r^\alpha V(-p_2^\alpha (-2 + r^\alpha)\gamma_2^\alpha + b^\alpha (p_2^\alpha V + \gamma_2^\alpha \mu^\alpha)) + r^\alpha (-p_2^{2\alpha}(-2 + r^\alpha) r^\alpha \gamma_2^{2\alpha} + b^{2\alpha} r^{2\alpha}(p_2^\alpha V$$
$$+ \gamma_2^\alpha \mu^\alpha)^2 + 2b^\alpha p_2^\alpha \gamma_2^\alpha (p_2^\alpha r^\alpha V - 2\sigma^\alpha p_3^\alpha \gamma_2^\alpha + r^\alpha \gamma_2^\alpha \mu^\alpha)) - d(-k_T^\alpha p_2^\alpha (-2 + r^\alpha)V + r^\alpha (p_2^\alpha (-2 + r^\alpha)\gamma_2^\alpha + b^\alpha r^\alpha (p_2^\alpha V + \gamma_2^\alpha \mu^\alpha))))))^{1/2}),$$
$$\lambda_4 = \frac{1}{(4b^\alpha p_2^\alpha r^{2\alpha} \gamma_2^{2\alpha})}((2b^\alpha + p_2^\alpha) r^\alpha (-d + k_T^\alpha p_2^\alpha V)\gamma_2^\alpha - b^\alpha r^{3\alpha} \gamma_2^\alpha (b^\alpha p_2^\alpha V - p_2^\alpha \gamma_2^\alpha + b^\alpha \gamma_2^\alpha \mu^\alpha)$$
$$+ r^{2\alpha} \gamma_2^\alpha (-p_2^{2\alpha} \gamma_2^\alpha + 2b^{2\alpha}(p_2^\alpha V + \gamma_2^\alpha \mu^\alpha) - b^\alpha (-d + p_2^\alpha ((k_T^\alpha + p_2^\alpha)V + \gamma_2^\alpha (2 + \mu^\alpha))))$$
$$+ (r^{2\alpha} \gamma_2^{2\alpha}((-p_2^\alpha (d + k_T^\alpha p_2^\alpha V - p_2^\alpha r^\alpha \gamma_2^\alpha) + b^{2\alpha}(-2 + r^\alpha) r^\alpha (p_2^\alpha V + \gamma_2^\alpha \mu^\alpha) + b^\alpha (d^\alpha (-2 + r^\alpha) - 2k_T^\alpha p_2^\alpha V + p_2^\alpha r^\alpha ((k_T^\alpha + p_2^\alpha)V +$$
$$\gamma_2^\alpha (2 - r^\alpha + \mu^\alpha))))^2 - 8b^\alpha p_2^\alpha (-k_T^{2\alpha} p_2^{2\alpha}(-2 + r^\alpha)V^2 - 2k_T^\alpha p_2^\alpha r^\alpha V^\alpha (-p_2^\alpha (-2 + r^\alpha)\gamma_2^\alpha + b^\alpha (p_2^\alpha V + \gamma_2^\alpha \mu^\alpha))$$
$$+ r^\alpha (-p_2^{2\alpha}(-2 + r^\alpha) r^\alpha \gamma_2^{2\alpha} + b^{2\alpha} r^{2\alpha}(p_2^\alpha V + \gamma_2^\alpha \mu^\alpha)^2 + 2b^\alpha p_2^\alpha \gamma_2^\alpha (p_2^\alpha r^\alpha V - 2\sigma^\alpha p_3^\alpha \gamma_2^\alpha$$
$$+ r^\alpha \gamma_2^\alpha \mu^\alpha)) - d(-k_T^\alpha p_2^\alpha (-2 + r^\alpha)V + r^\alpha (p_2^\alpha (-2 + r^\alpha)\gamma_2^\alpha + b^\alpha r^\alpha (p_2^\alpha V + \gamma_2^\alpha \mu^\alpha))))))^{1/2}).$$

From the conditions we have $\lambda_i < 0$ *for* $i = 1, 2, 3, 4$. Therefore, $|arg(\lambda_i)| > \frac{\alpha\pi}{2}$, and by Theorem (1), Eq_3 is locally asymptotically stable. ■

5 A numerical technique for the proposed fractional-order model

In this section, numerical solution of system (3) is carried out using the Predictor-Corrector method of Adams-Bashforth-Moulton [32, 33] for different $\alpha \in (0, 1]$. We implement the Caputo fractional operator to provide the numerical simulation of a nonlinear fractional order system. The following Cauchy-type ODE is taken into account with respect to the Caputo operator of order α:

$$_C D_t^\alpha D_t^\alpha \Phi(t) = f(t, \Phi(t)), \quad \Phi^{(k)}(0) = \Phi_0^k, \quad 0 < \alpha \leq 1, \quad 0 < t \leq \tau, \tag{7}$$

where $k = 0, 1, ..., n-1$, and $n = \lceil \alpha \rceil$. Equation (7) is equivalent to the following Volterra equation:

$$\Phi(t) = \sum_{k=0}^{n-1} \Phi_0^{(k)} \frac{t^k}{k!} + \frac{1}{\Gamma(\alpha)} \int_0^t (t - s)^{\alpha-1} f(s, \Phi(s))\, ds. \tag{8}$$

By considering this proposed predictor-corrector scheme associated with the Adam-Bashforth-Moulton algorithm [4, 6] to have the numerical solutions of the proposed model, we can take $h = \tau/N$, $t_z = zh$, and $z = 0, 1, ..., N \in Z^+$, by letting $\Phi_z \approx \Phi(t_z)$, it can be discretized as follows, i.e., the corresponding corrector formula [6]

$$S_{q+1} = \sum_{z=0}^{q-1} S_0^{(z)} \frac{t_{q+1}^z}{z!} + \frac{h^\alpha}{\Gamma(\alpha + 2)} \sum_{z=0}^{q} (p_{z,q+1})(\gamma_1^\alpha S_z - k_s^\alpha M_z S_z) + \frac{h^\alpha}{\Gamma(\alpha + 2)} \sum_{z=0}^{q} (p_{q+1,q+1}) \left(\gamma_1^\alpha S_{q+1}^{PF} - k_s^\alpha M_{q+1}^{PF} S_{q+1}^{PF}\right),$$

$$T_{q+1} = \sum_{z=0}^{q-1} T_0^{(z)} \frac{t_{q+1}^z}{z!} + \frac{h^\alpha}{\Gamma(\alpha + 2)} \sum_{z=0}^{q} (p_{z,q+1})(r^\alpha (1 - b^\alpha T_z) T_z - (p_3^\alpha E_z + k_t^\alpha M_z) T_z)$$
$$+ \frac{h^\alpha}{\Gamma(\alpha + 2)} \sum_{z=0}^{q} (p_{q+1,q+1}) \left(r^\alpha (1 - b^\alpha T_{q+1}^{PF}) T_{q+1}^{PF} - (p_3^\alpha E_{q+1}^{PF} + k_t^\alpha M_{q+1}^{PF}) T_{q+1}^{PF}\right),$$

$$E_{q+1} = \sum_{z=0}^{q-1} E_0^{(z)} \frac{t_{q+1}^z}{z!} + \frac{h^\alpha}{\Gamma(\alpha+2)} \sum_{z=0}^{q} (p_{z,q+1}) \left(a^\alpha - \mu^\alpha E_z + \frac{p_1^\alpha E_z S_z}{S_z + 1} - p_2^\alpha (T_z + M_z) E_z \right) + \frac{h^\alpha}{\Gamma(\alpha+2)} \sum_{z=0}^{q} (p_{q+1,q+1}) \left(a^\alpha - \mu^\alpha E_{q+1}^{PF} + \frac{p_1^\alpha E_{q+1}^{PF} S_{q+1}^{PF}}{S_{q+1}^{PF} + 1} - p_2^\alpha (T_{q+1}^{PF} + M_{q+1}^{PF}) E_{q+1}^{PF} \right),$$

$$M_{q+1} = \sum_{z=0}^{q-1} M_0^{(z)} \frac{t_{q+1}^z}{z!} + \frac{h^\alpha}{\Gamma(\alpha+2)} \sum_{z=0}^{q} (p_{z,q+1}) \left(-\gamma_2^\alpha M_z + V(t) \right) + \frac{h^\alpha}{\Gamma(\alpha+2)} \sum_{z=0}^{q} (p_{q+1,q+1}) \left(-\gamma_2^\alpha M_{q+1}^{PF} + V(t) \right),$$

where

$$p_{z,q+1} = \begin{cases} q^{\alpha+1} - (q-\alpha)(q+1)^\alpha, & \text{if } z = 0, \\ (q-z+2)^{\alpha+1} + (q-z)^{\alpha+1} - 2(q-z+1)^{\alpha+1}, & \text{if } 1 \le z \le q, \\ 1, & \text{if } z = q+1. \end{cases} \tag{9}$$

Subsequently, the following step is to construct the coincident predictor formula Φ_{q+1}^{PF}. One can compute the proposed predictor formula as

$$\begin{aligned} S_{q+1}^{PF} &= \sum_{z=0}^{q-1} S_0^{(z)} \frac{t_{q+1}^z}{z!} + \frac{h^\alpha}{\Gamma(\alpha+1)} \sum_{z=0}^{q} \left(j_{z,^\alpha q+1} \right) \left(\gamma_1^\alpha S_z - k_s^\alpha M_z S_z \right), \\ T_{q+1}^{PF} &= \sum_{z=0}^{q-1} T_0^{(z)} \frac{t_{q+1}^z}{z!} + \frac{h^\alpha}{\Gamma(\alpha+1)} \sum_{z=0}^{q} (j_{z,q+1}) \left(r^\alpha (1 - b^\alpha T_z) T_z - (p_3^\alpha E_z + k_t^\alpha M_z) T_z \right), \\ E_{q+1}^{PF} &= \sum_{z=0}^{q-1} E_0^{(z)} \frac{t_{q+1}^z}{z!} + \frac{h^\alpha}{\Gamma(\alpha+1)} \sum_{z=0}^{q} (j_{z,q+1}) \left(a^\alpha - \mu^\alpha E_z + \frac{p_1^\alpha E_z S_z}{S_z + 1} - p_2^\alpha (T_z + M_z) E_z \right), \\ M_{q+1}^{PF} &= \sum_{z=0}^{q-1} M_0^{(z)} \frac{t_{q+1}^z}{z!} + \frac{h^\alpha}{\Gamma(\alpha+1)} \sum_{z=0}^{q} (j_{z,q+1}) \left(-\gamma_2^\alpha M_z + V(t) \right), \end{aligned}$$

where

$$j_{z,q+1} = (q+1-z)^\alpha - (q-z)^\alpha.$$

6 Memory trace and hereditary traits

To examine the behaviour of the proposed model (2), we use the Caputo operator defined in (2). For $\alpha \in (0,1]$ derivative, let the fractional derivative of variable $\Phi(t)$ be

$${}_C D_t^\alpha \Phi(t) = \phi(\Phi(t), t). \tag{10}$$

Utilizing the one of most common numerical methods, the L1 scheme [22, 23, 24, 21], the numerical approximation of the FOD of $\Phi(t)$ is

$${}_C D_t^\alpha \Phi(t) \approx \frac{(dt)^{-\alpha}}{\Gamma(2-\alpha)} \left[\sum_{\rho=0}^{T-1} \left[\Phi(t_{\rho+1}) - \Phi(t_\rho) \right] \left[(T-\rho)^{1-\alpha} - (T-1-\rho)^{1-\alpha} \right] \right]. \tag{11}$$

One of the most powerful numerical methods for discretizing the Caputo-FOD in time is $L1$ scheme. The purpose of implementing the L1 scheme in this research study is its memory term and convergence rate. Memory term is also explicitly present in other numerical methods, but this memory integration term is more clearly defined in the $L1$ scheme. Considering (10) and (11) together, the numerical solution of Eq. (10) is as follows:

$$\Phi(t_T) \approx {}_C D_t^\alpha \Gamma(2-\alpha) H(\Phi(t), t) + \Phi(t_{T-1}) - \left[\sum_{\rho=0}^{T-2} \left[\Phi(t_{\rho+1}) - \Phi(t_\rho) \right] \left[(T-\rho)^{1-\alpha} - (T-1-\rho)^{1-\alpha} \right] \right].$$

Therefore, the solution of the FOD (fractional-order derivative) can be defined as the difference between the Markov term and the memory trace. The Markov term weighted by the Gamma function is as follows:

$$\text{Markov term} = {}_C D_t^\alpha \Gamma(2-\alpha) H(\Phi(t), t) + \Phi(t_{T-1}). \tag{12}$$

The memory trace (Φ-memory trace since it is related to variable $\Phi(t)$) is

$$\text{Memory trace} = \sum_{\rho=0}^{T-2} \left[\Phi(t_{\rho+1}) - \Phi(t_\rho) \right] \left[(T-\rho)^{1-\alpha} - (T-1-\rho)^{1-\alpha} \right]. \tag{13}$$

The memory trace is capable of integrating all past activities and takes into account the long-term history of the system. For $\alpha = 1$, the memory trace is 0 for any time t. Memory trace dynamics is highly dependent on time. When the fractional-order α is decreased from the

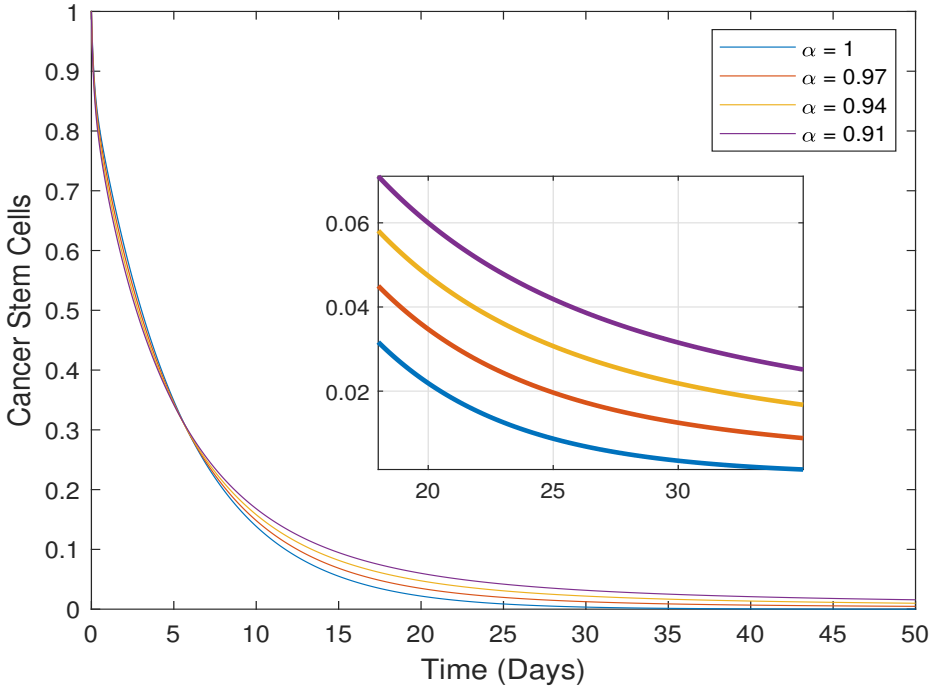

Figure 1. Change of the cancer stem cells over time for the varying fractional-order derivative

unit, the memory trace nonlinearly increases from 0. Hence, the fractional-order system dynamics quite different from the integer order dynamics.

7 Numerical simulations and data analysis

In this section, for the system (2), the numerical solutions are achieved using the Adams-Bashforth-Moulton Predictor-Corrector method [34] for the parameters in Table 1. With the help of numerical simulations, we have investigated the effects of changes in parameters on the system (2) and how different values of the fractional derivative α affect the behavior of the system. The parameter values that have been used for numerical simulations are given in Table 1. In Fig. 1, the variation of cancer stem cells with time for different fractional derivatives have been observed. As the α decreases from 1, that is, in the case of the Caputo fractional derivative, it takes a longer time for the stem cells to reach the equilibrium point. In Fig. 2, the change of tumor cells with time for different fractional derivatives have been observed. It has been seen that tumor cells disappear in a short time for the integer order case. In addition, since the fractional derivative decreases from 1 to zero (does not equal to zero) , the amount of decrease in tumor cells per unit time also decreases. In Fig. 3, it has been seen that the concentration of effector cells decreases in a short time, then their concentration suddenly increases and then reaches the equilibrium point. In addition, as α decreases from 1, it takes a longer time for effector cells to reach the equilibrium point. In Fig. 4, the variation of chemotherapy concentration drug with time for different fractional derivatives has been illustrated. It is understood from Fig. 4 that, the fractional order predicts more chemotherapy concentration drugs. Moreover, in Figs. 5,6,7, the changes of tumor cells and cancer stem cells with time have been investigated for different values of parameters. It is understood from Fig. 5 that as the γ_2 (decay rate of chemotherapy drug) increases, there is a significant increase in the number of tumor stem cells. In addition, we vary the parameter k_S and keep other parameters fixed in order to explore the effects of this parameter in Fig. 6. From Fig. 6, it has been shown that as k_S decreases, the number of stem cells also increases. In addition, it is clear from Fig. 7 that as k_T decreases, the number of tumor cells also increases. We also explore the effect of the memory trace in Figs. 8,9,10, 11. One can conclude that when $\alpha = 1$, the memory effect in the system is zero and as the α increases to 1 the memory effect of the system also emerges.

8 Results and discussion

In this paper, we have considered the Caputo fractional order cancer-immune system model that is given as a system of fractional differential equations (2) which have Caputo fractional derivative. We explore the local asymptotic stability of the tumor-free and tumor-infection fixed points of the system and we show that the equilibrium points of the model (2) is asymptotically stable under some certain conditions. Then, we have examined the existence and uniqueness of the solution. Moreover, we have achieved the numerical simulations to verify the theoretical results. In order to explore the effects of variation of the fractional order derivative and to examine the behavior of the system, we have obtained the figures for different α values. It is seen that as α decreases from 1, the cells reach the equilibrium points faster. In addition, we have investigated the effect of the memory trace, which is very important for biological models. When examining the effects of the memory trace, it is seen that there is no memory effect for $\alpha = 1$. However, as α decreases from 1, the memory effect of the system emerges. From the figures, we have concluded that the Caputo fractional derivative gives more realistic results than integer order derivatives. Although, there have been many studies that discuss the tumor-immune interaction in the literature, our model differs from them in terms of exploring the interaction between stem cells, tumor cells, effector cells and chemotherapy concentration drugs. In addition, also, it differs from other models in terms of the mathematical studies presented above.

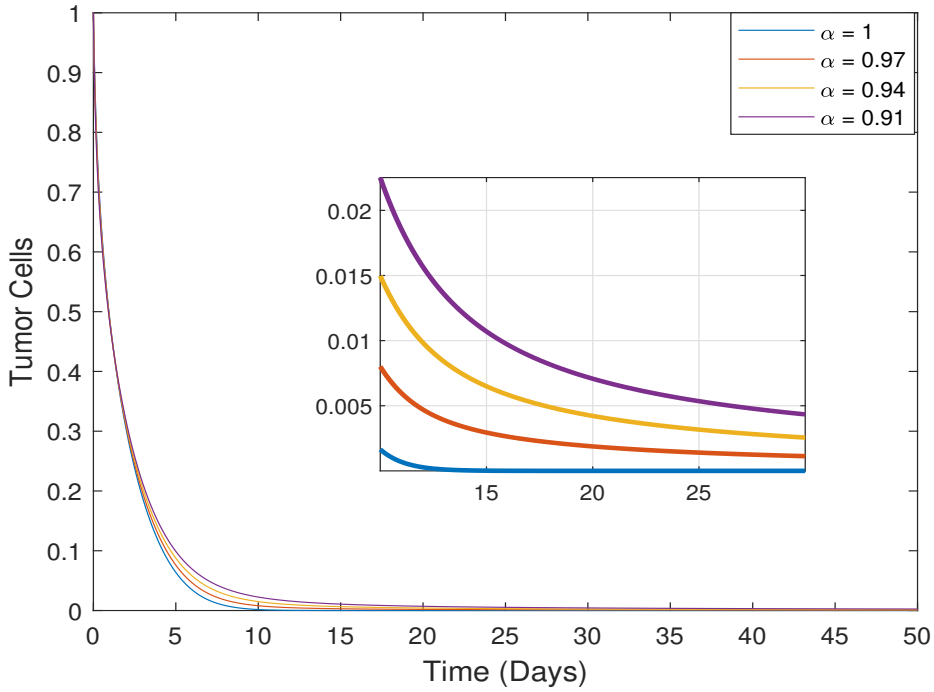

Figure 2. Change of the Tumor Cells over time for the varying fractional-order derivative

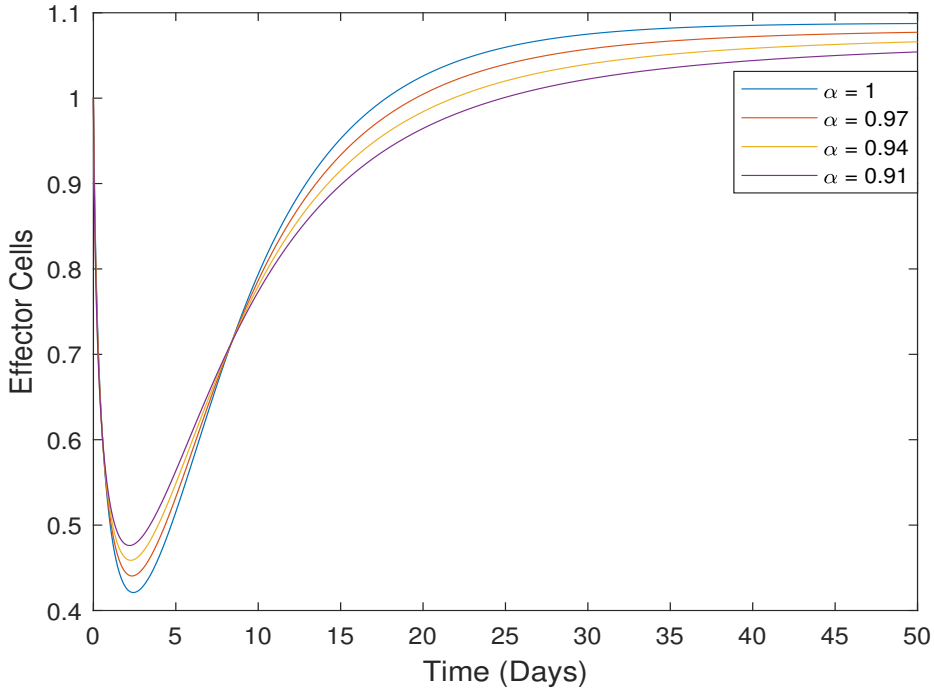

Figure 3. Change of the effector cells over time for the varying fractional-order derivative

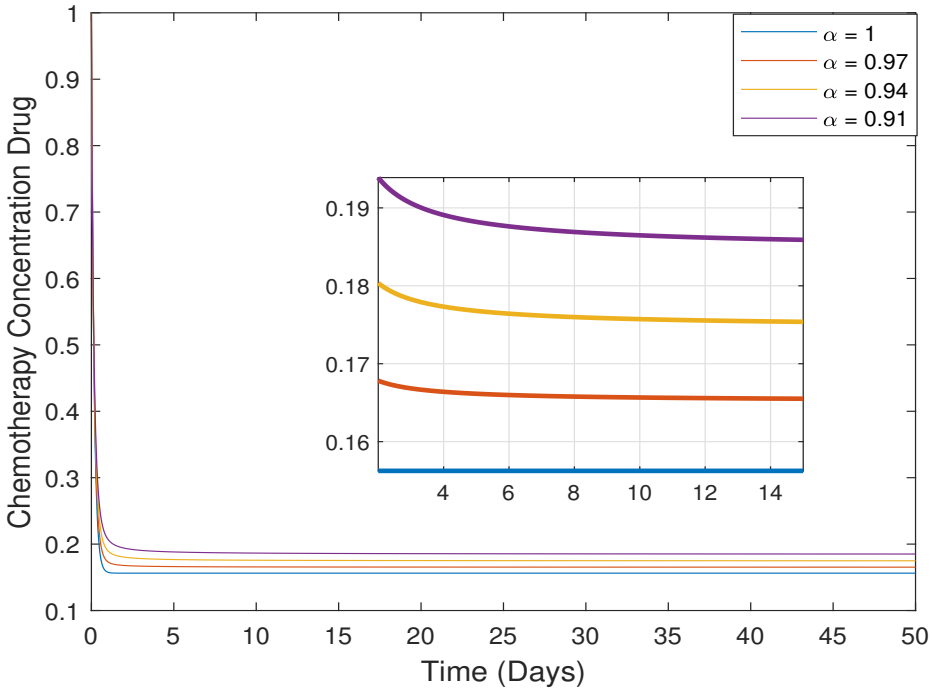

Figure 4. Change of the Chemotherapy drug concentration over time for the varying fractional-order derivative

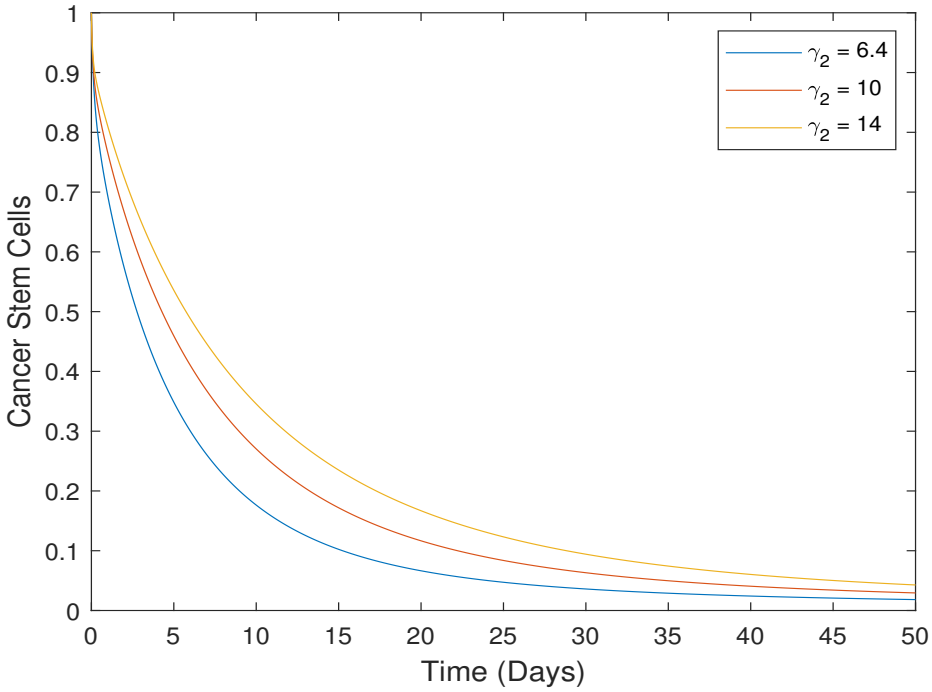

Figure 5. Change of the stem cells over time for the different γ_2 values, $\alpha = 0.9$

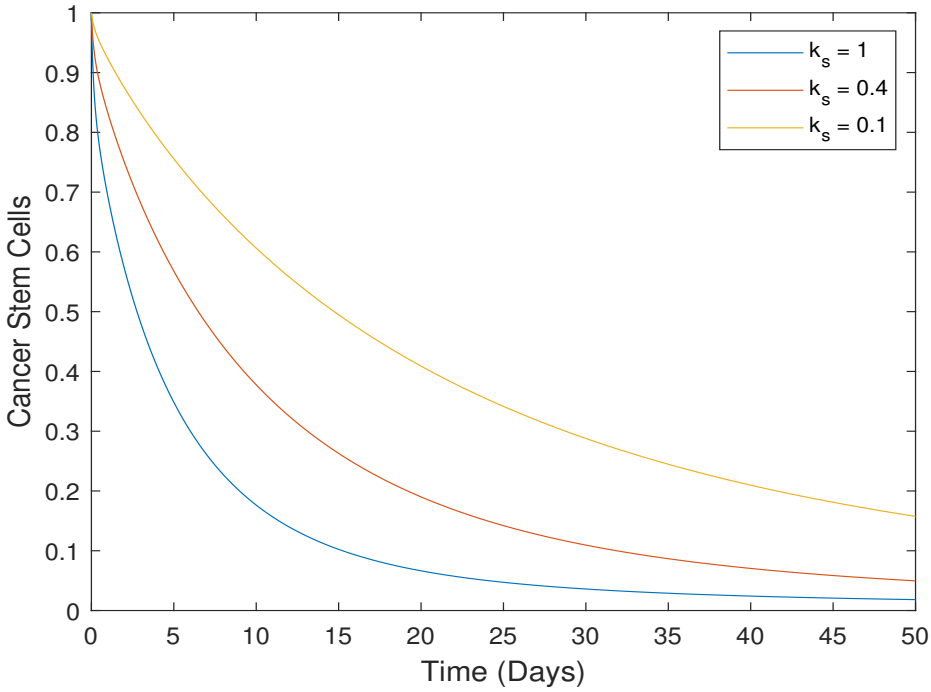

Figure 6. Change of the stem cells over time for the varying k_s values, $\alpha = 0.9$

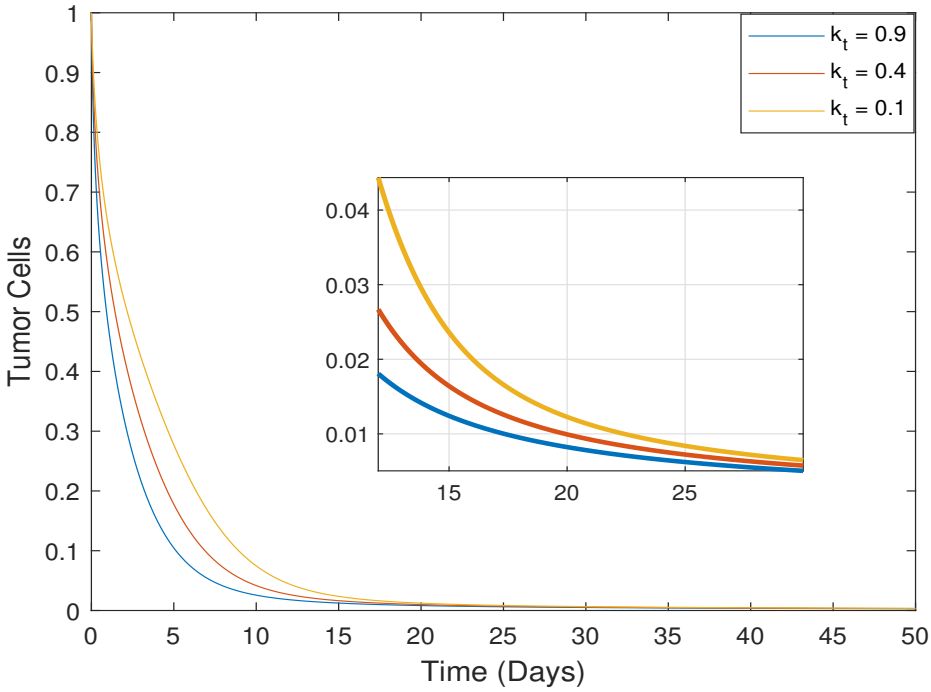

Figure 7. Change of the tumor cells over time for the varying k_t values, $\alpha = 0.9$

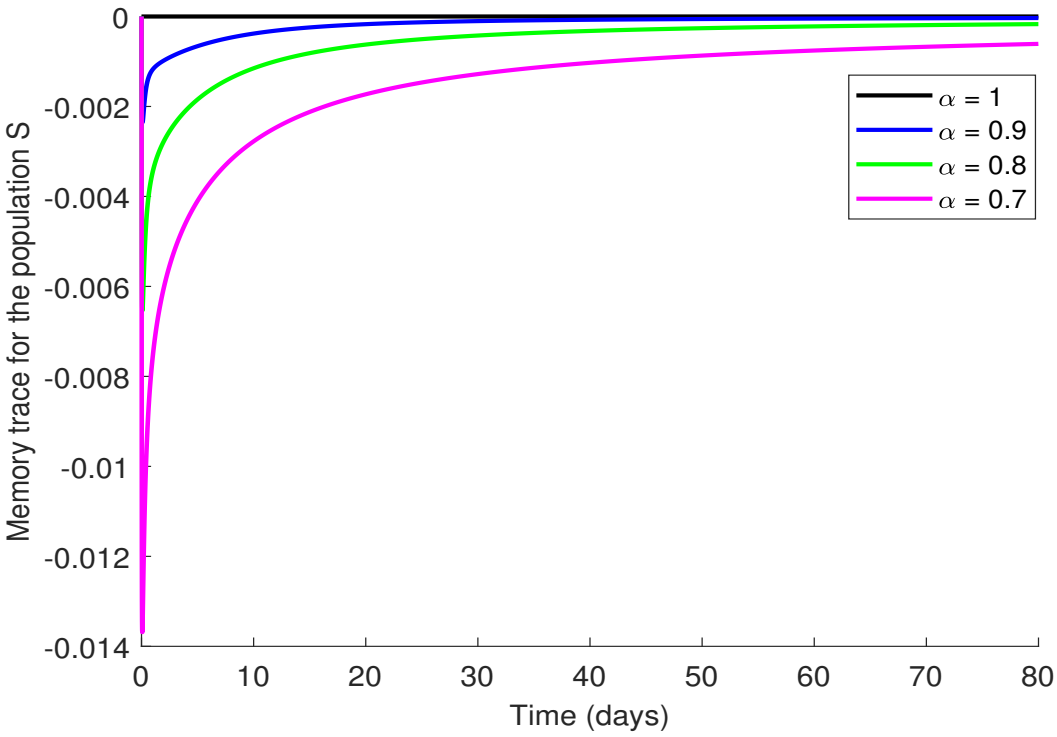

Figure 8. Change of the stem cells over time for the varying fractional-order derivative

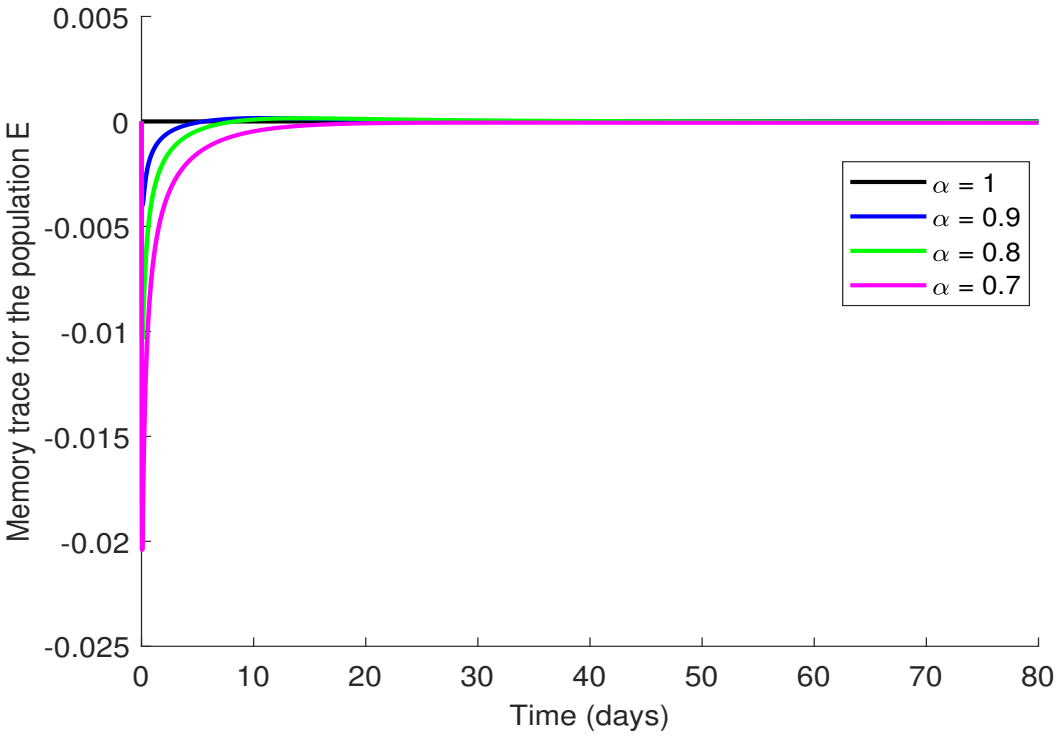

Figure 9. Change of the effector cells over time for the varying fractional-order derivative

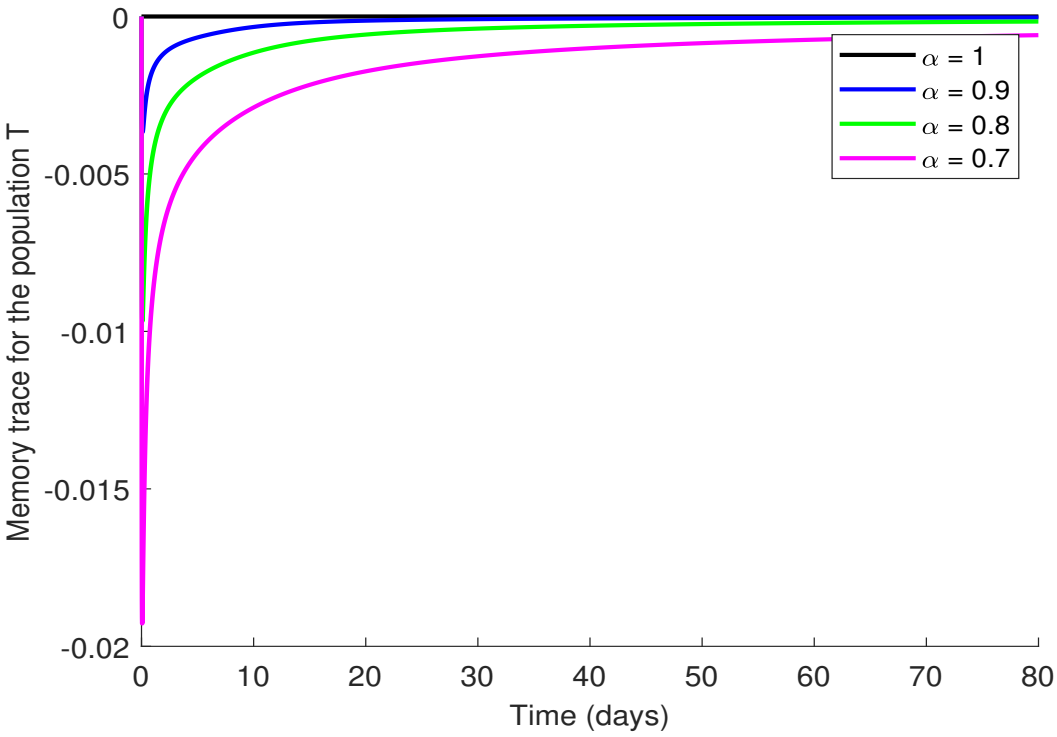

Figure 10. Change of the tumor cells over time for the varying fractional-order derivative

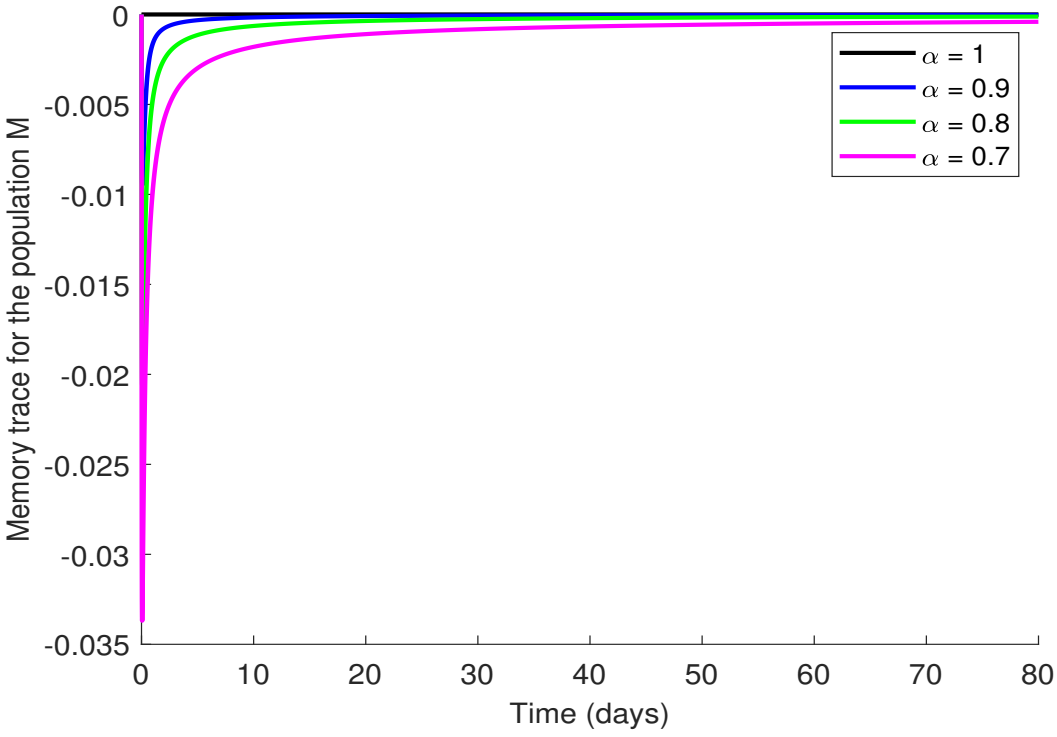

Figure 11. Change of the chemotherapy drug concentration over time for the varying fractional-order derivative

Chemotherapy concentration drug plays an important role in the prevention of tumor growth. According to the results, if the chemotherapy concentration drugs are high, then the tumor cells undergo a considerable loss. When the simulation results have been examined, it has been observed that as α changes, the stem cells, the number of tumor cells, number of effector cells and chemotherapy concentration drug also change significantly. We hope that this study will make very high contributions to academics both dealing with mathematics and working in the field of medicine.

Declarations

Consent for publication

Not applicable.

Conflicts of interest

The authors declare that they have no conflict of interests.

Author's contributions

F.Ö.: Conceptualization, Methodology, Investigation, Visualization, Writing, Software, Original draft preparation, Supervision, Validation, Writing-Reviewing and Editing. M.T.Ş.:Conceptualization, Writing-Original draft preparation, Software, Supervision, Validation, Writing-Reviewing and Editing. R.H.:Conceptualization, Visualization, Writing, Investigation, Validation, Original draft preparation, Writing-Reviewing and Editing. All authors discussed the results and contributed to the final manuscript.

Acknowledgements

This study was supported by Research Fund of the Erciyes University. Project Number: FDS-2021-11059.
The authors are very much thankful to the reviewers and editor for their valuable suggestions that have improved the quality of the manuscript.

References

[1] El-Gohary, A. Chaos and optimal control of cancer self-remission and tumor system steady states. *Chaos, Solutions and Fractals*, 37(5), 1305-1316, (2008). [CrossRef]
[2] El-Gohary, A. The chaos and optimal control of cancer model with complete unknown parameters. *Chaos, Solutions and Fractals*, 42(5), 2865-2874, (2009). [CrossRef]
[3] Kirschner, D., Panetta, J.C. Modeling immunotherapy of the tumor–immune interaction. *Journal of mathematical biology*, 37(3), 235–252, (1998). [CrossRef]
[4] Öztürk, I. & Özköse, F. Stability analysis of fractional order mathematical model of tumor-immune system interaction. *Chaos, Solitons & Fractals*, 133, 109614, (2020). [CrossRef]
[5] Hadamard, J. Essai sur l'étude des fonctions données par leur développement de Taylor (PDF). *Journal de Mathématiques Pures et Appliquées*, 4(8), 101–186, (1892).
[6] Li, C. & Tao, C. On the fractional Adams method. *Computers & Mathematics with Applications*, 58(8), 1573-1588, (2009). [CrossRef]
[7] Yavuz, M. & Sene, N. Stability analysis and numerical computation of the fractional predator–prey model with the harvesting rate. *Fractal and Fractional*, 4(3), 35, (2020). [CrossRef]
[8] Naik, P.A., Owolabi, K.M., Yavuz, M. & Zu, J. Chaotic dynamics of a fractional order HIV-1 model involving AIDS-related cancer cells. *Chaos, Solitons & Fractals*, 140, 110272, (2020). [CrossRef]
[9] Özköse, F. & Yavuz, M. Investigation of interactions between COVID-19 and diabetes with hereditary traits using real data: A case study in Turkey. *Computers in biology and medicine*, 105044, (2021). [CrossRef]
[10] Hammouch, Z., Yavuz, M. & Özdemir, N. Numerical solutions and synchronization of a variable-order fractional chaotic system. *Mathematical Modelling and Numerical Simulation with Applications*, 1(1), 11-23, (2021). [CrossRef]
[11] Naik, P.A., Yavuz, M. & Zu, J. The role of prostitution on HIV transmission with memory: A modeling approach. *Alexandria Engineering Journal*, 59(4), 2513-2531, (2020). [CrossRef]
[12] Naik, P.A., Yavuz, M., Qureshi, S., Zu, J., Townley, S. Modeling and analysis of COVID-19 epidemics with treatment in fractional derivatives using real data from Pakistan. *The European Physical Journal Plus*, 135(10), 1-42, (2020). [CrossRef]
[13] Thomson, J.A., Itskovitz-Eldor, J., Shapiro, S.S., Waknitz, M.A., Swiergiel, J.J., Marshall, V.S., Jones, J.M. Embryonic stem cell lines derived from human blastocysts. *Science*, 282(5391), 1145–1147, (1998). [CrossRef]
[14] Hernigou, P., Beaujean, F. Treatment of osteonecrosis with autologous bone marrow grafting. *Clinical Orthopaedics and Related Research*, 405, 14–23, (2002). [CrossRef]
[15] Körbling, M., Estrov, Z. Adult stem cells for tissue repair—a new therapeutic concept?. *New England Journal of Medicine*, 349(6), 570–582, (2003). [CrossRef]
[16] Chakrabarty, K., Shetty, R., Ghosh, A. Corneal cell therapy: with iPSCs, it is no more a far-sight. *Stem cell research & therapy*, 9(1), 1-15, (2018). [CrossRef]
[17] Alqudah, M.A. Cancer treatment by stem cells and chemotherapy as a mathematical model with numerical simulations. *Alexandria Engineering Journal*, 59, 1953–1957, (2020). [CrossRef]
[18] Naik, P.A., Zu, J. & Naik, M. Stability analysis of a fractional-order cancer model with chaotic dynamics. *International Journal of Biomathematics*, 14(6), 2150046, (2021). [CrossRef]

[19] Naik, P.A. Global dynamics of a fractional-order SIR epidemic model with memory. *International Journal of Biomathematics*, 13(8), 2050071, (2020). [CrossRef]
[20] Podlubny, I. Fractional Differential Equations. *Academic Press New York*, (1999).
[21] Naik, P.A., Zu, J., Owolabi, K.M. Global dynamics of a fractional order model for the transmission of HIV epidemic with optimal control. *Chaos, Solitons & Fractals*, 138, 109826, (2020). [CrossRef]
[22] Jin, B., Lazarov, R. & Zhou, Z. An analysis of the L1 scheme for the subdiffusion equation with nonsmooth data. *IMA Journal of Numerical Analysis*, 36(1), 197-221, (2016). [CrossRef]
[23] Du, M. & Wang, Z. Correcting the initialization of models with fractional derivatives via history-dependent conditions. *Acta Mechanica Sinica*, 32(2), 320-325, (2016). [CrossRef]
[24] Magin, R.L. Fractional Calculus in Bioengineering. Redding: Begell House, (2006).
[25] Ahmed, E., El-Sayed, A.M.A., El-Saka, H.A.A. Equilibrium points, stability and numerical solutions of fractional-order predator–prey and rabies models. *Journal of Matematical Analysis and Applications*, 325(1), 542-553, (2007). [CrossRef]
[26] El-Sayed, A.M.A., El-Mesiry, A.E.M., El-Saka, H.A.A. On the fractional- order logistic equation. *Applied Mathematics Letters*, (20), 817-823, (2007). [CrossRef]
[27] Petras, I. Fractional-Order Nonlinear Systems: Modeling, Analysis and Simulation. Springer Berlin, (2011).
[28] Baisad, K., Moonchai, S. Analysis of stability and hopf bifurcation in a fractional Gauss-type predator-prey model with Allee effect and Holling type-III functional response. *Advances in difference equations*, 2018(1), 1-20, (2018). [CrossRef]
[29] Daşbaşı, B., Öztürk, İ. & Özköse, F. Çoklu Antibiyotik Tedavisiyle Bakteriyel Rekabetin Matematiksel Modeli ve Kararlılık Analizi. *Karaelmas Science and Engineering Journal*, 6(2), 299-306, (2016). [CrossRef]
[30] Bozkurt, F. & Özköse, F. Stability analysis of macrophage-tumor interaction with piecewise constant arguments. *In AIP Conference Proceedings*, (Vol. 1648, No. 1, p. 850035), AIP Publishing LLC, (2015, March). [CrossRef]
[31] Özköse, F., Yılmaz, S., Yavuz, M., Öztürk, İ., Şenel, M.T., Bağcı, B.Ş. & Doğan, M., Önal, Ö. A fractional modelling of tumor-immune system interaction related to lung cancer with real data. *The European Physical Journal Plus*, (2022).
[32] Diethelm, K. An algorithm for the numerical solution of differential equations of fractional order. *Electronic transactions on numerical analysis*, 5(1), 1-6, (1997). [CrossRef]
[33] Diethelm, K., Ford, N.J., Freed, A.D. A predictor-corrector approch for the numerical solution of fractional differential equations. *Nonlinear Dynamics*, 29, 3-22, (2002). [CrossRef]
[34] Garrappa, R. On linear stability of predictor-corrector algorithms for fractional differential equations. *International Journal of Computer Mathematics*, 87(10), 2281-2290, (2010). [CrossRef]

Mathematical Modelling and Numerical Simulation with Applications (MMNSA) (http://www.mmnsa.org)

Mathematical Modelling and Numerical Simulation with Applications, 2021, 1(2), 84–94

https://www.mmnsa.org
ISSN Online: 2791-8564 / Open Access
https://doi.org/10.53391/mmnsa.2021.01.008

RESEARCH PAPER

Chaos of calcium diffusion in Parkinson's infectious disease model and treatment mechanism via Hilfer fractional derivative

Hardik Joshi[1,*,†,‡] and Brajesh Kumar Jha[2,†,‡]

[1]Department of Mathematics, LJ Institute of Engineering and Technology, LJ University, Ahmedabad-382210, Gujarat, India , [2]Department of Mathematics, School of Technology, Pandit Deendayal Energy University, Gandhinagar-382007, Gujarat, India

*Corresponding Author
†hardik.joshi8185@gmail.com (Hardik Joshi); brajeshjha2881@gmail.com (Brajesh Kumar Jha)
‡Contributed equally.

Abstract

Calcium is a vital element in our body and plays a crucial role to moderate the calcium signalling process. Calcium-dependent protein and flux through the sodium-calcium exchanger are also involved in signalling process to perform and execute necessary cellular activities. The loss or alteration in this cellular activity starts the early progress of Parkinson's disease. A mathematical calcium model is developed in the form of the Hilfer fractional reaction-diffusion equation to examine the calcium diffusion in the cells. The effect of calcium-dependent protein and flux through the sodium-calcium exchanger is incorporated in the model. The solution of the Hilfer fractional calcium model is obtained by using the Sumudu transform technique in the form of the Wright function and Mittag-Leffler function. The graphical results are obtained for the different amounts of proteins, presence, and absence of sodium-calcium exchanger, and various orders of Hilfer derivative. The obtained results show that the modified calcium model is a function of time, position, and Hilfer fractional derivative. Thus the modified Hilfer calcium model provides a rich physical interpretation of a calcium model as compared to the classical calcium model.

Key words: Calcium; sodium-calcium exchanger; Parkinson's disease; Hilfer fractional derivative; Sumudu transform
AMS 2020 Classification: 26A33; 35Q92; 35R11; 92B05

1 Introduction

Neurons a main component of the brain also refer as nerve cells that transfer the message from the brain to other parts in the form of electrochemical gradient and vice versa. The major part of a neuron is made by a combination of a cell body, axon, and dendrite. Dendrite is a long tree like structure that receives information from the other neurons and is passed to the cell body. The cell body is a central part of the neuron that analyzed the received information and prepared a necessary outcome. The axon received the outcomes and carries them to other neurons. This is the basic life cycle of a typical neuron. Our brain consists of around 80-90 billion neurons so it made a complex neuronal network to perform and execute cellular activities [1]. Besides neuron, astrocytes and glial cells are also supports and moderate the requisite cellular activities [2].

Calcium is also known as the second messenger and it is found in almost all kinds of nerve cells such as a neuron, astrocytes, oocytes, and many others. Calcium diffusion is a very dynamic process in the cells to understand the calcium signalling phenomena. Calcium diffuses

➤ **Received:** 06.11.2021 ➤ **Revised:** 06.12.2021 ➤ **Accepted:** 07.12.2021 ➤ **Published:** 16.12.2021

into the cell and reacts with protein, channels, pumps, and many other cellular entities. Due to the complexity, we have incorporated the flux through a sodium calcium exchanger in the presence of protein only. They diffused and produce the calcium depending protein as per a requirement of the calcium signalling process. The cytosol feels like a full of free calcium then the calcium buffering phenomena convert the level of free calcium into calcium dependent protein. That generated protein is utilized for fertilization, cell differentiation, synaptogenesis, and so on [3, 4]. The sodium calcium exchanger is also one of the major sources to transform free calcium from the cytosol to cells. They exchange three sodium ions against one calcium ion. That is three sodium ions enter into the cytosol and one calcium ion exists from the cytosol. In the present study, we have considered the sodium calcium exchanger with an exchange ratio of $3Na^{+} : 1Ca^{++}$ [5, 6, 7]. The alteration in the process to manage free calcium in the cells for long periods may result in various neurological diseases namely Parkinson's, Alzheimer's, Amyotrophic lateral sclerosis, etc [8, 9]. Parkinson's disease (PD) is a disorder of the nervous system strongly associated with the dysfunction or alteration of calcium signalling. There is numerous factor associated with it such as environmental effect, age, gene mutation, misfolded protein sequence, calcium homeostasis, etc [10, 11, 12].

Panday and Pardasani have employed the finite element method to study the role of sodium calcium exchanger on calcium diffusion in oocytes cells [5]. Tewari and Pardasani have employed Gear's method to study the role of sodium calcium exchanger, calcium channel, plasma membrane, sodium pump and buffer on calcium diffusion in neuron cells [6]. Jha et al. have employed the finite element method to study the role of sodium calcium exchanger by considering a point source and line source of calcium flux on calcium diffusion in neuron cells [7]. Also, there have been several experimental attempts that were performed in the past to identify the role and physiological impact of sodium calcium exchangers on various cells [13, 14, 15, 16]. Beside this a researches has explored the role of parameters of calcium toolkits on astrocytes [17, 18, 19, 20, 21, 22], neuron [23, 24, 25, 26, 27, 28, 29, 30], oocytes [31, 32], myocytes [33, 34, 35], hepatocytes [36], and *T* lymphocytes cells [37, 38]. Thus a very little amount of work has attempted to study parameters of calcium toolkits by using the fractional calculus approach. Also, the literature suggests that none of the researchers and scientists has studied the effect of sodium calcium exchanger and protein on calcium diffusion and related to Parkinson's disease. Therefore, in this paper, we have studied the role of sodium calcium exchanger and calcium dependent protein on calcium diffusion by using the fractional calculus approach.

The fractional calculus is a generalization of the integer-order calculus and it provides more accurate results as compared to classical calculus. Hence, it is widely used in mathematical modelling of science and engineering, medical, and almost all area of education [39, 40, 41, 42, 43, 44, 45, 46, 47, 48, 49, 50, 51, 52, 53, 54, 55, 56, 57, 58, 59, 60]. Nowadays, numbers of the fractional derivative are available to deal with real-world problems such as Caputo derivative, Caputo-Fabrizio derivative, Atangana-Baleneu derivative, Hilfer derivative, Weyl derivative, Conformable derivative and many more. We have used the Hilfer fractional derivative in this study because it is a generalization of the Caputo and Riemann-Liouville derivatives [61]. Also, there are a number of effective methods such as differential transform method, double Laplace transform, Fourier transform method, Sumudu transform method, iterative method, Adomian decomposition method, homotopy transform method, and many more. We have used the Sumudu transform method in this study because it is best to our problems and it provides a closed form solution of the calcium model in terms of Wright function and Mittag-Leffler function.

The structure of this study is as follows. In Section 2, we provide some basic definitions that are used in this study. In Section 3, we develop a mathematical formulation of the calcium model then, we modify the model in the sense of the Hilfer fractional calcium model. The results are obtained in Section 4 for different amounts of calcium protein and sodium calcium exchanger. In the last Section 5, some conclusions are derived from the proposed results.

2 Mathematical preliminaries

The mathematical model developed in the present study is solved by using the Hilfer fractional derivative and Sumudu transform technique. The basic definitions of the Hilfer derivative and Sumudu transform are provided here that can be used to solve the model [61, 62, 63, 64].

Definition 1 *The Riemann-Liouville fractional order integral for a function $y(t)$ is defined as*

$$I_a^u(y(t)) = \frac{1}{\Gamma(u)} \int_a^t (t-\xi)^{u-1} y(\xi) d\xi, \tag{1}$$

where $t > a$, and $R(u) > 0$.

Definition 2 *The Riemann-Liouville fractional order derivative for a function $y(t)$ of order u is defined as*

$${}_a^{RL}D_t^u(y(t)) = \left(\frac{d}{dt}\right)^n (I_a^{n-u} y(t)), \tag{2}$$

where $R(u) > 0$.

Definition 3 *The Caputo fractional order derivative for a function $y(t)$ of order u is defined as*

$${}_a^{C}D_t^u(y(t)) = \begin{cases} \frac{1}{\Gamma(m-u)} \int_a^t \frac{y^m(\xi)}{(t-\xi)^{u+1-m}} d\xi, & m-1 < u \le m, \\ \frac{d^m}{dt^m} y(t), & u = m, \end{cases} \tag{3}$$

where $R(u) > 0$ and $m \in N$.

Definition 4 *The Hilfer fractional derivative for a function $y(t)$ is defined as*

$$ {}^{H}_{a}D^{u,v}_{t}(y(t)) = I^{v(1-u)}_{t}\frac{\partial}{\partial t}(I^{(1-v)(1-u)}_{t}y(t)), 0 < u < 1, 0 \leq v \leq 1. \tag{4}$$

Remark 1 *The Hilfer fractional derivative is a generalization of the Riemann-Liouville and Caputo fractional definition. The Riemann-Liouville and Caputo fractional definitions are recovered by setting $v = 0$ and $v = 1$ respectively in equation (4).*

Definition 5 *Let consider a set A over the function $y(t)$ as*

$$A = \{y(t) : \exists M, \tau_1, \tau_2 > 0, |y(t)| < Me^{t/\tau_j}, t \in (-1)^j \times [0, \infty)\}, \tag{5}$$

then the Sumudu transform of function $y(t)$ over the set A is defined as

$$S\{y(t)\} = Y(p) = \int_0^\infty \frac{1}{p}e^{-\frac{t}{p}}y(t)dt, p \in (-\tau_1, \tau_2). \tag{6}$$

Definition 6 *The inverse Sumudu transform of function $Y(p)$ is defined as follows*

$$S^{-1}\{Y(p)\} = y(t) = \frac{1}{2\pi i}\int_{\gamma-i\infty}^{\gamma+i\infty} e^{\frac{t}{p}}Y(p)dp, \tag{7}$$

where $\gamma \in R$ is a fixed number.

3 Mathematical formulation of the calcium model

The calcium in the cytosol is diffuse with protein and produces a different chemical species that modulate the cellular process and is represented by the chemical equation as

$$Ca^{2+} + B_i \underset{k^-}{\overset{k^+}{\leftrightarrow}} CaB_i, \tag{8}$$

where Ca^{2+} represents calcium ion, B_i represents the proteins calbindin-D_{28k}, and CaB_i represents the produced calcium dependent protein.

The calcium flow in the cell at any position and time is determined by the following partial differential equation [23, 31, 32, 33]

$$\frac{\partial}{\partial t}[Ca^{2+}] = D_{Ca}\frac{\partial^2}{\partial x^2}[Ca^{2+}] + \sum_i R_i + f. \tag{9}$$

The rate of change of calcium is denoted by the first order derivative with time, the diffusion of calcium is denoted by the Laplacian operator, D_{Ca} is the diffusion coefficient, f denoted the calcium source from cellular entities, whereas the summation corresponds to multiple proteins and reaction term is a combination of chemical reactant and it is described as

$$R_i = -k^+[B_i][Ca^{2+}] + k^-[CaB_i]. \tag{10}$$

The similar chemical reaction for the proteins and calcium dependent protein follows the Fickian diffusion mechanism and is defined as [65, 66]

$$\frac{\partial}{\partial t}[B_i] = D_B \cdot \frac{\partial^2}{\partial x^2}[B_i] + R_i, \tag{11}$$

$$\frac{\partial}{\partial t}[CaB_i] = D_{CaB_i} \cdot \frac{\partial^2}{\partial x^2}[CaB_i] - R_i, \tag{12}$$

where D_B and D_{CaB_i} represent a diffusion coefficient of proteins and calcium dependent protein, respectively.

Thus to identify the calcium flow in the cell at any moment it is necessary to solve the given system of partial differential equation

$$\begin{aligned} &\tfrac{\partial}{\partial t}[Ca^{2+}] = D_{Ca}\tfrac{\partial^2}{\partial x^2}[Ca^{2+}] + \textstyle\sum_i R_i + f, \\ &\tfrac{\partial}{\partial t}[B_i] = D_B \cdot \tfrac{\partial^2}{\partial x^2}[B_i] + R_i, \\ &\tfrac{\partial}{\partial t}[CaB_i] = D_{CaB_i} \cdot \tfrac{\partial^2}{\partial x^2}[CaB_i] - R_i. \end{aligned} \tag{13}$$

Modified calcium model in form of Hilfer fractional derivative

The classical model is replaced by Hilfer fractional model to catch the memory of cells that increase the complexity of a model but simultaneously increase the accuracy of a model. The classical calcium model (13) become as

$$\begin{aligned} {}_0^H D_t^{\alpha,\beta}[Ca^{2+}](x,t) &= D_{Ca}\frac{\partial^2}{\partial x^2}[Ca^{2+}](x,t) + \sum_i R_i + f(x,t), \\ {}_0^H D_t^{\alpha,\beta}[B_i](x,t) &= D_B \cdot \frac{\partial^2}{\partial x^2}[B_i](x,t) + R_i(x,t), \\ {}_0^H D_t^{\alpha,\beta}[CaB_i](x,t) &= D_{CaB_i} \cdot \frac{\partial^2}{\partial x^2}[CaB_i](x,t) - R_i(x,t), \end{aligned} \tag{14}$$

where $0 < \alpha < 1, 0 \leq \beta \leq 1$.

The molecular weight of calcium is very small as compared to proteins and calcium dependent proteins. Hence by using this assumption we have $D_B = D_{CaB_i} = D_i$ and we get the following equation

$${}_0^H D_t^{\alpha,\beta}[B_i]_T(x,t) = D_i\frac{\partial^2}{\partial x^2}[B_i]_T(x,t), \tag{15}$$

where $[B_i]_T = [B_i] + [CaB_i]$.

The background concentration of proteins and calcium dependent protein in the terms of a total concentration and dissociate constant are given as [66]

$$[B_i]_\infty = \frac{K[B_i]_T}{K + [Ca^{2+}]_\infty}, \tag{16}$$

and

$$[CaB_i]_\infty = \frac{[Ca^{2+}]_\infty[B_i]_T}{K + [Ca^{2+}]_\infty}, \tag{17}$$

where $K = k^-/k^+$.

Thus by combining equations (15-17) the model (14) is converted to a Hilfer fractional reaction diffusion equation which is given as

$${}_0^H D_t^{\alpha,\beta}[Ca^{2+}](x,t) = D_{Ca}\frac{\partial^2}{\partial x^2}[Ca^{2+}](x,t) - \sum_i k_i^+[B_i]_\infty([Ca^{2+}](x,t) - [Ca^{2+}]_\infty) + f(x,t), \tag{18}$$

where $0 < \alpha < 1, 0 \leq \beta \leq 1$.

The sodium calcium exchanger flux is considered in the model whose electrochemical gradient is involved in the signalling phenomena. There are two valence ions of calcium they provide the given equation [5, 6, 7]

$$\Delta\mu_{Ca} = ZFV_m + RT\ln\left(\frac{Ca_i}{Ca_o}\right). \tag{19}$$

Similarly, there is one valence ion of sodium they generate the following equation as a result of electrochemical gradient as

$$\Delta\mu_{Na} = ZFV_m + RT\ln\left(\frac{Na_i}{Na_o}\right). \tag{20}$$

The exchange ratio of sodium and calcium ion is 3:1 that is three sodium ions enter into the cytosol and one calcium ion removed from the cytosol. The mathematical expression of the sodium calcium exchange ratio is given as

$$3\Delta\mu_{Na} = 1\Delta\mu_{Ca}. \tag{21}$$

By combining the electrochemical gradient and sodium calcium exchange ratio the equation (19-21) becomes as

$$2FV_m + RT\ln\left(\frac{Ca_i}{Ca_o}\right) = 3FV_m + 3RT\ln\left(\frac{Na_i}{Na_o}\right). \tag{22}$$

The rearrangement of equation (22) gives us the following equation

$$\frac{Ca_i}{Ca_o} = \left(\frac{Na_i}{Na_o}\right)^3 e^{\frac{FV_m}{RT}}. \tag{23}$$

Thus the mathematical expression for the sodium calcium flux becomes

$$f_{NCX} = Ca_o\left(\frac{Na_i}{Na_o}\right)^3 e^{\frac{FV_m}{RT}}, \tag{24}$$

where Ca_i, Ca_o, Na_i and Na_o are the intracellular and extracellular flux from the respective ions. By incorporating the flux through sodium calcium exchanger into the model the equation (18) becomes

$$ {}_0^H D_t^{\alpha,\beta}[Ca^{2+}](x,t) = D_{Ca}\frac{\partial^2}{\partial x^2}[Ca^{2+}](x,t) - \sum_i k_i^+[B_i]_\infty([Ca^{2+}](x,t) - [Ca^{2+}]_\infty) - f_{NCX}. \tag{25} $$

The initial and boundary conditions of a problem are as

$$ \lim_{x\to 0}\left(-D_{Ca}\frac{\partial}{\partial x}[Ca^{2+}]\right) = \sigma_{Ca}, t > 0, \tag{26} $$

$$ \lim_{x\to\infty}\left([Ca^{2+}]\right) = [Ca^{2+}]_\infty, t \geq 0, \tag{27} $$

$$ [Ca^{2+}]\Big|_{t=0} = 0, 0 \leq x < \infty. \tag{28} $$

For sake of simplicity the equation (25) rewritten as

$$ {}_0^H D_t^{\alpha,\beta}C(x,t) = D_{Ca}\frac{\partial^2}{\partial x^2}C(x,t) - \xi\cdot C(x,t) + \psi, \tag{29} $$

where $0 < \alpha < 1, 0 \leq \beta \leq 1, \xi = k^+[B_i]_\infty$, and $\psi = k^+[B_i]_\infty C_\infty - Ca_o\left(\frac{Na_i}{Na_o}\right)^3 e^{\frac{FV_m}{RT}}$.

The corresponding initial and boundary condition are

$$ \lim_{x\to 0}\left(\frac{\partial C}{\partial x}\right) = -\frac{\sigma_{Ca}}{D_{Ca}}, t > 0, \tag{30} $$

$$ \lim_{x\to\infty} C(x,t) = C_\infty, t \geq 0, \tag{31} $$

$$ C(x,0) = 0, 0 \leq x < \infty. \tag{32} $$

Applying Sumudu transform on both sides of equation (29) with respect to time then we get

$$ s^{-\alpha}\bar{C}(x,s) - s^{-1+\beta(1-\alpha)}\sum_{k=0}^{0}\frac{\partial^k}{\partial x^k}\left(I_0^{(1-\beta)(1-\alpha)}C(x,0)\right) = D_{Ca}\frac{\partial^2}{\partial x^2}\bar{C}(x,s) - \xi\cdot\bar{C}(x,s) + \psi, \tag{33} $$

Using the initial condition (32), equation (33) can be written as

$$ s^{-\alpha}\bar{C}(x,s) = D_{Ca}\frac{\partial^2}{\partial x^2}\bar{C}(x,s) - \xi\cdot\bar{C}(x,s) + \psi, \tag{34} $$

The equation (34) can be rewritten as

$$ \frac{\partial^2}{\partial x^2}\bar{C}(x,s) - \frac{1}{D_{Ca}}\left(s^{-\alpha}\bar{C}(x,s) - \xi\cdot\bar{C}(x,s) + \psi\right) = 0, \tag{35} $$

Further simplification of equation (35) lead us to the given equation

$$ \frac{\partial^2}{\partial x^2}\bar{C}(x,s) - \frac{s^{-\alpha}-\xi}{D_{Ca}}\bar{C}(x,s) - \frac{\psi}{D_{Ca}} = 0, \tag{36} $$

Thus the Sumudu transform of the equation (29) is obtained as

$$ \bar{C}(x,s) = C_1\exp\left(\sqrt{\frac{s^{-\alpha}-\xi}{D_{Ca}}}\right)x + C_2\exp\left(-\sqrt{\frac{s^{-\alpha}-\xi}{D_{Ca}}}\right)x - \frac{\psi}{s^{-\alpha}-\xi}, \tag{37} $$

By Applying the Sumudu transform on the boundary conditions (30-31), we get

$$ \frac{\partial}{\partial x}\bar{C}(0,s) = -\frac{\sigma_{Ca}}{D_{Ca}}, \tag{38} $$

and

$$\lim_{x\to\infty} \bar{C}(x,s) = 0. \tag{39}$$

By using equations (38-39), equation (37) turns out to be

$$\bar{C}(x,s) = \frac{\sigma_{Ca}}{\sqrt{D_{Ca}}} s^{\alpha/2} \exp\left(-\sqrt{\frac{s^{-\alpha}-\xi}{D_{Ca}}}\right) x - \frac{\psi}{s^{-\alpha}-\xi}, \tag{40}$$

To invert the Sumudu transform of equation (40) we use the following inequalities [64]

$$S^{-1}\left(p^{\alpha/2} e^{-\lambda p^{-\alpha/2}}\right) = t^{\alpha/2} W\left(-\frac{\alpha}{2}, \frac{\alpha}{2}+1, -\lambda t^{-\alpha/2}\right), \tag{41}$$

and

$$S^{-1}\left(\frac{p^{\beta-1}}{1-\lambda p^{\alpha}}\right) = t^{\beta-1} E_{\alpha,\beta}(\lambda t^{\alpha}), \tag{42}$$

By using equations (41-42) the inverse Sumudu transform of equation (40) gives the following results

$$C(x,t) = \frac{\sigma_{Ca}}{\sqrt{D_{Ca}}} e^{\sqrt{\frac{\xi}{D_{Ca}}}} t^{\alpha/2} W\left(-\frac{\alpha}{2}, \frac{\alpha}{2}+1, -\frac{x}{\sqrt{D_{Ca}}} t^{-\alpha/2}\right) - \psi t^{\alpha} E_{\alpha,\alpha+1}(\xi t^{\alpha}), \tag{43}$$

where $W(\alpha, \beta, \gamma)$ and $E_{\alpha,\beta}(z)$ are the Wright function and Mittag-Leffler function for two parameters respectively [61, 62, 63].

4 Results and discussion

The numerical values for the physical parameters are given in Table 1 and are used in the computation of the calcium profile.

Table 1. Values of physical parameters [5, 6, 7, 66]

Parameters	Values of parameters
Diffusion coefficient (D_{Ca})	200-300 ($\mu m^2/s$)
Buffer associate rate (k^+)	75 ($\mu M^{-1}s^{-1}$)
Concentration of protein ($[B_i]_\infty$)	100-360 (μM)
Intracellular sodium ($[Na^+])_i$	12 (mM)
Extracellular sodium ($[Na^+])_o$	145 (mM)
Intracellular calcium ($[Ca^{2+}])_i$	0.1 (μM)
Extracellular calcium ($[Ca^{2+}])_o$	1.8 (mM)
Source amplitude of calcium (σ_{Ca})	1.4 ($\mu M^{-1}s^{-1}$)
Faraday's constant (F)	96485 (C/mol)
Gas constant (R)	8.314 (J)
Temperature (T)	310 (^oK)
Membrane potential (V_m)	-0.06 (V)

The solution (43) of the modified calcium model (14) in form of Hilfer fractional derivative is used to obtain a graphical calcium profile for low and high proteins level and sodium calcium exchanger. The calcium profile simulated for the values $D_{Ca} = 250\mu m^2/s$, low protein level $[B_i]_\infty = 120\mu M$, high protein level $[B_i]_\infty = 340\mu M$ and for various values of α in Figures 1 to 6. Figures 1-3 show variations of calcium versus time for different biophysical parameters whereas Figures 4-6 show variations of calcium versus position for different biophysical parameters.

In Figure 1 we show calcium profile versus time near the source $x = 0$ for the low level of proteins level and presence of sodium calcium exchanger. The calcium profile is high for the lower values of fractional order up to 0.35 seconds then the calcium profile is high for the higher values of α and after 0.7 seconds the calcium profile achieves the steady level.

Figure 2 shows calcium profile versus time near the source $x = 0$ for a high level of proteins and presence of sodium calcium exchanger. The profile suddenly attains the peak near 0.1 second due to high level of proteins then decrease gradually to attain a steady level. The peak level of calcium profile in figure 2 is less compared to figure 1. This happened due to high proteins reacting with calcium in cytosol and producing calcium dependent protein that reduce the peak values of calcium profile and protect the neuron cells from the high level of calcium. A high level of calcium for large periods is toxic for cells and generates the symptoms of Parkinson's disease.

Figure 3 represents the calcium profile versus time for the low level of proteins level and absence of sodium calcium exchanger. The profile gradually rise and achieved a peak value due to low protein level. The profile attains more peak values as compared to Figure 1 due to the absence of sodium calcium exchanger as it removed the calcium from the cells against sodium. Thus the presence of sodium calcium

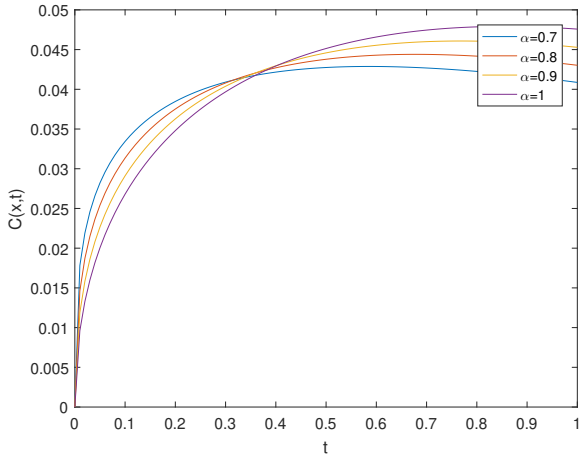

Figure 1. Calcium profile versus time for low amount of proteins at different values of α

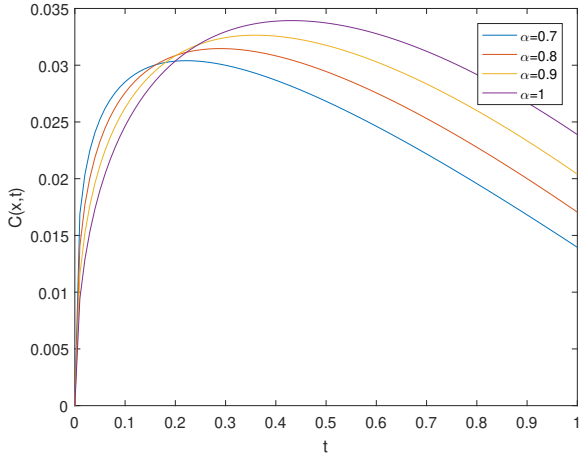

Figure 2. Calcium profile versus time for high amount of proteins at different values of α

exchanger plays a significant role in the presence of low proteins as high protein level reduces the significance of sodium calcium exchanger.

In Figure 4 we show calcium profile versus position for a $t = 0.5$ second at low proteins level and presence of sodium calcium exchanger. The calcium profile is high at the mouth of channels and slowly decrease as the position is increased. The profile is high for large values of α in the cells as the fractional order decreases the calcium profile also decreases and attains a steady level.

Figure 5 shows calcium profile versus position at $t = 0.5$ second for high proteins level and presence of sodium calcium exchanger. The profile is high at the mouth of the channel due to the high level of proteins then decreasing gradually to attain a steady level. The peak level of calcium profile in figure 5 is less compared to figure 4. The physiological results for this are the same as given in figure 2 that is high level proteins react with calcium and produce calcium protein that reduces the calcium profile and protect the cells from toxic level and symptoms of Parkinson's disease.

Figure 6 shows calcium profile versus position for low proteins level and absence of sodium calcium exchanger. The profile is at a peak level at the beginning due to the absence of sodium calcium exchanger as it did not remove the free calcium from the cells. The absence of sodium calcium exchanger and low proteins level results in an elevation in the calcium profile. It is observed that the sodium calcium exchanger is a good source of calcium flux to control the free calcium level in the cells and ultimately protect cells against Parkinson's disease.

The obtained results (43) show that the modified calcium model (14) is a function of time, position and Hilfer fractional derivative. Also, the graphical results show that the modified Hilfer calcium model provides a rich physical interpretation of a calcium model as compared to the classical calcium model.

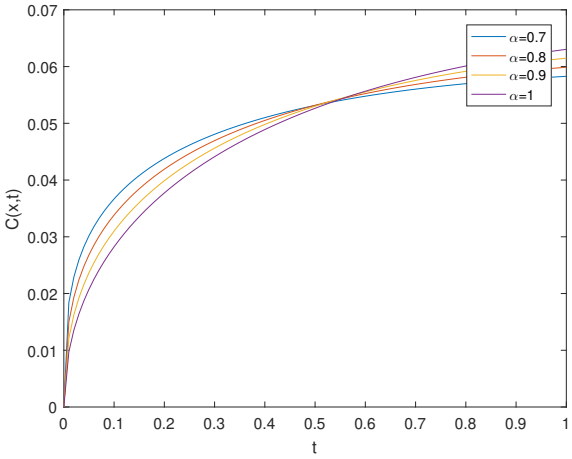

Figure 3. Calcium profile versus time for low amount of proteins and in absence of sodium calcium exchanger at different values of α

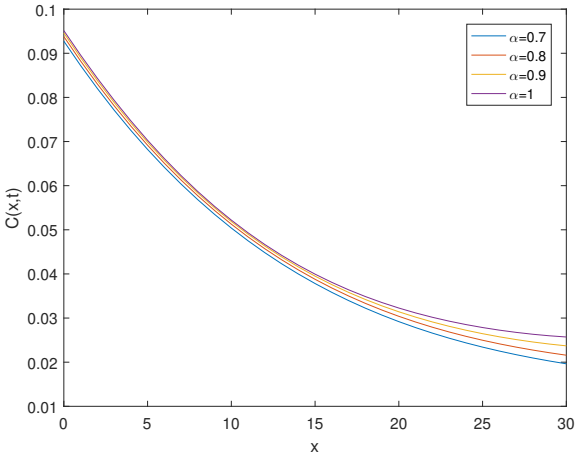

Figure 4. Calcium profile versus position for low amount of proteins at different values of α

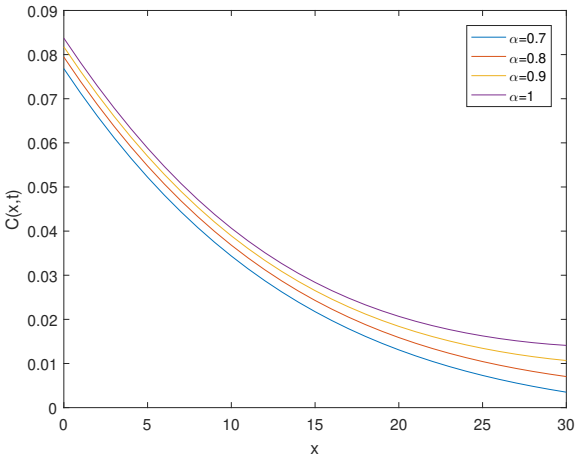

Figure 5. Calcium profile versus position for high amount of proteins at different values of α

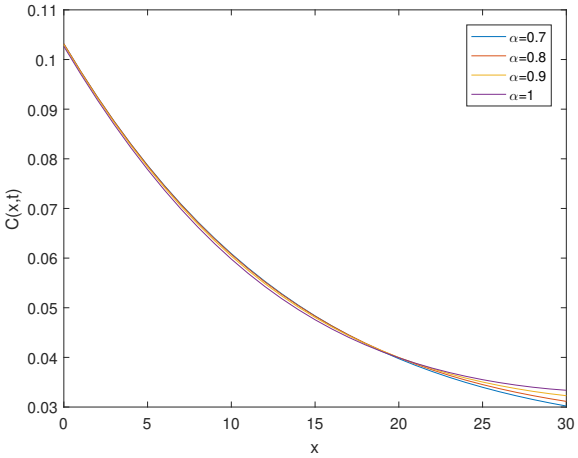

Figure 6. Calcium profile versus position for low amount of proteins and in absence of sodium calcium exchanger at different values of α

5 Conclusion

Hilfer fractional calcium model is a novel modification of the classical calcium model for neuron cells. We developed a Hilfer fractional calcium model to examine the role of calcium dependent protein, sodium calcium exchanger on calcium diffusion and related to Parkinson's disease. We obtained a closed form solution of the calcium model in the terms of Wright function and Mittag-Leffler function by using the Sumudu transform technique and Hilfer fractional derivative. High level proteins react with the calcium in cytosol and produce calcium dependent proteins that reduce the peak values of calcium profile and protect the neuron cells from the high level of calcium. A high level of calcium for large periods is toxic for cells and generates the symptoms of Parkinson's disease. The significant effect of sodium calcium exchanger has been observed for the low level of calcium dependent protein. The calcium dependent protein and sodium calcium exchanger play a crucial role to control the calcium level in the cytosol. Thus the amalgamation of the calcium dependent protein and sodium calcium exchanger control the calcium level and provide protection to neuron cell from the toxicity produced by the Parkinsonic cells. Thus Hilfer calcium model provides a rich physical interpretation of a calcium model as compared to the classical calcium model. The present model can be extended by considering the flux through various calcium channels, pumps, and receptors. A novel fractional model will be developed by considering the flux through all these parameters and expresses the obtained results with Parkinson's disease.

Declarations

Consent for publication

Not applicable.

Conflicts of interest

The authors declare that they have no conflict of interests.

Funding

Not applicable.

Author's contributions

H.J.: Conceptualization, Methodology, Investigation, Visualization, Writing, Software, Original draft preparation, Validation, Writing-Reviewing and Editing. B.K.J.: Conceptualization, Supervision, Validation, Writing-Reviewing and Editing. All authors discussed the results and contributed to the final manuscript.

Acknowledgements

The authors would like to thank the editor and reviewers for their fruitful comments and suggestions that improve the quality of the manuscript.

References

[1] Squire L.R., Berg D., Bloom F. E., Du Lac S., Ghosh A., and Spitzer N. C., *Fundamental Neuroscience*, (Vol. 4). Elsevier Inc., (2012).
[2] Verkhratsky A. & Butt A. *Glial neurobiology: a textbook*, John Wiley and Sons, (2007).

[3] Petersen, O.H., Michalak, M. & Verkhratsky A. Calcium signalling: past, present and future. *Cell Calcium*, 38(3-4), 161–169, (2005). [CrossRef]
[4] Clapham, D.E. Calcium Signaling. *Cell*, 131(6), 1047–1058, (2007). [CrossRef]
[5] Panday, S. & Pardasani, K.R. Finite element model to study effect of advection diffusion and Na +/Ca2+ exchanger on Ca2+ distribution in oocytes. *Journal of Medical Imaging and Health Informatics*, 3(3), 374–379, (2013). [CrossRef]
[6] Tewari, S.G. & Pardasani, K.R. Modeling effect of sodium pump on calcium oscillations in neuron cells. *Journal of Multiscale Modelling*, 4(3), 1250010, (2012). [CrossRef]
[7] Jha, A., Adlakha, N. & Jha, B.K. Finite element model to study effect of Na+ - Ca2+ exchangers and source geometry on calcium dynamics in a neuron cell. *Journal of Mechanics in Medicine and Biology*, 16(2), 1–22, (2015). [CrossRef]
[8] Mattson, M.P. Calcium and neurodegeneration. *Aging Cell*, 6(3), 337–350, (2007). [CrossRef]
[9] Bezprozvanny, I. Calcium signaling and neurodegenerative diseases. *Trends in molecular medicine*, 15(3), 89–100, (2009). [CrossRef]
[10] Surmeier, D.J. Calcium, ageing, and neuronal vulnerability in Parkinson's disease. *The Lancet Neurology*, 6(10), 933–938, (2007). [CrossRef]
[11] Zaichick, S.V., McGrath, K.M. & Caraveo, G. The role of Ca2+ signaling in Parkinson's disease. *Disease Models & Mechanisms*, 10(5), 519–535, (2017). [CrossRef]
[12] Calì, T., Ottolini, D. & Brini, M. Calcium signaling in Parkinson's disease. *Cell and tissue research*, 357(2), 439–454, (2014). [CrossRef]
[13] Blaustein, M.P. & Lederer, W.J. Sodium/calcium exchange: Its physiological implications. *Physiological Reviews*, 79(3), 763–854, (1999). [CrossRef]
[14] Sato, D., Despa, S. & Bers, D.M. Can the sodium-calcium exchanger initiate or suppress calcium sparks in cardiac myocytes? *Biophysical journal*, 102(8), L31–L33, (2012). [CrossRef]
[15] Philipson, K.D. & Nicoll, D.A. Sodium-calcium exchange: a molecular perspective. *Annual review of physiology*, 62(1), 111–133, (2000). [CrossRef]
[16] Noble, D., Noble, S.J., Bett, G.C.L., Earm, Y.E., Ho, W.K. & So, I.K. The Role of Sodium - Calcium Exchange during the Cardiac Action Potential a. *Annals of the New York Academy of Sciences*, 639(1), 334–353, (1991). [CrossRef]
[17] Jha, B.K., Adlakha, N. & Mehta, M.N. Two-Dimensional Finite Element Model To Study Calcium Distribution in Astrocytes in Presence of VGCC and Excess Buffer. *International Journal of Modeling, Simulation, and Scientific Computing*, 4(2), 1250030, (2013).
[18] Jha, B.K. & Jha, A. Two dimensional finite element estimation of calcium ions in presence of NCX and Buffers in Astrocytes. *Boletim da Sociedade Paranaense de Matemática*, 36(1), 151–160, (2018). [CrossRef]
[19] Jha, B.K., Jha, A. & Adlakha, N. Three-Dimensional Finite Element Model to Study Calcium Distribution in Astrocytes in Presence of VGCC and Excess Buffer. *Differential Equations and Dynamical Systems*, 28(3), 603–616,(2020).
[20] Jha, B.K., Adlakha, N. & Mehta, M.N. Two-dimensional finite element model to study calcium distribution in astrocytes in presence of excess buffer. *International Journal of Biomathematics*, 7(03), 1450031, (2014).
[21] Gill, V., Singh, Y., Kumar, D. & Singh, J. Analytical study for fractional Order mathematical model of concentration of Ca2+ in astrocytes cell with a composite fractional derivative. *Journal of Multiscale Modelling*, 11(3), 2050005, (2020). [CrossRef]
[22] Devi, A. & Jakhar, M. Analysis of Concentration of Ca2 + Arising in Astrocytes Cell. *International Journal of Applied and Computational Mathematics*, 7(1), 1–9, (2021). [CrossRef]
[23] Jha, A. & Adlakha, N. Two-dimensional finite element model to study unsteady state Ca2+ diffusion in neuron involving ER LEAK and SERCA. *International Journal of Biomathematics*, 8(01), 1550002, (2015). [CrossRef]
[24] Joshi, H. & Jha, B.K. Fractionally delineate the neuroprotective function of calbindin-28k in Parkinson's disease. *International Journal of Biomathematics*, 11(08), 1850103, (2018). [CrossRef]
[25] Joshi H. and Jha B. K. Generalized Diffusion Characteristics of Calcium Model with Concentration and Memory of Cells: A Spatiotemporal Approach. *Iranian Journal of Science and Technology, Transactions A: Science*, 1–14, (2021). [CrossRef]
[26] Joshi, H. & Jha, B.K. On a reaction–diffusion model for calcium dynamics in neurons with Mittag–Leffler memory. *The European Physical Journal Plus*, 136(6), 1–15, (2021). [CrossRef]
[27] Joshi, H. & Jha, B.K. Modeling the spatiotemporal intracellular calcium dynamics in nerve cell with strong memory effects. *International Journal of Nonlinear Sciences and Numerical Simulation*, (2021). [CrossRef]
[28] Joshi, H. & Jha, B.K. Fractional-order mathematical model for calcium distribution in nerve cells. *Computational and Applied Mathematics*, 39(2), 1–22, (2020). [CrossRef]
[29] Jha, B.K., Joshi, H. & Dave, D.D. Portraying the Effect of Calcium-Binding Proteins on Cytosolic Calcium Concentration Distribution Fractionally in Nerve Cells. *Interdisciplinary Sciences: Computational Life Sciences*, 10(4), 674–685, (2018). [CrossRef]
[30] Dave, D.D. & Jha, B.K. Mathematical Modeling of Calcium Oscillatory Patterns in a Neuron. *Interdisciplinary Sciences: Computational Life Sciences*, 13(1), 12–24, (2021). [CrossRef]
[31] Naik, P.A. & Pardasani, K.R. Finite element model to study calcium distribution in oocytes involving voltage gated Ca2 + channel, ryanodine receptor and buffers. *Alexandria Journal of Medicine*, 52(1), 43–49, (2016). [CrossRef]
[32] Naik, P.A. & Pardasani, K.R. Three-dimensional finite element Model to Study Effect of RyR Calcium Channel, ER Leak and SERCA Pump on calcium distribution in oocyte cell. *International Journal of Computational Methods*, 16(01), 1850091, (2019). [CrossRef]
[33] Pathak, K. & Adlakha, N. Finite element model to study two dimensional unsteady state calcium distribution in cardiac myocytes. *Alexandria Journal of Medicine*, 52(3), 261–268, (2016). [CrossRef]
[34] Chen, W., Aistrup, G., Wasserstrom J.A. & Shiferaw, Y. A mathematical model of spontaneous calcium release in cardiac myocytes. *American Journal of Physiology-Heart and Circulatory Physiology*, 300(5), H1794-H1805, (2011). [CrossRef]
[35] Singh, N. & Adlakha, N. A mathematical model for interdependent calcium and inositol 1,4,5-trisphosphate in cardiac myocyte. *Network Modeling Analysis in Health Informatics and Bioinformatics*, 8(1), 1–15, (2019). [CrossRef]
[36] Jagtap, Y. & Adlakha, N. Numerical study of one-dimensional buffered advection–diffusion of calcium and IP 3 in a hepatocyte cell. *Network Modeling Analysis in Health Informatics and Bioinformatics*, 8(1), 1–9, (2019). [CrossRef]
[37] Naik, P.A. & Zu, J. Modeling and simulation of spatial-temporal calcium distribution in T lymphocyte cell by using a reaction-diffusion equation. *Journal of bioinformatics and computational biology*, 18(2), 2050013, (2020). [CrossRef]
[38] Naik, P.A. Modeling the mechanics of calcium regulation in T lymphocyte: A finite element method approach. *International Journal of Biomathematics*, 13(05), 2050038, (2020). [CrossRef]

[39] Yavuz, M., Coşar, F.Ö., Günay F., & Özdemir, F.N. A new mathematical modeling of the COVID-19 pandemic including the vaccination campaign. *Open Journal of Modelling and Simulation*, 9(3), 299–321, (2021). [CrossRef]
[40] Özkose, F. & Yavuz M. Investigation of interactions between COVID-19 and diabetes with hereditary traits using real data: A case study in Turkey. *Computers in biology and medicine*, 105044, (2021). [CrossRef]
[41] Abboubakar, H., Kumar, P., Erturk V.S. & Kumar, A. A mathematical study of a tuberculosis model with fractional derivatives. *International Journal of Modeling, Simulation, and Scientific Computing*, 2150037, (2021). [CrossRef]
[42] Kumar, P. & Erturk, V.S. Environmental persistence influences infection dynamics for a butterfly pathogen via new generalised Caputo type fractional derivative. *Chaos, Solitons & Fractals*, 144, 110672, (2021). [CrossRef]
[43] Abboubakar, H., Kumar, P., Rangaig, N.A. & Kumar, S. A malaria model with Caputo-Fabrizio and Atangana-Baleanu derivatives. *International Journal of Modeling, Simulation, and Scientific Computing*, 12(2), 2150013, (2021). [CrossRef]
[44] Abu-Shady, M. & Kaabar, M.K. A Generalized Definition of the Fractional Derivative with Applications. *Mathematical Problems in Engineering*, 2021, (2021). [CrossRef]
[45] Debbouche, N., Ouannas, A., Batiha, I.M., Grassi, G., Kaabar, M.K., Jahanshahi, H., ... & Aljuaid, A.M. Chaotic Behavior Analysis of a New Incommensurate Fractional-Order Hopfield Neural Network System. *Complexity*, 2021, (2021). [CrossRef]
[46] Mohammadi, H., Kaabar, M.K.A, Alzabut, J., Selvam, A. & Rezapour, S. A Complete Model of Crimean-Congo Hemorrhagic Fever (CCHF) Transmission Cycle with Nonlocal Fractional Derivative. *Journal of Function Spaces*, 2021, (2021). [CrossRef]
[47] Kumar, P., Erturk, V.S., Banerjee, R., Yavuz, M. & Govindaraj, V. Fractional modeling of plankton-oxygen dynamics under climate change by the application of a recent numerical algorithm. *Physica Scripta*, 96(12), 124044, (2021). [CrossRef]
[48] Bonyah, E., Yavuz, M., Baleanu, D. & Kumar, S. A robust study on the listeriosis disease by adopting fractal-fractional operators. *Alexandria Engineering Journal*, 61(3), 2016-2028, (2021). [CrossRef]
[49] Veeresha, P. A Numerical Approach to the Coupled Atmospheric Ocean Model Using a Fractional Operator. *Mathematical Modelling and Numerical Simulation with Applications (MMNSA)*, 1(1), 1–10, (2021). [CrossRef]
[50] Erturk, V.S., Godwe, E., Baleanu, D., Kumar, P., Asad, J. & Jajarmi, A. Novel Fractional-Order Lagrangian to Describe Motion of Beam on Nanowire. *Acta Physica Polonica, A.*, 140(3), 265–272, (2021). [CrossRef]
[51] Allegretti, S., Bulai, I.M., Marino, R., Menandro, M.A. & Parisi, K. Vaccination effect conjoint to fraction of avoided contacts for a Sars-Cov-2 mathematical model. *Mathematical Modelling and Numerical Simulation with Applications (MMNSA)*, 1(2), 56–66, (2021). [CrossRef]
[52] Hammouch, Z., Yavuz, M. & Özdemir N. Numerical Solutions and Synchronization of a Variable-Order Fractional Chaotic System. *Mathematical Modelling and Numerical Simulation with Applications (MMNSA)*, 1(1), 11–23, (2021). [CrossRef]
[53] Naik, P.A., Yavuz, M., Qureshi, S., Zu, J. & Townley, S. Modeling and analysis of COVID-19 epidemics with treatment in fractional derivatives using real data from Pakistan. *The European Physical Journal Plus*, 135(10), 1-42, (2020). [CrossRef]
[54] Dasbasi, B. Stability Analysis of an Incommensurate Fractional-Order SIR Model. *Mathematical Modelling and Numerical Simulation with Applications (MMNSA)*, 1(1), 44–55, (2021). [CrossRef]
[55] Yokuş, A. Construction of Different Types of Traveling Wave Solutions of the Relativistic Wave Equation Associated with the Schrödinger Equation. *Mathematical Modelling and Numerical Simulation with Applications (MMNSA)*, 1(1), 24–31, (2021). [CrossRef]
[56] Kumar, P., Erturk, V.S., Yusuf, A. & Kumar, S. Fractional time-delay mathematical modeling of Oncolytic Virotherapy. *Chaos, Solitons & Fractals*, 150, 111123, (2021). [CrossRef]
[57] Kumar, P., Ertürk, V.S. & Nisar, K.S. Fractional dynamics of huanglongbing transmission within a citrus tree. *Mathematical Methods in the Applied Sciences*, 44(14), 11404–11424, (2021). [CrossRef]
[58] Kumar, P., Erturk, V.S., Yusuf, A., Nisar, K.S. & Abdelwahab, S.F. A study on canine distemper virus (CDV) and rabies epidemics in the red fox population via fractional derivatives. *Results in Physics*, 25, 104281, (2021). [CrossRef]
[59] Odibat, Z., Erturk, V.S., Kumar, P. & Govindaraj, V. Dynamics of generalized Caputo type delay fractional differential equations using a modified Predictor-Corrector scheme. *Physica Scripta*, 96(12), 125213, (2021). [CrossRef]
[60] Kumar, P., Erturk, V.S. & Almusawa, H. Mathematical structure of mosaic disease using microbial biostimulants via Caputo and Atangana–Baleanu derivatives. *Results in Physics*, 24, 104186, (2021). [CrossRef]
[61] Hilfer, R. *Applications of Fractional Calculus in Physics*, World Scientific: Singapore, (2000).
[62] Oldham, K.B. & Spanier, J. *The Fractional Calculus: Theory and Applications of differentiation and integration of arbitrary Order*, Elsevier, (2006).
[63] Podlubny, I. *Fractional differential equations: an introduction to fractional derivatives, fractional differential equations, to methods of their solution and some of their applications*, (Vol.1), Academic Press, Elsevier, (1998).
[64] Watugala, G.K. Sumudu transform: A new integral transform to solve differential equations and control engineering problems. *International Journal of Mathematical Education in Science and Technology*, 24(1), 35–43, (1993). [CrossRef]
[65] Crank, J. *The Mathematics of Diffusion*, (Vol.2), Oxford University Press: Oxford, (1975).
[66] Sherman, A., Smith, G.D., Dai, L. & Miura, R.M. Asymptotic analysis of buffered calcium diffusion near a point source. *SIAM Journal on Applied Mathematics*, 61(5), 1816–1838, (2001). [CrossRef]

Mathematical Modelling and Numerical Simulation with Applications, 2021, 1(2), 95–101

https://www.mmnsa.org
ISSN Online: 2791-8564 / Open Access
https://doi.org/10.53391/mmnsa.2021.01.009

RESEARCH PAPER

Flip and generalized flip bifurcations of a two-dimensional discrete-time chemical model

Parvaiz Ahmad Naik[1,*,‡], Zohreh Eskandari[2,‡] and Hossein Eskandari Shahraki[3,‡]

[1]School of Mathematics and Statistics, Xi'an Jiaotong University, Xi'an, Shaanxi 710049, P. R. China, [2]Department of Mathematical Sciences, Shahrekord University, P.O. Box 115, Shahrekord, Iran, [3]Amirkabir University of Technology, Faculty of Physics and Energy Engineering, No. 350, Hafez Ave, Valiasr Square, Tehran, Iran

*Corresponding Author
‡naik.parvaiz@xjtu.edu.cn (Parvaiz Ahmad Naik); z.eskandari@sku.ac.ir (Zohreh Eskandari); hes30377@aut.ac.ir (Hossein Eskandari Shahraki)

Abstract

This paper focuses on introducing a two-dimensional discrete-time chemical model and the existence of its fixed points. Also, the one and two-parameter bifurcations of the model are investigated. Bifurcation analysis is based on numerical normal forms. The flip (period-doubling) and generalized flip bifurcations are detected for this model. The critical coefficients identify the scenario associated with each bifurcation. To confirm the analytical results, we use the MATLAB package MatContM, which performs based on the numerical continuation method. Finally, bifurcation diagrams are presented to confirm the existence of flip (period-doubling) and generalized flip bifurcations for the glycolytic oscillator model that gives a better representation of the study.

Key words: Bifurcation; normal form; numerical continuation method; one-parameter bifurcation; two-parameter bifurcation
AMS 2020 Classification: 00A71; 80A30; 92C45

1 Introduction

Mathematical modelling is a powerful tool for understanding, designing, and predicting processes and process equipment in the chemical industry, including the conservation of momentum, energy, and material. Detailed modelling of complex reaction systems is becoming increasingly important in the development, analysis, design, and control of chemical reaction processes [1]. Numerical computer modelling can describe chemical reactions, composition, fluid flow, and temperature distribution in three dimensions and time. Chemical engineers frequently used fundamental dynamic models to develop new chemical processes and to predict the behavior of existing industrial processes accurately. For example, models can be used to simulate how a process will behave under new operating conditions, to indicate how new products can be made using an existing plant, to investigate product quality enhancements, and to achieve production rate improvements [2]. The systems of ordinary differential equations (ODEs) are involved in modelling the dynamics of reaction networks to track the time evolution of chemical concentrations for the species in the network. Through the differential equations using the theoretical results of dynamical systems, or numerical simulations, the study of the properties of the dynamics (e.g. stability of steady states, the existence of multiple steady states, etc.) are obtained [3].
Carden et al. [3] introduced a set of mathematical techniques for describing and characterizing a series of chemical processes (enzyme-substrate, protein-protein, etc.) that cells used to sense and respond to diverse stimuli during the progression and cellular behavior of cancers. Mahdy et al. [4], in their paper, combined the Sumudu decomposition method and the Hermite collocation method for the solutions

➤ **Received:** 06.11.2021 ➤ **Revised:** 16.12.2021 ➤ **Accepted:** 17.12.2021 ➤ **Published:** 18.12.2021

of a nonlinear biochemical reaction model. They have represented the signal flow graph and Simulink of MATLAB of the model in the paper. Besides, the stability of the equilibrium point was also studied. They show that the Sumudu decomposition method and Hermite collocation method are extremely symmetrical and similar. Apart from modelling chemical processes, mathematical modelling is not limited to any particular field but finds applications in different fields [5, 6, 7, 8, 9, 10, 11, 12, 13, 14, 15, 16, 17, 18]. Alidousti et al. [19] studied the dynamic behaviors of the discrete Bonhoeffer-van der Pol (BVP) model. Through their results, It was shown that the BVP model undergoes codimension one (codim-1) bifurcations such as pitchfork, fold, flip (period-doubling), and Neimark-Sacker. Instead of codimension one (codim-1) bifurcations, the codimension two (codim-2) bifurcations including resonance 1:2, 1:3, 1:4, and Chenciner were also achieved.

Bifurcation analysis can divide the parameter space into more regions and depict more complex dynamic behaviors. Bifurcation analysis traces time-varying change(s) at a particular state of the system in a multidimensional space where each dimension represents a particular concentration of the biochemical factor involved. It can happen that a slight variation in a parameter can have a significant impact on the solution. Bifurcation analysis finds application in different fields. Ghori et al. [20], in their paper, studied the global dynamics and bifurcation analysis of a fractional-order SEIR epidemic model with a saturation incidence rate. The outcome of their study reveals that the model undergoes a transcritical bifurcation and a Hopf bifurcation at the equilibrium points under certain conditions for all model parameters at fractional-order $\alpha = 1$. Wang and Jia [21] studied the stability and bifurcation analysis of a generalized Gray-Scott chemical reaction model. The results of their study show that the system exhibits abundant dynamical behaviors and the chemical reaction in the reactor will be in balance in the end under certain conditions. Khan [22], in his paper, studied the local dynamics and Neimark-Sacker bifurcation of a two-dimensional glycolytic oscillator model. It was found that the model has a unique equilibrium point for all α and β. Also, some bifurcation diagrams and the corresponding maximum Lyapunov exponent were presented for the model to verify the obtained results. Recently, Naik et al. [23] investigated the multiple bifurcations of a discrete-time prey-predator model with a mixed functional response. They detected the flip, Neimark-Sacker and strong resonance bifurcations of the model. The complex dynamical behavior of the model up to the 16^{th} iteration was investigated.

Although researchers tried to obtain the bifurcation results of the chemical model, none in the literature obtained the flip bifurcations of the model that motivates the authors to carry out this work and becomes the novelty of the present study. In this paper, we provide the dynamics of the glycolytic oscillator chemical model through the flip and generalized flip bifurcations analytically as well as numerically. Further, we calculate the critical coefficients of each bifurcation. The two-dimensional discrete-time chemical model under consideration is given as follows [22]

$$\begin{cases} x^{Ch} \mapsto -x^{Ch}\left(y^{Ch}\right)^2 - \beta\, x^{Ch} + \alpha + x^{Ch}, \\ y^{Ch} \mapsto x^{Ch}\left(y^{Ch}\right)^2 + \beta\, x^{Ch}, \end{cases} \tag{1}$$

where x^{Ch} and y^{Ch} are the substrate concentrations at time t and α and β are the dimensionless parameters.

The structure of the current study can be presented as follows. In Section 1, the introduction of the study is given. In Section 2, the analytical bifurcation results of the model are carried out in the form of theorems and proofs. Section 3 contains the numerical bifurcation analysis of the model to verify the analytical results. Finally, the concluding remarks about the proposed work are given in Section 4.

In the following section, we provide the existence of different types of bifurcations of the system (1).

2 Bifurcation analysis

Our first step is to obtain the fixed points of model (1) in order to investigate its bifurcations. Solving equations

$$\begin{cases} -x^{Ch}\left(y^{Ch}\right)^2 - \beta\, x^{Ch} + \alpha + x^{Ch} & = x^{Ch}, \\ x^{Ch}\left(y^{Ch}\right)^2 + \beta\, x^{Ch} & = y^{Ch}, \end{cases}$$

yields that model (1) has a unique fixed point

$$x_*^{Ch} = \frac{\alpha}{\alpha^2 + \beta}, \quad y_*^{Ch} = \alpha.$$

Analyzing the bifurcations of map

$$\begin{pmatrix} x^{Ch} \\ y^{Ch} \end{pmatrix} \mapsto M^{Ch}(\mathcal{X}, \Lambda) = \begin{pmatrix} -x^{Ch}\left(y^{Ch}\right)^2 - \beta\, x^{Ch} + \alpha + x^{Ch} \\ x^{Ch}\left(y^{Ch}\right)^2 + \beta\, x^{Ch} \end{pmatrix}, \tag{2}$$

is discussed in this section, where $\mathcal{X} = (x^{Ch}, y^{Ch})^T$ and $\Lambda = (\alpha, \beta)^T$.

Jacobian matrix, second-order multi-linear form, and third-order multi-linear form of (2) are as follows:

$$A^{Ch}(\mathcal{X}, \Lambda) = \begin{pmatrix} -\left(y^{Ch}\right)^2 - \beta + 1 & -2\, x^{Ch} y^{Ch} \\ \left(y^{Ch}\right)^2 + \beta & 2\, x^{Ch} y^{Ch} \end{pmatrix},$$

$$B^{Ch}(\widehat{X^{Ch}}, \widehat{Y^{Ch}}) = \begin{pmatrix} -2\, y^{Ch}(x_1 y_2 + x_2 y_1) - 2\, x^{Ch} x_2 y_2 \\ 2\, y^{Ch}(x_1 y_2 + x_2 y_1) + 2\, x^{Ch} x_2 y_2 \end{pmatrix},$$

$$C^{Ch}(\widehat{X^{Ch}}, \widehat{Y^{Ch}}, \widehat{Z^{Ch}}) = \begin{pmatrix} -2x_1y_2z_2 - 2x_2y_1z_2 - 2x_2y_2z_1 \\ 2x_1y_2z_2 + 2x_2y_1z_2 + 2x_2y_2z_1 \end{pmatrix},$$

where $\widehat{X^{Ch}} = (x_1, x_2)^T$, $\widehat{Y^{Ch}} = (y_1, y_2)^T$ and $\widehat{Z^{Ch}} = (z_1, z_2)^T$.

Flip bifurcation of $\mathcal{X}_*^{Ch}$

The bifurcation parameter β and the fixed parameter α are considered here.

Theorem 1 *At $\alpha = \alpha_{PD} = -\alpha^2 + 1 + \sqrt{4\alpha^2 + 1}$, a flip bifurcation occurs for $\mathcal{X}_*^{Ch}$.*

Proof As we can see, the multipliers of

$$A^{Ch}(\mathcal{X}_*^{Ch}, \Lambda_{PD}) = \begin{pmatrix} -\sqrt{4\alpha^2+1} & -2\frac{\alpha^2}{1+\sqrt{4\alpha^2+1}} \\ 1+\sqrt{4\alpha^2+1} & 2\frac{\alpha^2}{1+\sqrt{4\alpha^2+1}} \end{pmatrix}, \quad \Lambda_{PD} = (\alpha, \beta_{PD})^T,$$

where $\Lambda_{PD} = (\alpha_{PD}, \beta)^T$, are the following

$$\lambda_1^{PD} = -1, \qquad \lambda_2^{PD} = -1/2\sqrt{4\alpha^2+1} + 1/2.$$

If $\lambda_2^{PD} \neq \pm 1$, $A^{Ch}(\mathcal{X}_*^{Ch}, \Lambda_{PD})$ has a simple multiplier -1 on the unit circle. So $M^{Ch}(\mathcal{X}_*^{Ch}, \Lambda_{PD})$ is possible to write as

$$\eta \mapsto -\eta + \widehat{b_{PD}}\eta^3 + \mathcal{O}(\eta^4),$$

where

$$\widehat{b_{PD}} = \frac{1}{6}\left\langle w_{PD}, C^{Ch}(v_{PD}, v_{PD}, v_{PD}) + 3B^{Ch}\left(v_{PD}, \left(I_2 - A^{Ch}(\mathcal{X}_*^{Ch}, \Lambda_{PD})\right)^{-1} B^{Ch}(v_{PD}, v_{PD})\right)\right\rangle,$$

and

$$A^{Ch}(\mathcal{X}_*^{Ch}, \Lambda_{PD})v_{PD} = -v_{PD}, \quad \left(A^{Ch}(\mathcal{X}_*^{Ch}, \Lambda_{PD})\right)^T w_{PD} = -w_{PD}, \quad \langle w_{PD}, v_{PD}\rangle = 1.$$

As a result

$$v_{PD} = \begin{pmatrix} -1/2 \\ 1 \end{pmatrix}, \quad w_{PD} = \begin{pmatrix} 2\frac{1+\sqrt{4\alpha^2+1}}{\sqrt{4\alpha^2+1}-3} \\ 2\frac{\sqrt{4\alpha^2+1}-1}{\sqrt{4\alpha^2+1}-3} \end{pmatrix},$$

and

$$\widehat{b_{PD}} = -4\frac{2\alpha^2\sqrt{4\alpha^2+1} - 2\alpha^2 - \sqrt{4\alpha^2+1} - 1}{\left(1+\sqrt{4\alpha^2+1}\right)^2\left(\sqrt{4\alpha^2+1}-3\right)}.$$

$\widehat{b_{PD}} \neq 0$ yields a generic bifurcation. This bifurcation is supercritical (subcritical) if $\widehat{b_{PD}} > 0$ ($\widehat{b_{PD}} < 0$) and 2-period points bifurcated from $\mathcal{X}_*^{Ch}$ are stable (unstable). For more details see [24, 25, 26]. ■

Generalized flip bifurcation of $\mathcal{X}_*^{Ch}$

The bifurcation parameters β and α are considered here.

Theorem 2 *At $\alpha = \alpha_{GPD} = 1/2\sqrt{2+2\sqrt{2}}$ and $\beta = \beta_{GPD} = 3/2 + 1/2\sqrt{2}$, a generalized flip bifurcation occurs for $\mathcal{X}_*^{Ch}$.*

Proof Based on an assumption

$$\alpha = \alpha_{GPD} = 1/2\sqrt{2+2\sqrt{2}}, \quad \beta = \beta_{GPD} = 3/2 + 1/2\sqrt{2},$$

the Jacobian matrix

$$A^{Ch}(\mathcal{X}_*^{Ch}, \Lambda_{GPD}) = \begin{pmatrix} -1-\sqrt{2} & -\frac{\sqrt{2}+1}{2+\sqrt{2}} \\ 2+\sqrt{2} & \frac{\sqrt{2}+1}{2+\sqrt{2}} \end{pmatrix}, \quad \Lambda_{GPD} = (\alpha_{PD}, \beta_{PD})^T,$$

has a simple critical multiplier $\lambda_1^{GPD} = 1$, and no other multiplier is not on the unit circle and $\widehat{b_{PD}} = 0$. So $M^{Ch}(\mathcal{X}_*^{Ch}, \Lambda_{GPD})$ is possible to write as

$$\eta \mapsto -\eta + \widehat{c_{GPD}}\eta^5 + \mathcal{O}(\eta^6),$$

where

$$\begin{aligned}
\widehat{c_{GPD}} &= \frac{1}{120}\left\langle w_{GPD}, 5\,B^{Ch}(v_{GPD}, h_4^{Ch}) + 10\,C^{Ch}(v_{GPD}, v_{GPD}, h_3^{Ch}) + 10\,B^{Ch}(h_2^{Ch}, h_3^{Ch})\right.\\
&\quad \left. +15\,C^{Ch}(v_{GPD}, h_2^{Ch}, h_2^{Ch})\right\rangle,\\
h_2^{Ch} &= (I_2 - A^{Ch})^{-1}B^{Ch}(v_{GPD}, v_{GPD}),\\
h_3^{Ch} &= -(A^{Ch} + I_2)^{INV}\left(C^{Ch}(v_{GPD}, v_{GPD}, v_{GPD}) + 3B^{Ch}(v_{GPD}, h_2^{Ch})\right),\\
h_4^{Ch} &= (I_2 - A^{Ch})^{-1}\left(4\,B^{Ch}(v_{GPD}, h_3^{Ch}) + 3\,B^{Ch}(h_2^{Ch}, h_2^{Ch}) + 6\,C^{Ch}(v_{GPD}, v_{GPD}, h_2)\right),
\end{aligned}$$

and

$$A^{Ch}(\mathcal{X}_*^{Ch}, \Lambda_{GPD})\,v_{PD} = -v_{GPD}, \quad \left(A^{Ch}(\mathcal{X}_*^{Ch}, \Lambda_{GPD})\right)^T w_{GPD} = -w_{GPD}, \quad \langle w_{GPD}, v_{GPD}\rangle = 1.$$

As a result

$$v_{GPD} = \begin{pmatrix} -1/2 \\ 1 \end{pmatrix}, \qquad w_{GPD} = \begin{pmatrix} -\frac{(2+\sqrt{2})\sqrt{2}}{\sqrt{2}-1} \\ -2\,(\sqrt{2}-1)^{-1} \end{pmatrix},$$

$$h_2^{Ch} = \begin{pmatrix} \frac{\sqrt{2+2\sqrt{2}}(\sqrt{2}+1)}{(2+\sqrt{2})^2} \\ 0 \end{pmatrix}, \qquad h_3^{Ch} = \begin{pmatrix} 0 \\ 0 \end{pmatrix}, \qquad h_4^{Ch} = \begin{pmatrix} -12\,\frac{\sqrt{2+2\sqrt{2}}(\sqrt{2}+1)}{(2+\sqrt{2})^3} \\ 0 \end{pmatrix}.$$

So $\widehat{c_{GPD}}$ can be obtained as follows:

$$\widehat{c_{GPD}} = -1.$$

Since $\widehat{c_{GPD}}$, the generalized flip is generic. ■

3 Numerical continuation of $M^{Ch}(\mathcal{X}, \Lambda)$

To confirm the analytical results, we use MATCONTM, a toolbox of MATLAB and works based on the numerical continuation method, for more details, see [27, 28]. Here α and β are considered as a free parameter and a fixed parameter, respectively. Here we consider $\alpha = 1$, by varying β the flip bifurcations occurs at $\mathcal{X}_*^{Ch} = (.309017, 1.00000)$ for $\beta\,\beta_{PD} = 2.23606$ where $\widehat{b_{PD}} = -3.05573 \times 10^{-1}$. According to the sign of $\widehat{b_{PD}}$result in the flip bifurcation is sub-critical. Continuation of $\mathcal{X}_*^{Ch}$ in (x^{Ch}, β)−space is shown in Figure 1.

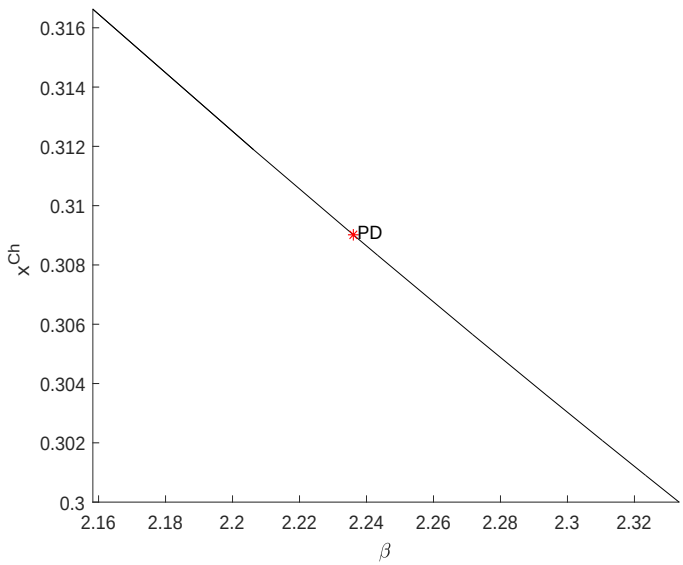

Figure 1. Continuation of $\mathcal{X}_*^{Ch}$ in (x^{Ch}, β)−space.

Selecting this PD point and starting the continuation of a PD bifurcation curve in two control parameters α and β, yield a generalized flip bifurcation at $\mathcal{X}_*^{Ch} = (0.321797, 1.098684)$ for $\alpha = \alpha_{GPD} = 1.098684$ and $\beta = \beta_{GPD} = 2.207106$ with $\widehat{c_{GPD}} = -6.400000 \times 10^{-1}$, see Figure 2.

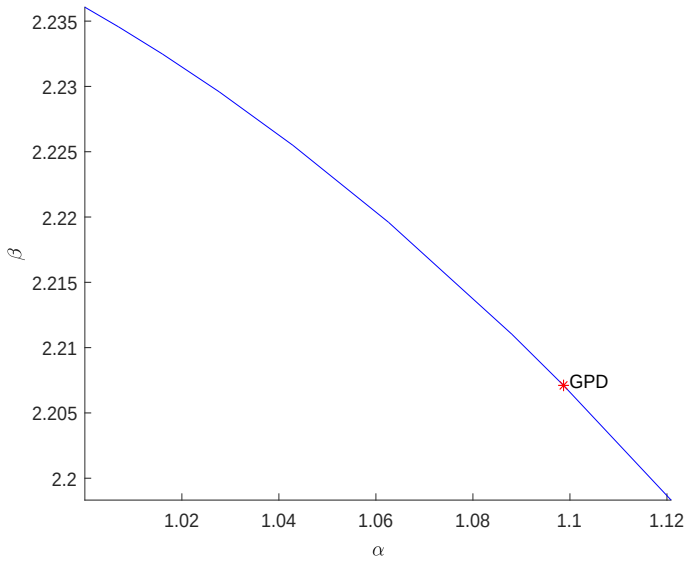

Figure 2. Flip bifurcation curve.

We compute a branch of fold points of the second iterate by switching at the GPD point, see Figure 3.

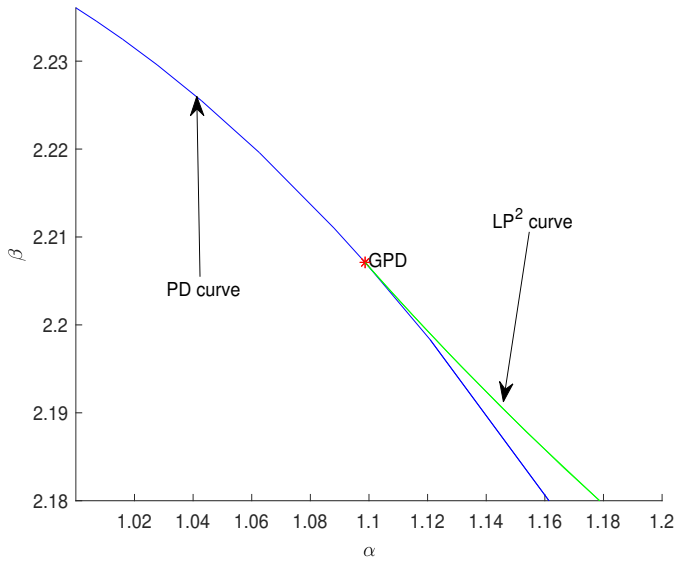

Figure 3. A curve of fold bifurcations of the second iterate, LP^2, which emanates tangentially at a GPD point on a flip curve.

4 Conclusion

In this paper, we provided the dynamics of the glycolytic oscillator chemical model through the flip and generalized flip bifurcations analytically as well as numerically. To investigate the bifurcations of this model, we calculated the critical coefficients of each bifurcation. These coefficients determined whether a bifurcation is non-degenerate and determined the scenario of each bifurcation. The results obtained in Sections 2 and 3 show excellent agreement between the analytical predictions and the numerical observations. From the obtained results, it is concluded that the model shows flip and generalized flip bifurcation indicating that the substrate concentrations vary from one period to another. Although the current paper studied a standard two-dimensional discrete-time chemical model but can be extended to fractional-order derivatives with the operators known as Caputo, Atangana-Gomez, Atangana-Baleanu, Caputo-Fabrizio, and others discover more causative factors that are not covered in this paper, such is left for future research direction.

Declarations

Consent for publication

Not applicable.

Conflicts of interest

The authors declare that they have no conflict of interests.

Funding

Not applicable.

Author's contributions

P.A.N.: Conceptualization, Methodology, Supervision, Investigation, Writing-Original draft. Z.E.: Software, Methodology, Data Curation, Writing-Original draft. H.E.S.: Visualization, Investigation, Software, Writing-Reviewing and Editing. All authors discussed the results and contributed to the final manuscript.

Acknowledgements

Not applicable.

References

[1] Okino, M.S. & Mavrovouniotis, M.L. Simplification of mathematical models of chemical reaction systems. *Chemical Reviews*, 98(2), 391-408, (1998).
[2] McLean, K.A.P. & McAuley, K.B. Mathematical modelling of chemical processes-obtaining the best model predictions and parameter estimates using identifiability and estimability procedures. *Canadian Journal of Chemical Engineering*, 90(2), 351-366, (2012). [CrossRef]
[3] Carden, J., Pantea, C., Craciun, G., Machiraju, R. & Mallick, P. Mathematical methods for modeling chemical reaction networks. *bioRxiv*, 070326, (2016). [CrossRef]
[4] Mahdy, A.M.S. & Higazy, M. Numerical different methods for solving the nonlinear biochemical reaction model.*International Journal of Applied and Computational Mathematics*, 5(6), 1-17, (2019). [CrossRef]
[5] Yavuz, M. & Sene, N. Fundamental calculus of the fractional derivative defined with Rabotnov exponential kernel and application to nonlinear dispersive wave model.*Journal of Ocean Engineering and Science*, 6(2), 196-205, (2021). [CrossRef]
[6] Naik, P.A., Yavuz, M., Qureshi, S., Zu, J. & Townley, S. Modeling and analysis of COVID-19 epidemics with treatment in fractional derivatives using real data from Pakistan. *The European Physical Journal Plus*, 135(10), 1-42, (2020). [CrossRef]
[7] Dasbasi, B. Stability analysis of an incommensurate fractional-order SIR model. *Mathematical Modelling and Numerical Simulation with Applications (MMNSA)*, 1(1), 44-55, (2021). [CrossRef]
[8] Naik, P.A., Owolabi, K.M., Zu, J. & Naik, M.U.D. Modeling the transmission dynamics of COVID-19 pandemic in Caputo type fractional derivative.*Journal of Multiscale Modelling*, 12(3), 2150006-107, (2021). [CrossRef]
[9] Hammouch, Z., Yavuz, M. & Özdemir, N. Numerical solutions and synchronization of a variable-order fractional chaotic system. *Mathematical Modelling and Numerical Simulation with Applications (MMNSA)*, 1(1), 11-23, (2021). [CrossRef]
[10] Naik, P.A., Owolabi, K.M., Yavuz, M. & Zu, J. Chaotic dynamics of a fractional order HIV-1 model involving AIDS-related cancer cells. *Chaos Solitons & Fractals*, 140, 110272, (2020). [CrossRef]
[11] Eskandari, Z., Alidousti, J., Avazzadeh, Z. & Machado, J.T. Dynamics and bifurcations of a discrete-time prey-predator model with Allee effect on the prey population. *Ecological Complexity*, 48, 100962, (2021). [CrossRef]
[12] Naik, P.A., Yavuz, M. & Zu, J. The role of prostitution on HIV transmission with memory: A modeling approach. Alexandria Engineering Journal, 59(4), 2513-2531,(2020). [CrossRef]
[13] Yavuz, M. European option pricing models described by fractional operators with classical and generalized Mittag-Leffler kernels. *Numerical Methods for Partial Differential Equations*, (2020). [CrossRef]
[14] Naik, P.A., Zu, J. & Ghori, M.B. Modeling the effects of the contaminated environments on COVID-19 transmission in India.*Results in Physics*, 29, 104774, (2021). [CrossRef]
[15] Owolabi, K.M. & Baleanu, D. Emergent patterns in diffusive Turing-like systems with fractional-order operator. *Neural Computing and Applications*, 1-18, (2021). [CrossRef]
[16] Joshi, H. & Jha, B.K. Modeling the spatiotemporal intracellular calcium dynamics in nerve cell with strong memory effects. *International Journal of Nonlinear Sciences and Numerical Simulation*. [CrossRef]
[17] Owolabi, K.M., Karaagac, B. & Baleanu, D. Dynamics of pattern formation process in fractional-order super-diffusive processes: a computational approach. *Soft Computing*, 1-18, (2021). [CrossRef]
[18] Dave, D.D. & Jha, B.K. On finite element estimation of calcium advection diffusion in a multipolar neuron. *Journal of Engineering Mathematics*, 128(1), 1-15, (2021). [CrossRef]
[19] Alidousti, J., Eskandari, Z., Fardi, M. & Asadipour, M. Codimension two bifurcations of discrete Bonhoeffer-van der Pol oscillator model. *Soft Computing*, 25(7), 5261-5276, (2021). [CrossRef]

[20] Naik, P.A., Ghori, M.B., Zu, J., Eskandari, Z. & Naik, M. Global dynamics and bifurcation analysis of a fractional-order SEIR epidemic model with saturation incidence rate. Mathematical Methods in the Applied Sciences, 45(3), 1-24, (2022). [CrossRef]
[21] Wang, J. & Jia, Y. Analysis on bifurcation and stability of a generalized Gray-Scott chemical reaction model. *Physica A: Statistical Mechanics and its Applications*, 528, 121394, (2019). [CrossRef]
[22] Khan, A.Q. Neimark-Sacker bifurcation of a two-dimensional discrete-time chemical model. *Mathematical Problems in Engineering*, 2020, 3936242, (2020). [CrossRef]
[23] Naik, P.A., Eskandari, Z., Zu, J. & Avazzadeh, Z. Multiple bifurcations of a discrete-time prey-predator model with mixed functional response. *International Journal of Bifurcation and Chaos*, 32(3), 1-15, (2022).
[24] Kuznetsov, Y.A. Elements of Applied Bifurcation Theory (Vol. 112). *Springer Science & Business Media*, (2013).
[25] Eskandari, Z., Alidousti, J. & Ghaziani, R.K. Codimension-one and -two bifurcations of a three-dimensional discrete game model. *International Journal of Bifurcation and Chaos*, 31(02), 2150023, (2021). [CrossRef]
[26] Kuznetsov, Y.A. & Meijer, H.G. Numerical normal forms for codim 2 bifurcations of fixed points with at most two critical eigenvalues. *SIAM Journal on Scientific Computing*, 26(6), 1932-1954, (2005). [CrossRef]
[27] Govaerts, W., Ghaziani, R.K., Kuznetsov, Y.A. & Meijer, H.G. Numerical methods for two-parameter local bifurcation analysis of maps. SIAM Journal on Scientific Computing, 29(6), 2644-2667, (2007). [CrossRef]
[28] Kuznetsov, I.A. & Meijer, H.G.E. Numerical Bifurcation Analysis of Maps: From Theory to Software. *Cambridge University Press*, (2019).

Mathematical Modelling and Numerical Simulation with Applications (MMNSA) (http://www.mmnsa.org)

Mathematical Modelling and Numerical Simulation with Applications, 2021, 1(2), 102–111

https://www.mmnsa.org
ISSN Online: 2791-8564 / Open Access
https://doi.org/10.53391/mmnsa.2021.01.010

RESEARCH PAPER

Dynamics of cholera disease by using two recent fractional numerical methods

Pushpendra Kumar[1,*,‡] and Vedat Suat Erturk[2,‡]

[1]Department of Mathematics and Statistics, School of Basic and Applied Sciences, Central University of Punjab, Bathinda, Punjab-151001, India , [2]Department of Mathematics, Ondokuz Mayis University, Atakum-55200, Samsun, Turkey

*Corresponding Author
‡kumarsaraswatpk@gmail.com (Pushpendra Kumar); vserturk@omu.edu.tr (Vedat Suat Erturk)

Abstract

In this paper, we simulate an epidemic model of cholera disease in the sense of generalized Liouville-Caputo fractional derivative. We provide the results related to the existence of a unique solution by using some well-known theorems. Numerical solutions of the given model are derived by using two different numerical methods along with their importance. A number of graphs are plotted to understand the given cholera disease dynamics. The main motivation to do this research is to understand the given disease dynamics as well as the efficiency of both methods which are very recent to the literature.

Key words: Cholera disease; mathematical model; generalized Liouville-Caputo fractional derivative; numerical methods; graphical simulations
AMS 2020 Classification: 26A33; 34C60; 92C60; 92D30

1 Introduction

The bacterium 'Vibrio Cholerae' causes cholera, which is a bacterial illness. This bacterium is commonly found in contaminated foods. It's a Gram-negative bacteria which is curved and comma-shaped. It may be found in sewage and coastal saltwater environments. It's also found where there aren't enough sanitary facilities. During the 1800s, this illness was initially discovered in the United States. For hundreds of years, humans have been suffering from cholera sickness. If left untreated, this condition can cause severe diarrhoea and dehydration in the body. It can sometimes result in a deadly condition. They cling to shellfish, crabs, and other creatures' shells. Various illnesses, including cholera, are spread by drinking polluted water. This bacteria dwells in the human body's small intestine and releases an exotoxin, which induces a flow of water and electrolytes into the small intestine, including sodium bicarbonate, chloride, and others [1, 2].

Causes of cholera: (i) It is brought on by causes such as a polluted water source. (ii) It occurs as a result of the intake of tainted foods and beverages offered by street vendors. (iii) Vegetables that are cultivated with the help of human waste and water. (iv) Contaminated seafood, which has been contaminated by sewage. (v) Foods that have an adverse effect on the digestive system are to blame. Some of the symptoms of Cholera are: (i) High fever. (ii) Weight loss. (iii) Increased thirst. (iv) Feeling of Nausea. (v) Vomiting sensation. (vi) A kind bloating in the belly. (vii) Blood pressure becomes low. (viii) The elasticity of the skin is lost. (ix) Develop cramps in the muscles. (x) A rapid increase in the heart rate. (xi) Dryness in the mouth, nose, and eyelids. (xii) Formation of blood or mucus or sometimes undigested materials in the stool [1, 2].

Replacement of lost fluid and electrolytes is part of the cholera therapy. Dehydration may be avoided by drinking enough of ORS (Oral Rehydration Solution). Intravenous fluid replacement may be necessary if the disease worsens. Antibiotics and zinc supplements may be

➤ **Received:** 30.10.2021 ➤ **Revised:** 18.12.2021 ➤ **Accepted:** 20.12.2021 ➤ **Published:** 21.12.2021

prescribed by doctors to treat diarrhoea. Recently, some novel mathematical studies have been come out to define the dynamics of cholera. In [3], a cholera disease model with optimal control treatment is defined. Authors in ref. [4] have given some mathematical modelling related analysis on the dynamics of cholera. Study given in ref. [5] describes the transmission dynamics of cholera by using a mathematical modeling along with control strategies. In [6], spatial synchrony in fractional order metapopulation cholera transmission is given.

As we know that the fractional derivatives [7, 8] are helpful operators to study real-world problems in the sense of mathematical modeling. Recently, a number of studies have been coming to the literature on this topic. In the epidemic modelings, disease like COVID-19 [9, 10, 11, 12, 13, 14, 15, 16, 17, 18], cancer therapy [19], tuberculosis [20], malaria [21], lassa hemorrhagic fever [22], and canine distemper virus [23], etc. have been successfully studied. Applications of fractional derivatives in psychology [24], ecology [25, 26], and plant epidemiology [27, 28] have been derived by many researchers. Several novel fractional-order mathematical models for studying the calcium distribution in nerve cells are introduced in refs. [29, 30, 31, 32]. Also, some novel recent applications of fractional-order computational methods in different real-world problems can be studied from refs. [33, 34, 35, 36, 37]. Nowadays, scientists use different types of fractional derivatives with or without singular kernels in a huge amount to solve various types of real-world problems. In our study, we use the generalised Liouville-Caputo fractional derivative to simulate a mathematical model of the cholera epidemic. The novelty of this work is to explore the given disease dynamics as well as the efficiency of both numerical schemes which are very recent to the literature.

This article is divided into number of sections. After defining cholera epidemic, we mention two necessary definitions in Section 2. In Section 3, a cholera model followed by the fractional model is proposed. In Section 4, results related to existence and uniqueness analysis are given. The solution of the model by using two different numerical methods is given in Section 5. All results and discussion are explained in Section 6. Finally, concluding remarks are given in the last Section 7.

2 Preliminaries

Here we recall the definitions of two fractional derivatives.

Definition 1 *[8] The Liouville-Caputo non-integer order derivative of* $\mathcal{L} \in C^{d}_{-1}$ *is defined by*

$$D^{\varrho}_{t}\mathcal{L}(t) = \begin{cases} \frac{d^{q}\mathcal{L}(t)}{d\zeta^{q}}, & \varrho = q \in \mathbb{N} \\ \frac{1}{\Gamma(q-\varrho)}\int_{0}^{t}(t-\vartheta)^{q-\varrho-1}\mathcal{L}^{(q)}(\vartheta)\,d\vartheta, & q-1<\varrho<q, q\in\mathbb{N}. \end{cases} \tag{1}$$

Definition 2 *[38] The generalized Liouville-Caputo-type non-integer order derivative,* $D^{\varrho,\rho}_{d_+}$ *of order* $\varrho > 0$ *is given by*

$$(D^{\varrho,\rho}_{d_+}\mathcal{L})(\xi) = \frac{\rho^{\varrho-q+1}}{\Gamma(q-\varrho)}\int_{d}^{\xi} s^{\rho-1}(\xi^{\rho}-s^{\rho})^{q-\varrho-1}\left(s^{1-\rho}\frac{d}{ds}\right)^{q}\mathcal{L}(s)ds,\ \ \xi > d, \tag{2}$$

where $\rho > 0, d \geq 0,$ *and* $q-1<\varrho\leq q$.

3 Model description

Now we describe the dynamics of the mathematical model used to study the cholera epidemic. Recently, authors in ref. [4] proposed an integer-order mathematical model consisting following ordinary differential equations

$$\begin{cases} S' = b - dS - \beta SI + \nu V + \gamma R, \\ I' = -dI + \beta SI - \sigma I - \omega I - \alpha I, \\ R' = -dR + \alpha I - \gamma R, \\ V' = \sigma I - \nu V, \end{cases} \tag{3}$$

where $N = S + I + R + V$. In this model, the cholera disease is distributed into four classes. S is for susceptible class, I is for infected individuals at contact rate β, R is for recovered humans at a rate α and V is for the environment. A brief description of all parameter values is given in Table 1. The disease-free equilibrium is defined by

$$(S^{*}, 0, 0, 0) = \left(\frac{b}{d}, 0, 0, 0\right). \tag{4}$$

The endemic equilibrium is

$$(S^{**}, I^{**}, R^{**}, V^{**}) = \left(\frac{(d+\omega+\sigma+\alpha)}{\beta}, \frac{(d+\gamma)R^{*}}{\alpha}, \frac{(d+\beta I^{*})S^{*}-b}{\gamma}, \frac{\sigma(d+\gamma)R^{*}}{\nu\alpha}\right), \tag{5}$$

and then the basic reproductive number is calculated as

$$\mathcal{R}_{0} = \frac{\beta b}{d} - (d+\omega+\sigma+\alpha). \tag{6}$$

Table 1. Parameter values cited from [4]

Parameter	Description	Values
b	Recruitment rate	0.000096274
d	Natural death rate	0.00002537
ω	Disease induced death rate	0.0004
α	Recovery rate	0.2
γ	Rate of recovered humans return to the susceptible class	0.002
σ	Rate of infectious humans contaminate the environment	0.1
ν	Environment infect humans with the bacteria at a rate	0.075
β	Contact rate with infectious humans	0.011

To capture the hysteresis memory effects in the given model, the generalization of the proposed model (3) in the generalised Liouville-Caputo sense is described as follows:

$$\begin{cases} {}^{C}D_t^{\varrho,\rho} S = b - dS - \beta SI + \nu V + \gamma R, \\ {}^{C}D_t^{\varrho,\rho} I = -dI + \beta SI - \sigma I - \omega I - \alpha I, \\ {}^{C}D_t^{\varrho,\rho} R = -dR + \alpha I - \gamma R, \\ {}^{C}D_t^{\varrho,\rho} V = \sigma I - \nu V. \end{cases} \tag{7}$$

where ${}^{C}D_t^{\varrho,\rho}$ is the notation of generalised Caputo type fractional derivative operator with fractional order ϱ and the extra parameter ρ.

4 Existence and uniqueness analysis

In this section, we do the analysis for the existence of a unique solution to the proposed model with the help of the consequences of fixed point theory. We perform the analysis for class $S(t)$ and it is relevant to write that the same analysis will be applicable for the rest of the equations of model (7). Let us write the model (7) in the following compact form:

$$\begin{cases} {}^{C}D_t^{\varrho,\rho} S(t) = \mathcal{L}_1(t, S), \\ {}^{C}D_t^{\varrho,\rho} I(t) = \mathcal{L}_2(t, I), \\ {}^{C}D_t^{\varrho,\rho} R(t) = \mathcal{L}_3(t, R), \\ {}^{C}D_t^{\varrho,\rho} V(t) = \mathcal{L}_4(t, V), \end{cases} \tag{8}$$

with the initial conditions $S(0) = S_0, I(0) = I_0, R(0) = R_0$, and $V(0) = V_0$.
For proving the analysis for $S(t)$ class, define the initial value problem (IVP)

$$ {}^{C}D_t^{\varrho,\rho} S(t) = \mathcal{L}_1(t, S), \tag{9a}$$

$$ S(0) = S_0. \tag{9b}$$

The relative Volterra integral equation of the above IVP is

$$S(t) = S(0) + \frac{\rho^{1-\varrho}}{\Gamma(\varrho)} \int_0^t \theta^{\rho-1}(t^\rho - \theta^\rho)^{\varrho-1} \mathcal{L}_1(\theta, S) d\theta. \tag{10}$$

Now we proceed to the following results:

Theorem 1 *[39, 40] Let $0 < \varrho \leq 1$, $S_0 \in \mathbb{R}$, $K > 0$ and $T^* > 0$. Consider $\mathcal{L} := \{(t, S) : t \in [0, T^*], |S - S_0| \leq K\}$ and let the function $\mathcal{L}_1 : \mathcal{L} \to \mathbb{R}$ be continuous. Also, let $M := \sup_{(t,S)\in\mathcal{L}} |\mathcal{L}_1(t, S)|$ and*

$$T = \begin{cases} T^*, & \text{if} \quad M = 0, \\ min\{T^*, \left(\frac{K\Gamma(\varrho+1)\rho^\varrho}{M}\right)^{\frac{1}{\varrho}}\} & \text{otherwise.} \end{cases} \tag{11}$$

Then, there exists a function $S \in C[0, T]$ that satisfies the IVP (9a) and (9b).

Theorem 2 *[39, 40] Let $S(0) \in \mathbb{R}$, $K > 0$, $T^* > 0$, $0 < \varrho \leq 1$. Define the set $\mathcal{L}$ as in Theorem 1 and let the function $\mathcal{L}_1 : \mathcal{L} \to \mathbb{R}$ be continuous and satisfies a Lipschitz condition with respect to the second variable, i.e.*

$$|\mathcal{L}_1(t, S_1) - \mathcal{L}_1(t, S_2)| \leq L|S_1 - S_2|,$$

for some constants $L > 0$ independent to $t, S_1,$ and S_2. Then, there exists a unique solution $S \in C[0, T]$ for the IVP (9a) and (9b).

5 Numerical solution of the model

Solution of the projected model using modified Predictor-Corrector algorithm

Nowadays, a number of numerical methods are available in the literature. Recently, a modified version of the Predictor-Corrector (P-C) scheme to solve delay-type fractional initial value problems has been proposed in ref. [41]. In this part of the study, we write the numerical solution of the proposed cholera model with the help of the generalised P-C method investigated in ref. [38]. The reason to use this generalised Liouville-Caputo derivative is its features to generate more varieties in the graphical observations in the presence of both parameters ϱ and ρ. Now first we consider the solution for the first equation of the cholera model (7) by taking equivalent Volterra integral equation

$$S(t) = S(0) + \frac{\rho^{1-\varrho}}{\Gamma(\varrho)} \int_0^t \theta^{\rho-1}(t^\rho - \theta^\rho)^{\varrho-1}\mathcal{L}_1(\theta, S)d\theta. \tag{12}$$

Now by dividing the interval $[0, T]$ into N unequal sub-intervals $\{[t_k, t_{k+1}],\ k = 0, 1, ..., N-1\}$ taking the mesh points

$$\begin{cases} t_0 = 0, \\ t_{k+1} = (t_k^\rho + h)^{1/\rho}, \quad k = 0, 1, ..., N-1, \end{cases} \tag{13}$$

where $h = \dfrac{T^\rho}{N}$. Now, to evolute the approximations $S_k,\ k = 0, 1, ..., N$, we are assuming that we have already derived the approximations $S_j \approx S(t_j)(j = 1, 2, ..., k)$, and we want to calculate the approximation $S_{k+1} \approx S(t_{k+1})$ by means of the integral equation

$$S(t_{k+1}) = S(0) + \frac{\rho^{1-\varrho}}{\Gamma(\varrho)} \int_0^{t_{k+1}} \theta^{\rho-1}(t_{k+1}^\rho - \theta^\rho)^{\varrho-1}\mathcal{L}_1(\theta, S)d\theta. \tag{14}$$

Let us take $z = \theta^\rho$, we get

$$S(t_{k+1}) = S(0) + \frac{\rho^{-\varrho}}{\Gamma(\varrho)} \int_0^{t_{k+1}^\rho} (t_{k+1}^\rho - z)^{\varrho-1}\mathcal{L}_1(z^{1/\rho}, S(z^{1/\rho}))dz. \tag{15}$$

That is

$$S(t_{k+1}) = S(0) + \frac{\rho^{-\varrho}}{\Gamma(\varrho)} \sum_{j=0}^{k} \int_{t_j^\rho}^{t_{k+1}^\rho} (t_{k+1}^\rho - z)^{\varrho-1}\mathcal{L}_1(z^{1/\rho}, S(z^{1/\rho}))dz. \tag{16}$$

To approximate the right-hand side of Eq. (16), we use the trapezoidal quadrature rule with respect to the weight function $(t_{k+1}^\rho - z)^{\varrho-1}$, by replacing the function $\mathcal{L}_1(z^{1/\rho}, S(z^{1/\rho}))$ by its piecewise linear interpolant with nodes chosen at the t_j^ρ $(j = 0, 1, ..., k+1)$, then we obtain

$$\begin{aligned} &\int_{t_j^\rho}^{t_{k+1}^\rho} (t_{k+1}^\rho - z)^{\varrho-1}\mathcal{L}_1(z^{1/\rho}, S(z^{1/\rho}))dz \approx \frac{h^\varrho}{\varrho\,(\varrho+1)}\Big[\Big((k-j)^{\varrho+1} - (k-j-\varrho)(k-j+1)^\varrho\Big)\mathcal{L}_1(t_j, S(t_j)) \\ &+ \Big((k-j+1)^{\varrho+1} - (k-j+\varrho+1)(k-j)^\varrho\Big)\mathcal{L}_1(t_{j+1}, S(t_{j+1}))\Big]. \end{aligned} \tag{17}$$

Now putting the above approximations into Eq. (16), we obtain the corrector formula for $S(t_{k+1}),\ k = 0, 1, ..., N-1$,

$$S(t_{k+1}) \approx S(0) + \frac{\rho^{-\varrho}h^\varrho}{\Gamma(\varrho+2)} \sum_{j=0}^{k} a_{j,k+1}\mathcal{L}_1(t_j, S(t_j)) + \frac{\rho^{-\varrho}h^\varrho}{\Gamma(\varrho+2)}\mathcal{L}_1(t_{k+1}, S(t_{k+1})), \tag{18}$$

where

$$a_{j,k+1} = \begin{cases} k^{\varrho+1} - (k-\varrho)(k+1)^\varrho \ \text{ if } j = 0, \\ (k-j+2)^{\varrho+1} + (k-j)^{\varrho+1} - 2(k-j+1)^{\varrho+1} \ \text{ if } 1 \le j \le k. \end{cases} \tag{19}$$

In order to obtain the predictor value $S^P(t_{k+1})$, we apply the one-step Adams- Bashforth method to the integral equation (15). In this case, by replacing the function $\mathcal{L}_1(z^{1/\rho}, S(z^{1/\rho}))$ by the quantity $\mathcal{L}_1(t_j, S(t_j))$ at each integral in Eq. (16), we get

$$\begin{aligned} S^P(t_{k+1}) &\approx S(0) + \frac{\rho^{-\varrho}}{\Gamma(\varrho)} \sum_{j=0}^{k} \int_{t_j^\rho}^{t_{j+1}^\rho} (t_{k+1}^\rho - z)^{\varrho-1}\mathcal{L}_1(t_j, S(t_j))dz \\ &= S(0) + \frac{\rho^{-\varrho}h^\varrho}{\Gamma(\varrho+1)} \sum_{j=0}^{k} [(k+1-j)^\varrho - (k-j)^\varrho]\mathcal{L}_1(t_j, S(t_j)). \end{aligned} \tag{20}$$

Now replacing $S(t_{k+1})$ given in the right side of (18) by $S^P(t_{k+1})$, our P-C algorithm, for finding the approximation $S_{k+1} \approx S(t_{k+1})$, is completely expressed by the formula

$$S_{k+1} \approx S(0) + \frac{\rho^{-\varrho} h^{\varrho}}{\Gamma(\varrho+2)} \sum_{j=0}^{k} a_{j,k+1} \mathcal{L}_1(t_j, S_j) + \frac{\rho^{-\varrho} h^{\varrho}}{\Gamma(\varrho+2)} \mathcal{L}_1(t_{k+1}, S^P_{k+1}), \tag{21}$$

where $S_j \approx S(t_j)$, $j = 0, 1, \ldots, k$, and the predicted value $S^P_{k+1} \approx S^P(t_{k+1})$ is given in Eq. (20) with the weights $a_{j,k+1}$ being defined according to (19).
So, the Predictor-Corrector formulae for the system (7) are given by

$$\begin{aligned}
S_{k+1} &\approx S(0) + \frac{\rho^{-\varrho} h^{\varrho}}{\Gamma(\varrho+2)} \sum_{j=0}^{k} a_{j,k+1} \mathcal{L}_1(t_j, S_j) + \frac{\rho^{-\varrho} h^{\varrho}}{\Gamma(\varrho+2)} \mathcal{L}_1(t_{k+1}, S^P_{k+1}),\\
I_{k+1} &\approx I(0) + \frac{\rho^{-\varrho} h^{\varrho}}{\Gamma(\varrho+2)} \sum_{j=0}^{k} a_{j,k+1} \mathcal{L}_2(t_j, I_j) + \frac{\rho^{-\varrho} h^{\varrho}}{\Gamma(\varrho+2)} \mathcal{L}_2(t_{k+1}, I^P_{k+1}),\\
R_{k+1} &\approx R(0) + \frac{\rho^{-\varrho} h^{\varrho}}{\Gamma(\varrho+2)} \sum_{j=0}^{k} a_{j,k+1} \mathcal{L}_3(t_j, R_j) + \frac{\rho^{-\varrho} h^{\varrho}}{\Gamma(\varrho+2)} \mathcal{L}_3(t_{k+1}, R^P_{k+1}),\\
V_{k+1} &\approx V(0) + \frac{\rho^{-\varrho} h^{\varrho}}{\Gamma(\varrho+2)} \sum_{j=0}^{k} a_{j,k+1} \mathcal{L}_4(t_j, V_j) + \frac{\rho^{-\varrho} h^{\varrho}}{\Gamma(\varrho+2)} \mathcal{L}_4(t_{k+1}, V^P_{k+1}),
\end{aligned} \tag{22}$$

where

$$\begin{aligned}
S^P(t_{k+1}) &\approx S(0) + \frac{\rho^{-\varrho} h^{\varrho}}{\Gamma(\varrho+1)} \sum_{j=0}^{k} [(k+1-j)^{\varrho} - (k-j)^{\varrho}] \mathcal{L}_1(t_j, S(t_j)),\\
I^P(t_{k+1}) &\approx I(0) + \frac{\rho^{-\varrho} h^{\varrho}}{\Gamma(\varrho+1)} \sum_{j=0}^{k} [(k+1-j)^{\varrho} - (k-j)^{\varrho}] \mathcal{L}_2(t_j, I(t_j)),\\
R^P(t_{k+1}) &\approx R(0) + \frac{\rho^{-\varrho} h^{\varrho}}{\Gamma(\varrho+1)} \sum_{j=0}^{k} [(k+1-j)^{\varrho} - (k-j)^{\varrho}] \mathcal{L}_3(t_j, R(t_j)),\\
V^P(t_{k+1}) &\approx V(0) + \frac{\rho^{-\varrho} h^{\varrho}}{\Gamma(\varrho+1)} \sum_{j=0}^{k} [(k+1-j)^{\varrho} - (k-j)^{\varrho}] \mathcal{L}_4(t_j, V(t_j)).
\end{aligned} \tag{23}$$

Theorem 3 *[39] Assume that $\mathcal{L}_1(t, S)$, $\mathcal{L}_2(t, I)$, $\mathcal{L}_3(t, R)$, $\mathcal{L}_4(t, V)$ satisfy the Lipschitz condition and S_j, I_j, R_j, V_j $(j = 1, \ldots, k+1)$ are the solutions of the Predictor-Corrector method (22) and (23). Then, the proposed numerical scheme is conditionally stable.*

Solution of the model by *Kumar-Erturk (K-E)* fractional numerical algorithm

Now we utilize one more method which is a very recent numerical method given by *Kumar et al.* in [42] to simulate nonlinear fractional-order IVPs. The scheme is defined by the following theorem:

Theorem 4 *Recall the IVP (9a)-(9b). Let*

$$\mathcal{F}(\nu, S_*(\nu)) = \mathcal{L}_1\left(\left\{t^{\rho} - (t^{\varrho} - \nu\Gamma(\varrho+1)\rho^{\varrho})^{\frac{1}{\varrho}}\right\}^{\frac{1}{\rho}}, S(t^{\rho} - (t^{\varrho} - \nu\Gamma(\varrho+1)\rho^{\varrho})^{\frac{1}{\varrho}})^{\frac{1}{\rho}}\right),$$

with the assumption of Theorem 1 hold. Then, a solution of (9a)-(9b) is defined by

$$S(t) = S_*(t^{\varrho}\rho^{-\varrho}/\Gamma(\varrho+1)),$$

where $S_*(\nu)$ is a solution of classical differential equations

$$\frac{dS_*(\nu)}{d\nu} = \mathcal{F}(\nu, S_*(\nu)), \tag{24}$$

and

$$S_*(0) = S_0. \tag{25}$$

Proof Let us assume from Theorem 1 that $S(t)$ is a solution of (9a)-(9b) which also satisfies (10). Let $\tau^{\rho} = t^{\rho} - (t^{\varrho} - \nu\Gamma(\varrho+1)\rho^{\varrho})^{1/\varrho}$. Then Eq. (10) can be re-written as

$$\begin{aligned} S(t) &= S_0 + \int_0^{t^{\varrho}\rho^{-\varrho}/\Gamma(\varrho+1)} \mathcal{L}_1\left(\left\{t^{\rho} - (t^{\varrho} - \nu\Gamma(\varrho+1)\rho^{\varrho})^{\frac{1}{\varrho}}\right\}^{\frac{1}{\rho}}, S(t^{\rho} - (t^{\varrho} - \nu\Gamma(\varrho+1)\rho^{\varrho})^{\frac{1}{\varrho}})^{\frac{1}{\rho}}\right) d\nu \\ &= S_0 + \int_0^{t^{\varrho}\rho^{-\varrho}/\Gamma(\varrho+1)} \mathcal{F}(\nu, S_*(\nu))d\nu. \end{aligned} \tag{26}$$

Also, every solution of (24)-(25) is the solution of the VIE given below and vice versa.

$$S_*(\nu) = S_0 + \int_0^{\nu} \mathcal{F}(s, S_*(s))ds, \quad 0 \le \nu \le a^{\varrho}\rho^{-\varrho}/\Gamma(\varrho+1). \tag{27}$$

Since, $0 \le t^{\varrho}\rho^{-\varrho}/\Gamma(\varrho+1) \le a^{\varrho}\rho^{-\varrho}/\Gamma(\varrho+1)$, the right-hand side of equation (26) is equal to $S_*(t^{\varrho}\rho^{-\varrho}/\Gamma(\varrho+1))$. ■

Now we derive the numerical solution of the considered model (7) based on the above methodology. Firstly, the corresponding classical model is

$$\begin{aligned} \frac{dS_*}{d\nu} &= b - S_* - \beta S_* I_* + \nu V_* + \gamma R_*, \\ \frac{dI_*}{d\nu} &= -dI_* + \beta S_* I_* - \sigma I_* - \omega I_* - \alpha I_*, \\ \frac{dR_*}{d\nu} &= -dR_* + \alpha I_* - \gamma R_*, \\ \frac{dV_*}{d\nu} &= \sigma I_* - \nu V_*. \end{aligned} \tag{28}$$

If the solution of this system is $(S_*(\nu), I_*(\nu), R_*(\nu)), V_*(\nu))$, then the solution of the model is $(S_*(t^{\varrho}/\Gamma(\varrho+1)), I_*(t^{\varrho}/\Gamma(\varrho+1)), R_*(t^{\varrho}/\Gamma(\varrho+1)), V_*(t^{\varrho}/\Gamma(\varrho+1)))$.

Remark 1 *This method is one of the fast numerical methods as compared to other available methods to solve the fractional-order initial value problems. The output processing time of the algorithm is very less,which means the scheme gives the outputs in a very short of time. Also, it is very easy to code this algorithm via any software like, Mathematica, Maple or MATLAB.*

6 Simulation results

Now we perform the analysis for the given cholera model (7) with the help of real parameter values given in Table 1. For the initial values of all four classes of cholera model, we assume $S(0) = 20000, I(0) = 30, R(0) = 0$ and $V(0) = 1000000$. In Figure 1, we plotted the graphs of infectious class $I(t)$ versus time variable t at various fractional order values along with the fixed values of extra parameter $\rho = 0.75$ by using both (K-E and P-C) numerical methods. Where-from sub-figure 1a we can observe the variations in the infected individuals by K-E method and from sub-figure 1b by using P-C method. We can see that the outputs of both methods are slightly different. In the case of K-E method, as much as time increasing, the infectious population is converging to the lower values much faster than the case of P-C method.

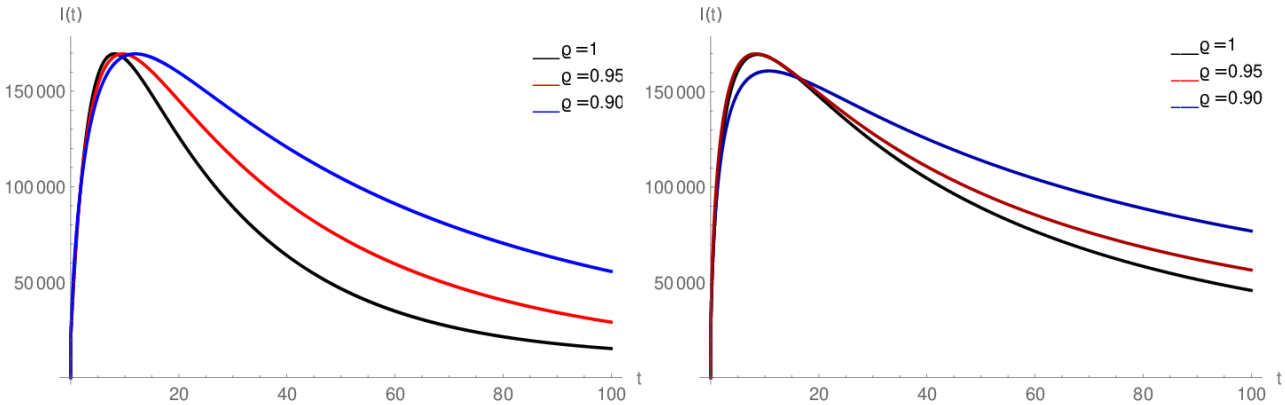

(a) Output via K-E method **(b)** Output via modified P-C method

Figure 1. Dynamics of infectious class $I(t)$ at fractional-order values $\varrho = 1,\ 0.95,\ 0.90$.

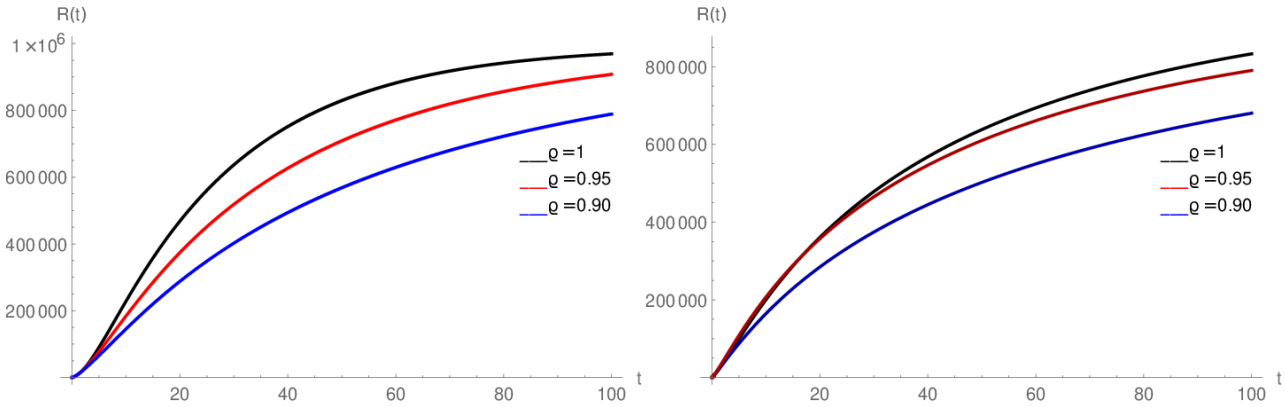

(a) Output via K-E method **(b)** Output via modified P-C method

Figure 2. Dynamics of recovered class $R(t)$ at fractional-order values $\varrho = 1,\ 0.95,\ 0.90$.

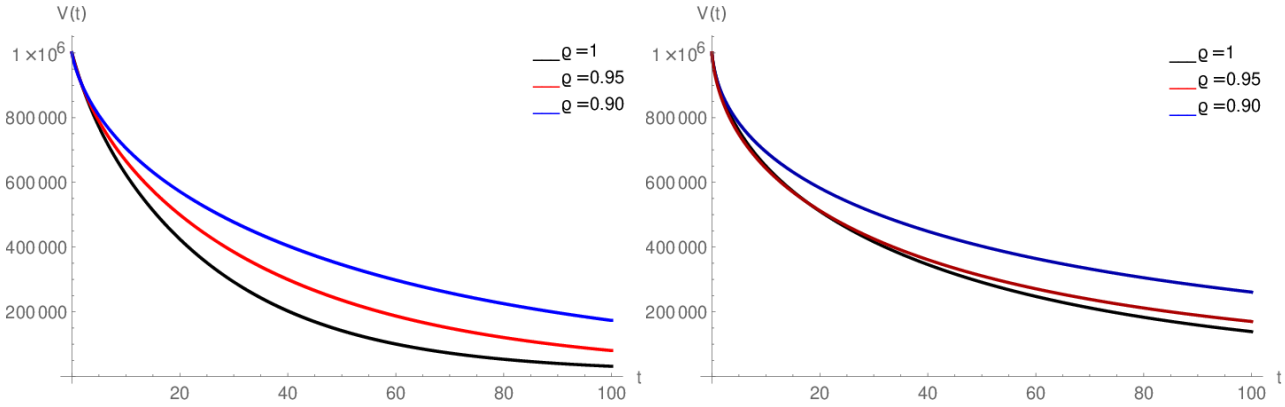

(a) Output via K-E method **(b)** Output via modified P-C method

Figure 3. Dynamics of enviroment $V(t)$ at fractional-order values $\varrho = 1,\ 0.95,\ 0.90$.

In Figure 2, the graphs of recovered class $R(t)$ versus time variable t at various fractional orders along with $\rho = 0.75$ by using both numerical methods are given. From sub-figure 2a, we can see the variations in the recovered individuals by K-E method and from sub-figure 2b by using P-C method. Again the outputs of both methods are slightly different. In the case of K-E method, the recovered population is increasing much faster then the case of P-C method. Similarly, decrement in the environmental infection or the number of bacteria concentrations $V(t)$ can be observed from Figure 3 (sub-figure 3a via K-E method and sub-figure 3b via P-C method). For understanding the role of extra parameter ρ, we plotted the group of Figures 4, 5, and 6. Here we notice that the variations caused by extra parameter ρ in K-E method (sub-figures 4a, 5a, 6a) are totally reverse to the variations caused by ρ in P-C method (sub-figures 4b, 5b, 6b). It means that both methods process the role of ρ in a different way, which makes their comparison more interesting.

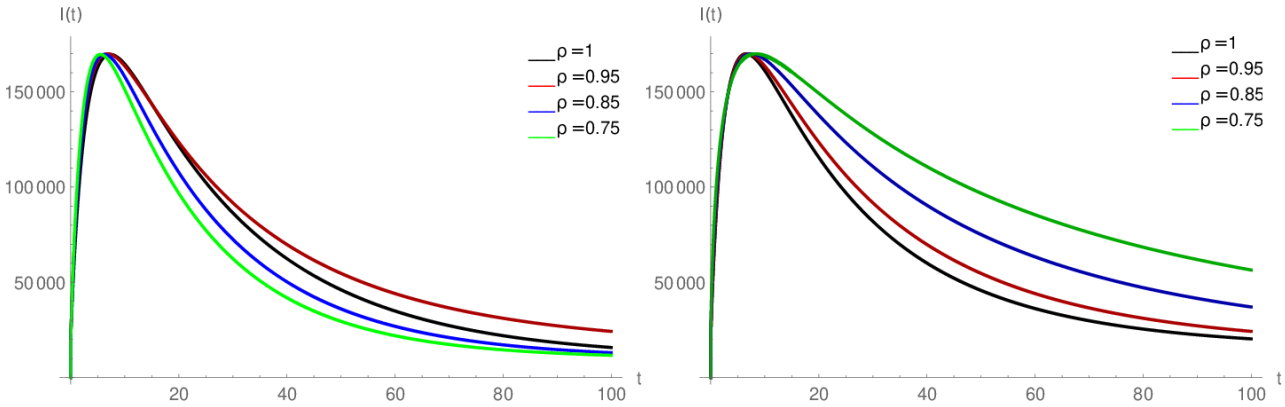

(a) Output via K-E method **(b)** Output via modified P-C method

Figure 4. Variations caused by extra parameter ρ in class $I(t)$ at fractional-order $\varrho = 0.95$.

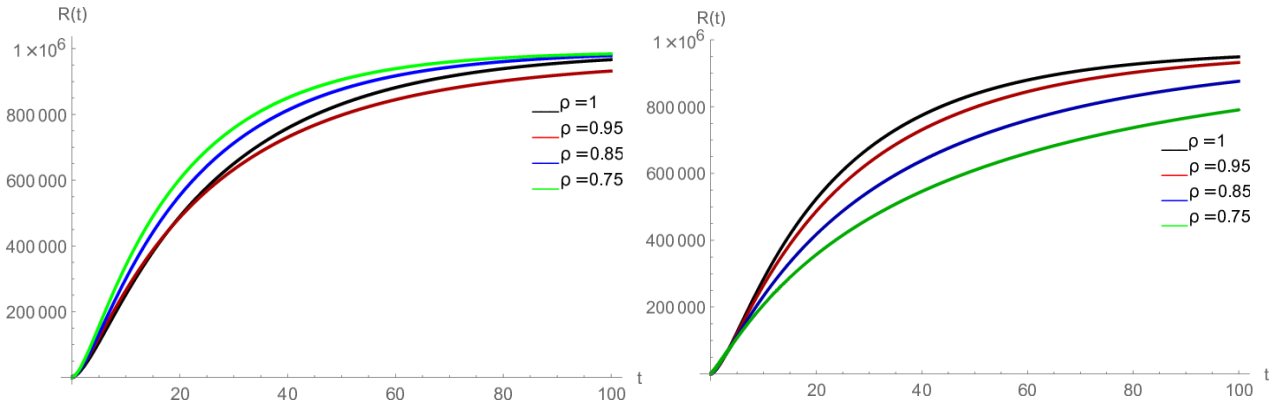

(a) Output via K-E method

(b) Output via modified P-C method

Figure 5. Variations caused by extra parameter ρ in class $R(t)$ at fractional-order $\varrho = 0.95$.

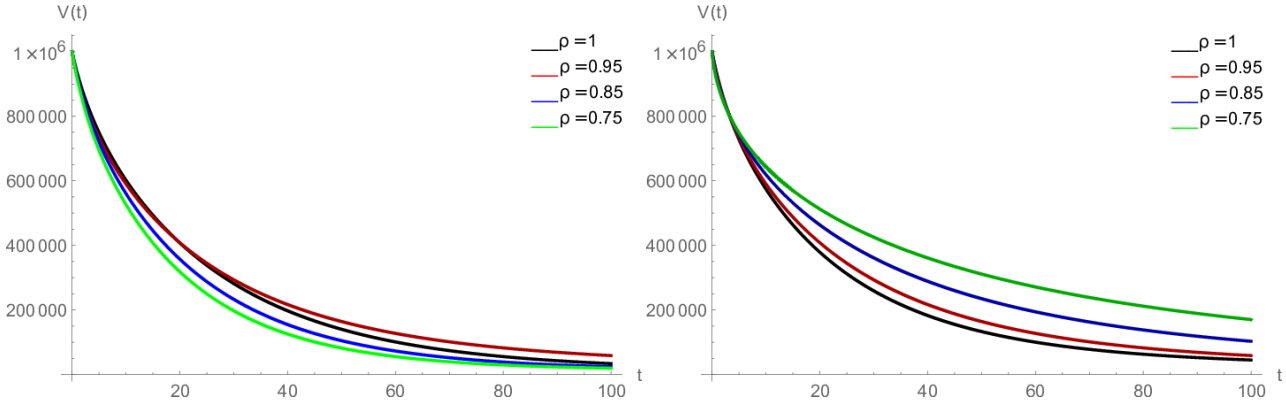

(a) Output via K-E method

(b) Output via modified P-C method

Figure 6. Variations caused by extra parameter ρ in class $V(t)$ at fractional-order $\varrho = 0.95$.

From the above given graphical simulations, we can see that both methods perform well to simulate the dynamics of the given cholera model. The outputs of both methods are slightly different which justify the importance of both schemes in this study. But when we compare the processing speed of both methods then K-E method is very fast as compared to P-C scheme because it takes only $1/4th$ processing time of the P-C method. The stability of the given P-C method is available as mentioned in Theorem 3 but the analysis related to the stability of K-E method still needs to be studied.

7 Conclusion

In this research work, we have investigated a mathematical model of cholera disease in the sense of the generalised Liouville-Caputo fractional derivative. We have proved the results for the existence of a unique solution. Numerical solutions to the considered model have been derived with the help of two different methods and the importance of both schemes has been justified. A couple of figures are simulated to explore the given cholera disease dynamics. The main aim of this work has been to explore the given disease dynamics as well as the efficiency, accuracy, and differences of both numerical methods. In the future, the given model can be solved by using any other fractional derivatives and the proposed schemes can be utilized to solve different types of non-linear fractional order models.

Declarations

Consent for publication

Not applicable.

Data availability statement

The data used in this study are mentioned/available in the manuscript.

Conflicts of interest

The authors declare that they have no conflict of interests.

Funding

Not applicable.

Author's contributions

P.K.: Conceptualization, Investigation, Formal analysis, Resources, Visualization, Writing - original draft. V.S.E.: Investigation, Software, Writing-Reviewing and Editing. All authors discussed the results and contributed to the final manuscript.

Acknowledgements

Not applicable.

References

[1] Piarroux, R., Barrais, R., Faucher, B., Haus, R., Piarroux, M., Gaudart, J., Magloire, R. & Raoult, D. Understanding the cholera epidemic, Haiti. *Emerging infectious diseases*, 17(7), 1161, (2011). [CrossRef]
[2] Tappero, J.W. & Tauxe, R.V. Lessons learned during public health response to cholera epidemic in Haiti and the Dominican Republic. *Emerging infectious diseases*, 17(11), 2087,(2011). [CrossRef]
[3] Lemos-Paião, A.P., Silva, C.J. & Torres, D.F. An epidemic model for cholera with optimal control treatment. *Journal of Computational and Applied Mathematics*, 318, 168-180, (2017). [CrossRef]
[4] Eustace, K.A., Osman, S. & Wainaina, M. Mathematical modelling and analysis of the dynamics of cholera. *Global Journal of Pure and Applied Mathematics*, 14(9), 1259-1275, (2018). [CrossRef]
[5] Sun, G.Q., Xie, J.H., Huang, S.H., Jin, Z., Li, M.T. & Liu, L. Transmission dynamics of cholera: Mathematical modeling and control strategies. *Communications in Nonlinear Science and Numerical Simulation*, 45, 235-244, (2017). [CrossRef]
[6] Njagarah, J.B.H. & Tabi, C.B. Spatial synchrony in fractional order metapopulation cholera transmission. *Chaos, Solitons & Fractals*, 117, 37-49, (2018). [CrossRef]
[7] Kilbas, A., Srivastava, H.M., and Trujillo, J.J. *Theory and Applications of Fractional Differential Equations*. Elsevier Science, (2006).
[8] Podlubny, I. *Fractional Differential Equations: An Introduction to Fractional Derivatives, Fractional Differential Equations, to Methods of their Solution and Some of their Applications*. Elsevier, (1998).
[9] Kumar, P. & Erturk, V.S. The analysis of a time delay fractional COVID-19 model via Caputo type fractional derivative. *Mathematical Methods in the Applied Sciences*, (2020). [CrossRef]
[10] Kumar, P., Erturk, V.S., Abboubakar, H. & Nisar, K.S. Prediction studies of the epidemic peak of coronavirus disease in Brazil via new generalised Caputo type fractional derivatives. *Alexandria Engineering Journal*, 60(3), 3189-3204, (2021). [CrossRef]
[11] Gao, W., Veeresha, P., Baskonus, H.M., Prakasha, D.G. & Kumar, P. A New Study of Unreported Cases of 2019-nCOV Epidemic Outbreaks. *Chaos, Solitons & Fractals*,138, 109929, (2020). [CrossRef]
[12] Nabi, K.N., Abboubakar, H. & Kumar, P. Forecasting of COVID-19 pandemic: From integer derivatives to fractional derivatives. *Chaos, Solitons & Fractals*, 141, 110283, (2020). [CrossRef]
[13] Nabi, K.N., Kumar, P. & Erturk, V.S. Projections and fractional dynamics of COVID-19 with optimal control strategies. *Chaos, Solitons & Fractals*, 145, 110689, (2021). [CrossRef]
[14] Kumar, P., Erturk, V.S., & Murillo-Arcila, M. A new fractional mathematical modelling of COVID-19 with the availability of vaccine.*Results in Physics*, 24, 104213, (2021). [CrossRef]
[15] Naik, P.A., Yavuz, M., Qureshi, S., Zu, J. & Townley, S. Modeling and analysis of COVID-19 epidemics with treatment in fractional derivatives using real data from Pakistan. *The European Physical Journal Plus*, 135(10), 1-42, (2020). [CrossRef]
[16] Özköse, F., & Yavuz, M. Investigation of interactions between COVID-19 and diabetes with hereditary traits using real data: A case study in Turkey. *Computers in biology and medicine,* 105044, (2022). [CrossRef]
[17] Ikram, R., Khan, A., Zahri, M., Saeed, A., Yavuz, M. & Kumam, P. Extinction and stationary distribution of a stochastic COVID-19 epidemic model with time-delay. *Computers in Biology and Medicine*, 141, 105115, (2022). [CrossRef]
[18] Allegretti, S., Bulai, I.M., Marino, R., Menandro, M.A. & Parisi, K. Vaccination effect conjoint to fraction of avoided contacts for a Sars-Cov-2 mathematical model. *Mathematical Modelling and Numerical Simulation with Applications (MMNSA)*, 1(2), 56-66, (2021). [CrossRef]
[19] Kumar, P., Erturk, V.S., Yusuf, A. & Kumar, S. Fractional time-delay mathematical modeling of Oncolytic Virotherapy. *Chaos, Solitons & Fractals*, 150, 111123, (2021). [CrossRef]
[20] Abboubakar, H., Kumar, P., Erturk, V.S. & Kumar, A. A mathematical study of a Tuberculosis model with fractional derivatives. *International Journal of Modeling, Simulation, and Scientific Computing*, 2150037, (2021). [CrossRef]
[21] Abboubakar, H., Kumar, P., Rangaig, N.A. & Kumar, S. A Malaria Model with Caputo-Fabrizio and Atangana-Baleanu Derivatives. *International Journal of Modeling, Simulation, and Scientific Computing*, 12(02), 2150013, (2020). [CrossRef]
[22] Kumar, P., Erturk, V.S., Yusuf, A. & Sulaiman, T.A. Lassa hemorrhagic fever model using new generalized Caputo-type fractional derivative operator. *International Journal of Modeling, Simulation, and Scientific Computing*, 12(06), 2150055, (2021). [CrossRef]
[23] Kumar, P., Erturk, V.S., Yusuf, A., Nisar, K.S. & Abdelwahab, S.F. A study on canine distemper virus (CDV) and rabies epidemics in the red fox population via fractional derivatives. *Results in Physics*, 25, 104281, (2021). [CrossRef]

[24] Kumar, P., Erturk, V.S. & Murillo-Arcila, M. A complex fractional mathematical modeling for the love story of Layla and Majnun. *Chaos, Solitons & Fractals*, 150, 111091, (2021). [CrossRef]
[25] Kumar, P. & Erturk, V.S. Environmental persistence influences infection dynamics for a butterfly pathogen via new generalised Caputo type fractional derivative. *Chaos, Solitons & Fractals*, 144, 110672, (2021). [CrossRef]
[26] Kumar, P., Erturk, V.S., Banerjee, R., Yavuz, M. & Govindaraj, V. Fractional modeling of plankton-oxygen dynamics under climate change by the application of a recent numerical algorithm. *Physica Scripta*, 96(12), 124044, (2021). [CrossRef]
[27] Kumar, P., Erturk, V.S. & Nisar, K.S. Fractional dynamics of huanglongbing transmission within a citrus tree. *Mathematical Methods in the Applied Sciences*, (2021). [CrossRef]
[28] Kumar, P., Erturk, V.S. & Almusawa, H. Mathematical structure of mosaic disease using microbial biostimulants via Caputo and Atangana–Baleanu derivatives. *Results in Physics*, 24, 104186, (2021). [CrossRef]
[29] Joshi, H. & Jha, B.K. Fractional-order mathematical model for calcium distribution in nerve cells. *Computational and Applied Mathematics*, 39(2), 1-22, (2020). [CrossRef]
[30] Joshi, H. & Jha, B.K. On a reaction–diffusion model for calcium dynamics in neurons with Mittag–Leffler memory. *The European Physical Journal Plus*, 136(6), 1-15, (2021). [CrossRef]
[31] Joshi, H. & Jha, B.K. Chaos of calcium diffusion in Parkinson's infectious disease model and treatment mechanism via Hilfer fractional derivative. *Mathematical Modelling and Numerical Simulation with Applications (MMNSA)*, 1(2), 84-94, (2021). [CrossRef]
[32] Joshi, H. & Jha, B.K. Modeling the spatiotemporal intracellular calcium dynamics in nerve cell with strong memory effects. *International Journal of Nonlinear Sciences and Numerical Simulation*, (2021). [CrossRef]
[33] Veeresha, P. A numerical approach to the coupled atmospheric ocean model using a fractional operator. *Mathematical Modelling and Numerical Simulation with Applications (MMNSA)*, 1(1), 1-10, (2021). [CrossRef]
[34] Baishya, C. & Veeresha, P. Laguerre polynomial-based operational matrix of integration for solving fractional differential equations with non-singular kernel. *Proceedings of the Royal Society A*, 477(2253), 20210438, (2021). [CrossRef]
[35] Veeresha, P. & Baleanu, D. A unifying computational framework for fractional Gross–Pitaevskii equations. *Physica Scripta*, 96(12), 125010, (2021). [CrossRef]
[36] Akinyemi, L., Nisar, K.S., Saleel, C.A., Rezazadeh, H., Veeresha, P., Khater, M.M. & Inc, M. Novel approach to the analysis of fifth-order weakly nonlocal fractional Schrödinger equation with Caputo derivative. *Results in Physics*, 31, 104958, (2021). [CrossRef]
[37] Okposo, N.I., Veeresha, P. & Okposo, E.N. Solutions for time-fractional coupled nonlinear Schrödinger equations arising in optical solitons. *Chinese Journal of Physics*, (2021). [CrossRef]
[38] Odibat, Z. and Baleanu, D. Numerical simulation of initial value problems with generalized caputo-type fractional derivatives. *Applied Numerical Mathematics*, 156, 94-105, (2020). [CrossRef]
[39] Erturk, V.S. & Kumar, P. Solution of a COVID-19 model via new generalized Caputo-type fractional derivatives. *Chaos, Solitons & Fractals*, 139, 110280, (2020). [CrossRef]
[40] Kumar, P. & Erturk, V.S. A case study of Covid-19 epidemic in India via new generalised Caputo type fractional derivatives. *Mathematical Methods in the Applied Sciences*, 1-14, (2021). [CrossRef]
[41] Odibat, Z., Erturk, V.S., Kumar, P. & Govindaraj, V. Dynamics of generalized Caputo type delay fractional differential equations using a modified Predictor-Corrector scheme. *Physica Scripta*, 96(12), 125213, (2021). [CrossRef]
[42] Kumar, P., Erturk, V.S. & Kumar, A. A new technique to solve generalized Caputo type fractional differential equations with the example of computer virus model. *Journal of Mathematical Extension*, 15, (2021). [CrossRef]

Mathematical Modelling and Numerical Simulation with Applications (MMNSA) (http://www.mmnsa.org)